THE UNIVERSITY OF MANITOBA

AN INVESTIGATION OF POSSIBLE SUPERPLASTIC CONDITIONS IN DUCTILE CAST IRON

BY

KENNETH G SIMONITE

A Thesis
Submitted to the Faculty of Graduate Studies
In Partial Fulfillment of the Requirements for the Degree of
Master of Science

Winnipeg, Manitoba
1992

ISBN 0-315-77879-2

AN INVESTIGATION OF POSSIBLE SUPERPLASTIC CONDITIONS IN DUCTILE CAST IRON

By

KENNETH G SIMONITE

A dissertation submitted to the Faculty of Graduate Studies of the University of Manitoba in partial fulfillment of the requirements of the degree of

MASTER OF SCIENCE

ACKNOWLEDGEMENTS

The author wishes to thank Dr. J. R. Cahoon for his constant guidance and patience throughout the entire course of this study. I would also like to recognize the many students and staff members in the material science lab who provided their time and thoughts. I would like to acknowledge Ancast Industries Limited for providing the material for this work and in particular Jose Castillo for his advice. And lastly, but not least, I would like to thank my wife, Gloria, and family members for providing lasting patience and encouragement.

ABSTRACT

An attempt was made to determine the possibilities of producing a superplastic ductile cast iron. Ductile cast iron is a material that, despite its name, is quite brittle. It lacks the ability to be processed and consequently applied using thermomechanical forming. This investigation attempts to change this by determining the feasibility of producing a more versatile superplastic material.

In order to achieve a refined microstructure the ductile cast iron in this study was subjected to a mechanical process called swaging. The material underwent hot swaging at temperatures in the order of 850°C, a temperature close to that at which it was anticipated that superplastic properties would be realized. The swaged material, after further preparation, was subjected to compression and tension tests over temperature ranges of 750°C to 950°C and strain rates of 1 $X10^{-5}$ to 2 X 10^{-3} sec^{-1}. Ductile cast iron not subjected to the swaging process was also tested under the same conditions as the swaged material for comparison purposes.

Similar results were obtained for both the swaged material and the as received material. Strain rate sensitivity values were generally in the range of 0.20 to 0.35 and elongation to failure values ranged from 40% to 106%. A notable difference between the two materials was that the swaged material exhibited catastrophic failure in compression while the as received material did not fail in such a dramatic fashion.

The swaged material did not exhibit the required grain refinement since the graphite nodules (second phase) did not fragment and recrystallize as expected.

This material did not perform well over the range of superplastic forming temperatures. Under these conditions the material is not superplastic and the prime reason seems to be due to the lack of graphite refinement and recrystallization.

TABLE OF CONTENTS

LIST OF FIGURES

LIST OF TABLES

1. INTRODUCTION

Upon considering some of the essentials of superplasticity and relating them to some of the characteristics of ductile cast iron, one may come to the conclusion, that on the surface at least, the existence of a superplastic ductile cast iron is possible. Prerequisites inherent to superplastic materials and that exist in ductile cast iron is the presence of two phases in which the grains are equiaxed in nature, stable and uniformly distributed throughout the matrix at the elevated temperature where deformation is taking place.

The two phases that exist in ductile cast iron at elevated temperatures are graphite and austenite. The spheroidal shape of the graphite nodules is proof enough that it exists in an equiaxed form. It is also suggested that graphite will retain this shape over the range of test temperatures.[1] Austenite is also equiaxed in shape in ductile cast iron at the test temperatures.

There are however other preconditions necessary for the existence of the phenomena of superplasticity. These include such things as ultrafine grain size, high angle grain boundaries and highly mobile grains resistant to tensile separation.

In the following chapters aspects of superplasticity will be related to ductile cast iron under theoretical and experimental conditions. The reasons as to whether or not this material is superplastic will become clear and this knowledge will lead to recommendations on the future directions of ductile cast iron in the area of superplasticity. Before this happens it is important to understand the intricacies of both ductile cast iron and superplasticity, paying particular attention to the most recent and

relevant advances in these areas. This is accomplished in the following two chapters.

2. CHARACTERISTICS OF DUCTILE CAST IRON

2.1 General

Ductile cast iron is a relatively new material that has gained considerable importance over the last 40 years. Ductile iron is described by one author as being "a high carbon containing, iron-base alloy in which graphite is present in compact, spheroidal shapes"[2], whereas another author refers to it as "an as-cast structure containing graphite particles in the form of small, rounded, spheroidal nodules in a ductile metallic matrix."[3] Because of these spheroidal nodules of graphite, ductile cast iron is also referred to as nodular cast iron and spheroidal graphite cast iron.

There are several grades of ductile cast iron. These are shown in Figure 1, which gives several of the common grades according to matrix structure, and indicates where they stand with respect to yield strength and percent elongation. These different grades are achieved through varying cooling rates, heat treatments, alloying additions, etc... The various grades are also shown in Figure 2 according to their respective standards. These standards are based on a combination of tensile strength, 0.2% offset yield strength and percent elongation. It is obvious, from Figure 1 and Figure 2, that the differences in the metallic matrices between grades has a pronounced effect on tensile strength, yield strength and percent elongation along with other mechanical and physical properties.

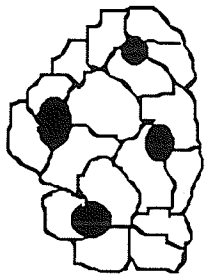

1 Ferritic; may be annealed
Used in shock resistant parts
and low temperature service.

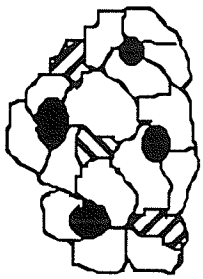

2 Mostly ferritic; as cast or
annealed. Used in general
service.

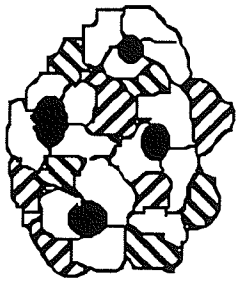

3 Ferritic/pearlitic; as cast
Used in general service.

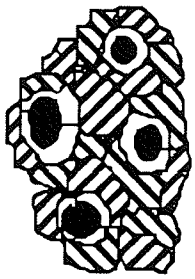

4 Mostly pearlitic; may be
normalized. Exhibits the
best combination of strength,
wear resistance and response
to surface hardening.

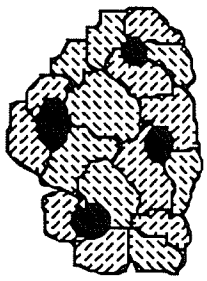

5 Martensitic; oil quenched
and tempered. Has the highest
strength and wear resistance.

Figure 1 Structure of five grades of ductile cast iron. 1) Grade 60-40-18, 2) Grade 65-45-12, 3) Grade 80-55-06, 4) Grade 100-70-06, 5) Grade 120-90-02. The first number in each grade represents Ultimate Strength (Ksi), the second number represents Yield Strength (Ksi) and the third number represents percent elongation.

2.2 Elemental Influence

There are approximately 50 elements that affect the structure and properties of ductile iron to a varying degree, and therefore must be controlled. A given element can promote the existence or nonexistence of carbides, influence the shape and distribution of graphite or be involved in the characteristics of the matrix. The more important of these elements are discussed below.

Both carbon and silicon promote a carbide free as-cast structure, which is of primary importance in producing ductile cast iron. The optimum range for carbon is between 3.4 and 3.8% and is dependent upon the silicon content which ranges between 2.0 and 2.8%. Too much carbon leads to possible graphite flotation (in heavier sections) and an increase in the expansion of the casting; too little carbon can result in unsoundness of the casting and the formation of carbides. Low levels of silicon will also promote the formation of carbides. High levels of silicon reduce impact energy, increase the ductile to brittle transition temperature and decrease thermal conductivity.

Manganese promotes carbide and pearlite formation. The maximum amount of manganese is dependent on the amount of silicon and the thickness of the casting. Other elements that promote carbide formation include chromium, vanadium, boron, tellurium and molybdenum.

The primary element that is used to give the graphite its spheroidal shape is magnesium. The amount of magnesium necessary to accomplish this is in the range of 0.04 to 0.06%. Too much magnesium can promote the formation of carbides while too

little can result in compacted graphite structures rather than the desired spheroidal shape.

Some elements that disrupt the spheroidal graphite shape are lead, antimony, bismuth, titanium, sulphur, aluminum and arsenic. Additions of cerium which promote spheroidization will neutralize the effect of the above elements.

Copper promotes hardness and pearlite formation. Phosphorous must be kept low, as it promotes unsoundness and lowers ductility.

2.3 Mechanical Properties

From Figure 2 it is apparent that in the grades of iron shown, as both tensile strength and yield strength increase, hardness also increases. Percentage elongation decreases as hardness increases, however. It can be inferred therefore, that percentage elongation will decrease as tensile and yield strength increase. Various mechanical properties in tension, compression and torsion for some of these grades are given in Table 1. These are not average values for these grades of iron, but they are certainly in the acceptable range. Yield strengths in compression are reported as being 1.0 to 1.2 times as high as yield strengths in tension. Ductile iron could be fully pearlitic, fully ferritic or some combination of the two. As the pearlite content increases, the strength and hardness of the material will also increase. A desired matrix structure can be achieved through heat treatment. Carbides in the matrix are undesirable because they reduce ductility and result in premature failure in tension, fatigue and impact loading.

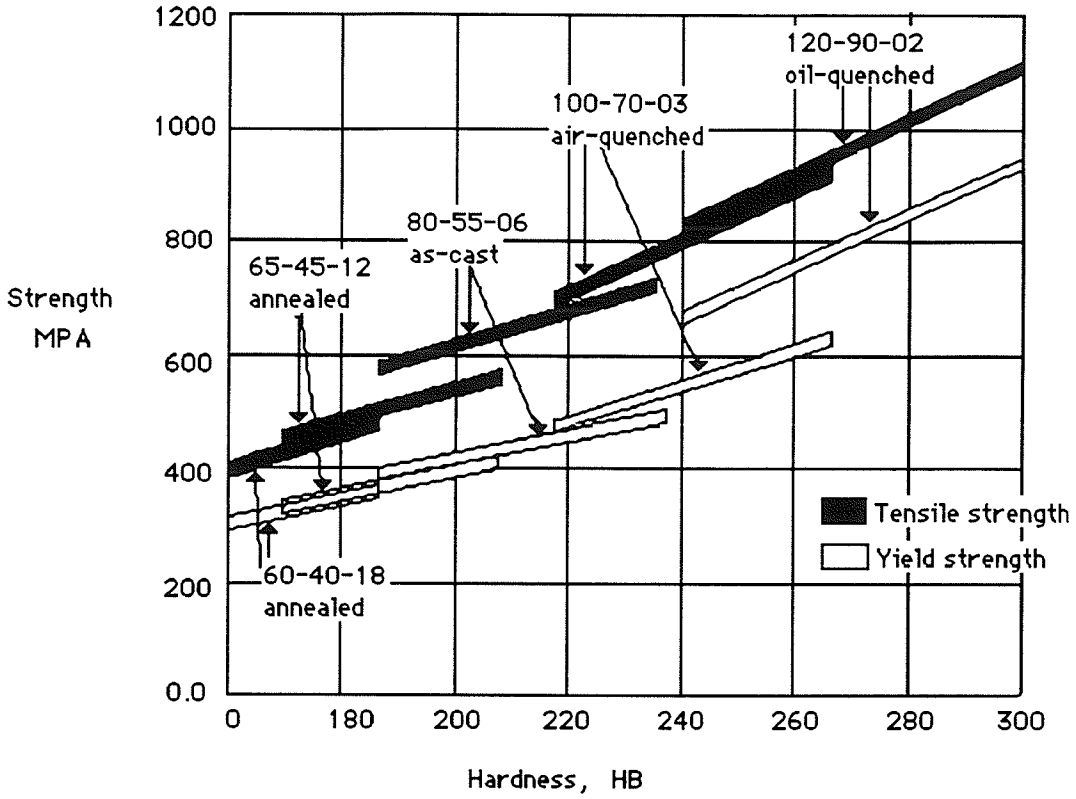

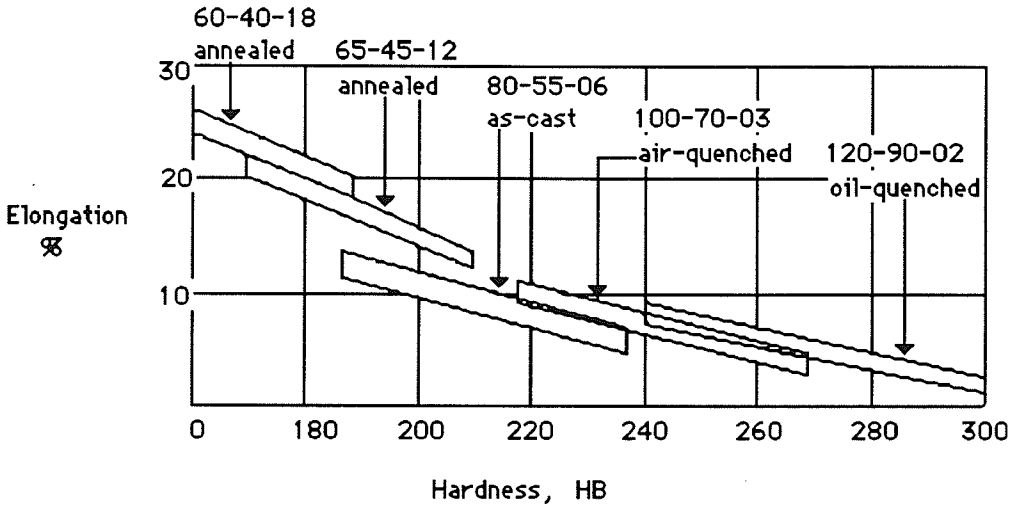

Figure 2 Mechanical properties of ductile cast irons

Table 1 Average mechanical properties of ductile irons heated to various levels. (a)

Nearest standard grade	Hardness HB	Ultimate Strength MPa	Ksi	Yield strength Mpa	ksi	Elongation %(b)	Modulus GPa	10^6 psi	Poisson's ratio
Tension									
60-40-18	167	461	66.9	329(c)	47.7(c)	15.0	169	24.5	0.29
65-45-12	167	464	67.3	332(c)	48.2(c)	15.0	168	24.4	0.29
80-55-06	192	559	81.1	362(c)	52.5(c)	11.2	168	24.4	0.31
120-90-02	331	974	141.3	864(c)	125.3(c)	1.5	164	23.8	0.28
Compression									
60-40-18	167	...	...	359(c)	52.0(c)	...	164	23.8	0.26
65-45-12	167	...	...	362(c)	52.5(c)	...	163	23.6	0.31
80-55-06	192	...	...	386(c)	56.0(c)	...	165	23.9	0.31
120-90-02	331	...	...	920(c)	133.5(c)	...	164	23.8	0.27
Torsion									
60-40-18	167	472	68.5	195(d)	28.3(d)	...	63	9.1	...
							65.5(e)	9.5(e)	
65-45-12	167	475	68.9	297(d)	30.0(d)	...	64	9.3	...
							65(e)	9.4(e)	
80-55-06	192	504	73.1	193(d)	28.0(d)	...	62	9.0	...
							64(e)	9.3(e)	
120-90-02	331	875	126.9	492(d)	71.3(d)	...	63.4	9.2	...
							64(e)	9.3(e)	

(a) Determined for a single heat of ductile iron, heat treated to approximate various standard grades. Properties were obtained using test bars machined from 25 mm (1 in) keel. (b) In 50 mm, or 2 in. (c) 0.2% offset. (d) 0.0375% offset. (e) Calculated from tensile modulus and Poisson's ratio in tension.

2.4 The Importance of Graphite

Graphite is an integral part of ductile cast iron. The size, shape and distribution of graphite influences the material's performance. Graphite shape is the most important and influential factor affecting the material's properties. "The conversion of graphite from flakes to nodules results in a fivefold to sevenfold increase in the strength of the cast metal."[4] "All of the mechanical and physical properties characteristic of this class of materials are a result of the graphite being substantially or wholly in the spheroidal nodular shape, and any departure from this shape in a proportion will cause some deviation from these properties."[5] It is therefore important that 85 to 100% of the graphite retains its spheroidal form.

An increase in the amount of graphite results in a decrease in strength and ductility. An increase in tensile properties is evident when the nodules are small but numerous.

3. SUPERPLASTICITY

3.1 General

The phenomenon of superplasticity has been observed in various metallic alloys, including aluminum, iron, titanium, nickel and copper as well as some ceramics. One definition of superplasticity comes from Padmanabhan and Davies. "Superplasticity is the deformation process that produces essentially neck-free elongations of many hundreds of percent in metallic materials deformed in tension."[6] To the layman this macroscopic definition is sufficient, but to the metallurgist a more in depth understanding is necessary, one that explains the very nature of the process and the mechanisms involved. A further classification as to what constitutes superplasticity is given by Ridley and Pilling; "Micrograin superplasticity" as opposed to environmental superplasticity, which is not dealt with in this thesis, "is shown by materials with a fine grain size, usually less than 10 μm, when they are deformed within the strain rate range 10^{-5} to 10^{-1} s^{-1} at temperatures greater than 0.5 T_m, where T_m is the melting point in degrees Kelvin."[7] Superplastic deformation also exhibits low flow stresses along with highly uniform plastic flow. Both of these factors make a superplastic material extremely attractive commercially.

3.1.1 Strain Rate Sensitivity

A high strain rate sensitivity along with an ultra fine grain size should result in the necessary low tensile flow stresses that produce the abnormally large elongations inherent to superplastic

deformation. The strain rate sensitivity, m, is seen in the power law equation relating flow stress, σ, and strain rate, $\dot{\varepsilon}$:

$$\sigma = K\dot{\varepsilon}^m \quad \text{.....(1)}$$

where K is a material constant.

A material is not considered superplastic if the strain rate sensitivity is less than 0.3. Ideally, m values between 0.4 to 0.8 are desired.

The localized strain rate is affected by the presence of a neck in the gauge length of a tensile specimen. A locally high strain rate will appear in the necked region and if m is high, there will be a sharp rise in flow stress in this area. The necked region will consequently become strain rate hardened, and necking in this region will essentially stop. Further neck regions will develop and stop, and the material will become highly elongated as a result of the high strain rate sensitivity.

If log σ is plotted versus log $\dot{\varepsilon}$, then from equation #1 it is obvious that the slope will be equivalent to m. The plot of stress versus strain rate is usually sigmoidal in nature for superplastic materials. Figure 3 gives an example of flow stress versus strain rate for an aluminum alloy subjected to a step strain rate test. Figure 4 shows the strain rate sensitivity, derived from Figure 3, versus strain rate. It is apparent that within the superplastic regime there is a maximum m value which represents the best testing condition for superplastic deformation at the test temperature.

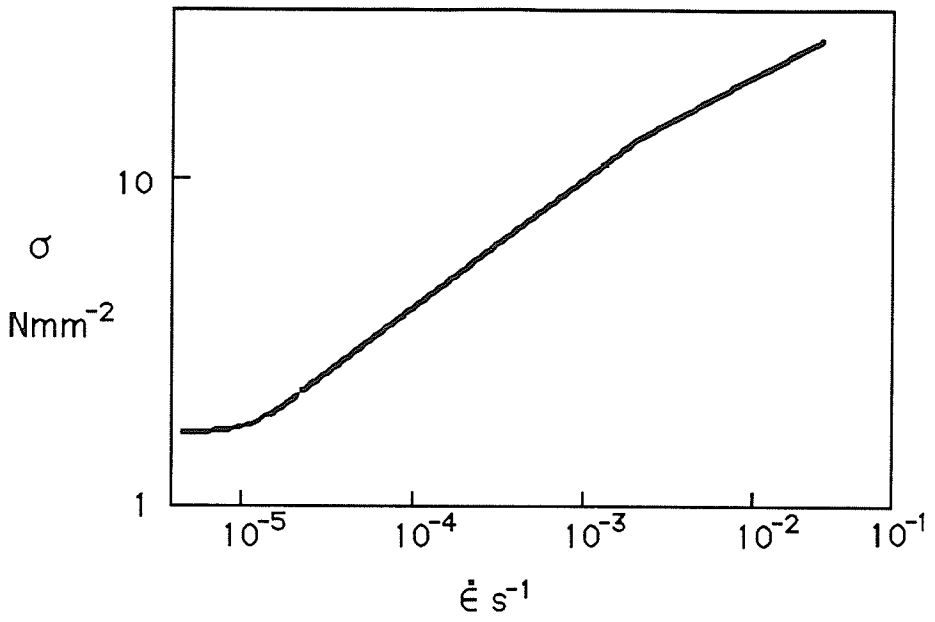

Figure 3 Logarithmic plot of flow stress versus strain rate.

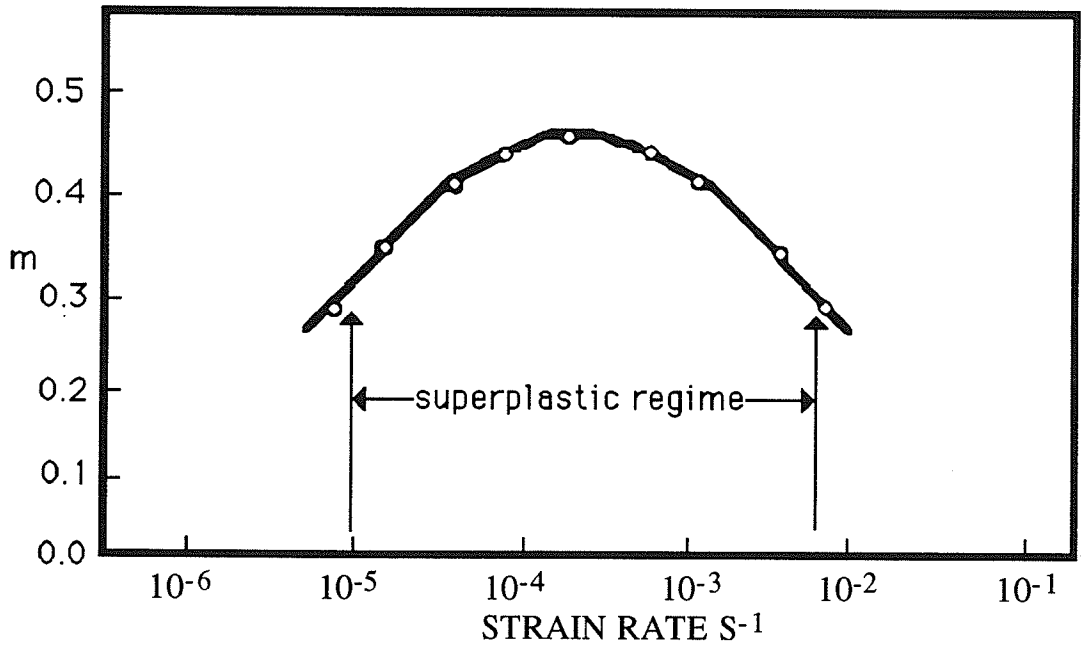

Figure 4 The variation of strain rate sensitivity (m) with strain rate.

The step strain rate test mentioned above was suggested by Backofen et al.[8] It is used to determine strain rate sensitivity values at various strains and strain rates. Each test is carried out at a constant temperature with two variations shown in Figures 5 and 6.

The first involves two constant strain rates as shown in Figure 5. The base strain rate must reach equilibrium before it is increased to the second constant strain rate, which also has to attain equilibrium before it is decreased back to the base. This test takes into account the way strain influences strain rate sensitivity, because the same two strain rates are used throughout the duration of the test.

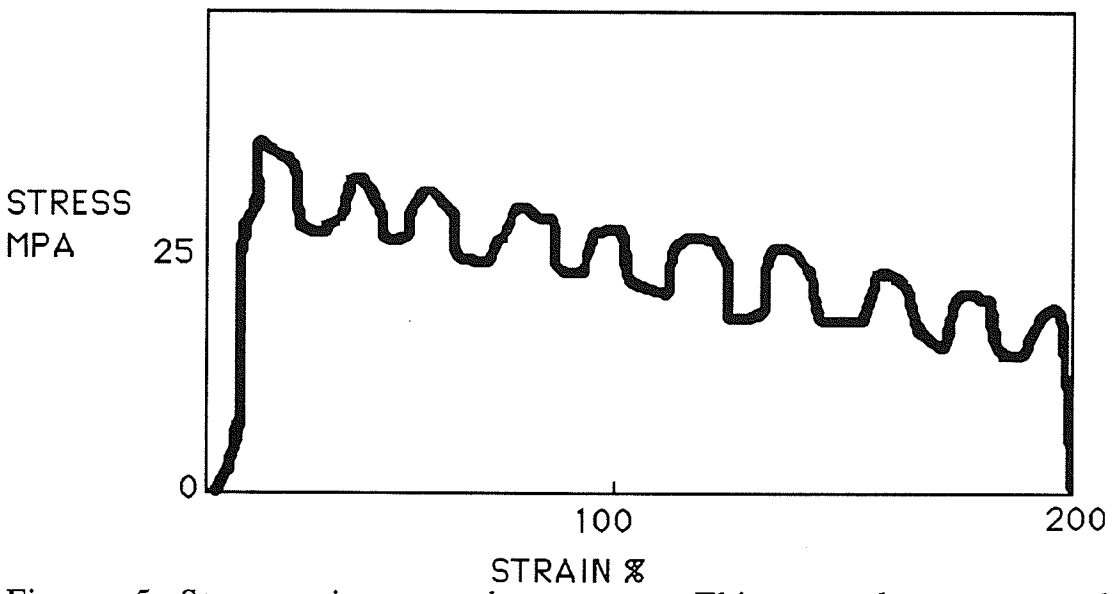

Figure 5 Step strain rate change test. This test demonstrates how strain affects strain rate sensitivity.

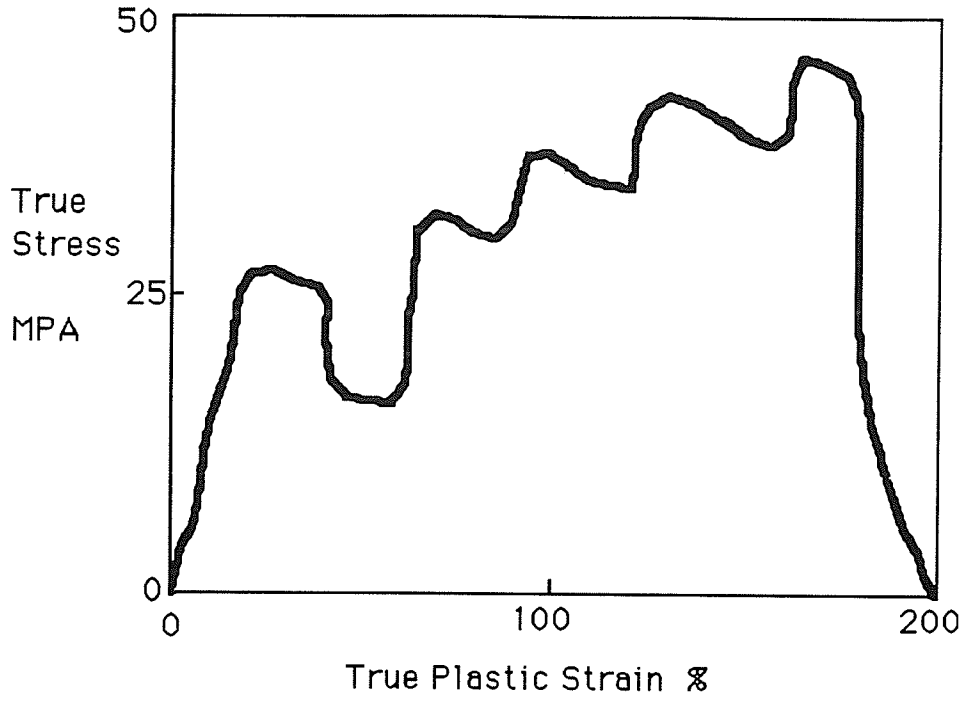

Figure 6 The step strain rate test. Each sharp jump in stress represents a change in strain rate. This test predicts how sensitive a material is to a change in strain rate, hence it is also known as a "strain rate sensitivity test".

The other test involves continual incremental increases in strain rate as shown in Figure 6. A base strain rate, with a value at approximately the mid-point of the range of strain rates used in the experiment, is allowed to stabilize before it is lowered to the slowest strain rate. This slow strain rate, after stabilization, is then increased to the next slowest strain rate and the process continues in this fashion until the end of the test. The increments chosen for this test are arbitrary and not necessarily the same throughout. This test is a function of strain rate.

The ideal conditions for superplasticity are determined from these experiments and constant strain rate tension tests can be run at these conditions to determine resulting elongations.

3.1.2 Fine Grain Size

A fine grain size capable of remaining stable during deformation is a necessary ingredient for the making of a superplastic material. Furthermore, it is imperative that these fine equiaxed grains have grain boundaries that are high-angled, mobile and resistant to separation. It is necessary that each phase be fairly equivalent in strength at the temperature at which superplastic deformation is occurring.

Superplastic materials can be categorized into two fundamental groups; pseudo single phase and microduplex. Pseudo single phase materials are not discussed in this investigation, as the ductile cast iron scrutinized is microduplex in nature.

Microduplex materials attain their fine grain size by thermomechanical processing. The grains will remain stable after refinement if there are approximately an equal amount of two or more chemically and structurally different phases that are randomly dispersed throughout the matrix. Grain growth usually does occur to an extent in many superplastic materials, with the majority of the growth occurring in the deformed region. There are several methods utilized to refine grains. These include phase separation, phase transformation and mechanical working.

In mechanical working the material is worked at a temperature close to that where it will be superplasticly deformed. The refining process occurs as follows: if the two phases differ greatly in hardness, the harder phases will fragment and the softer phase will penetrate through these fragments, thus causing separation.

Recrystallization usually takes place during the refining process. If however, the two phases are relatively equal in hardness, the grains will elongate simultaneously and then fragment due to the formation of intense shear bands. Recrystallization occurs in the same way as above. Both of these cases are shown in Figure 7. Grain growth is kept relatively minimal because the separate fine grains are of different composition. Diffusion from smaller grains to larger grains has to occur for grain growth to take place. Diffusion is restricted by the solubility of the two phases in each other since the grains are fairly evenly distributed. Phase transformation and phase separation are not discussed in this section.

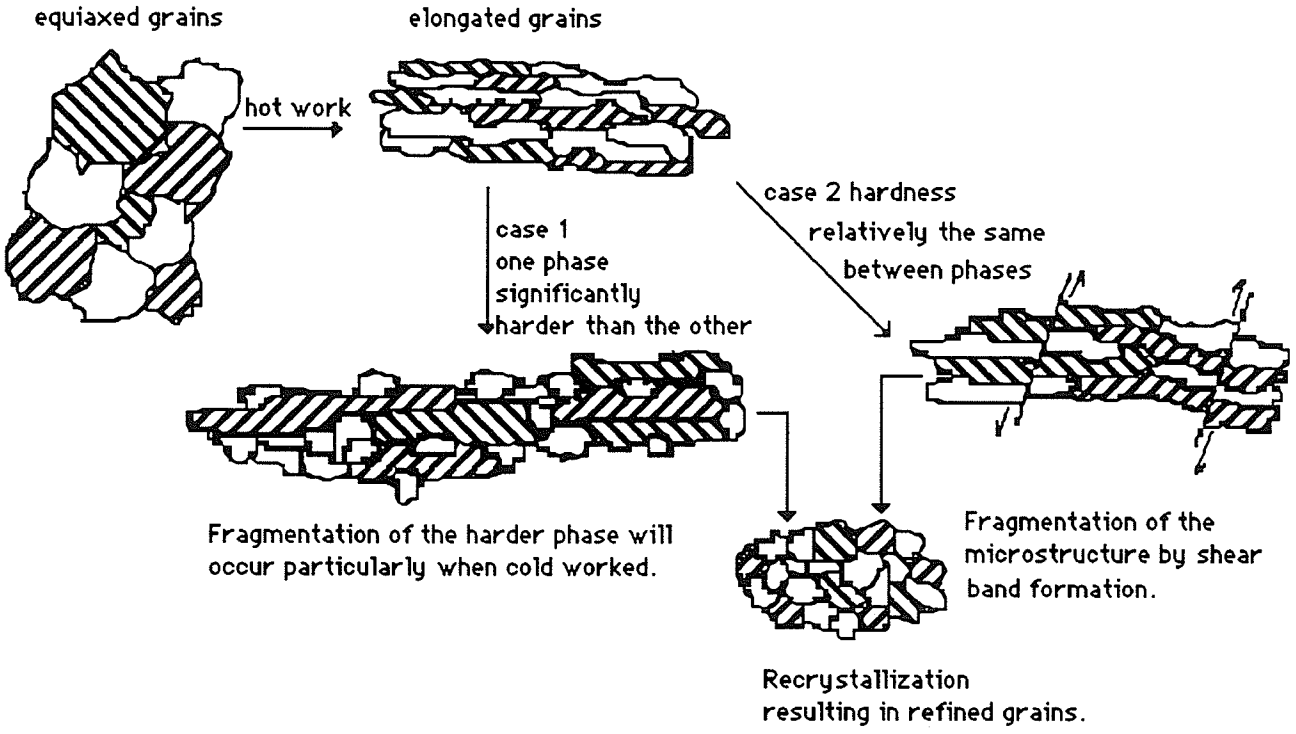

Figure 7 Grain refining process for two types of materials.

3.1.3 Grain Boundary Sliding and Grain Rotation

In the region of superplastic deformation the rate controlling mechanisms are as yet unclear. However, it is clear that grain boundary sliding and grain rotation occur during deformation. This motion by the grains is in effect the strain which develops as loading progresses. An individual grain will move in a way that depends on how the normal and shear stresses act on its grain boundary. It is clear that motion is dependent on grain shape and grain orientation. Due to the randomness of the distribution of grains, sliding and rotation will take place in different directions and in different amounts. On the surface it appears that large elongations result due to the accommodation made by the grains when sliding and rotating, limiting the formation of cracks and voids. Many theories relating to this and other mechanisms of deformation exist but are beyond the scope of this thesis.

3.2 Iron Alloys

3.2.1 General

Iron and its alloys are one of the most commonly used materials in the world. Their importance can be further enhanced if they can become even more versatile. To be made superplastic, with good room temperature properties, would certainly make iron alloys more versatile. This feat has been achieved in various alloys (at least the superplastic aspect) and they can be broken up into two groups: particle stabilized and segregation stabilized. This thesis is mainly concerned with the particle stabilized alloys.

3.2.2 Particle Stabilized

Plain carbon and low alloy steels are the main materials that comprise particle stabilized alloys. These alloys acquire their fine grain size by thermal and thermomechanical processing, and are thereby stabilized by carbides during deformation.

Sherby et al[9], worked with ultra-high carbon steels containing 1.3 to 1.9% carbon. Their reasons for using such high carbon contents was so that they could take advantage of the proeutectoid cementite that forms in hypereutectoid steels, to stabilize the ferrite grains. They also reasoned that even above the A_1 temperature, the austenite grains should remain fine because there would still be undissolved proeutectoid cementite present. They reasoned therefore, that superplasticity could be achieved between 650 to 900°C for these alloys. The alloys tested had cementite grain sizes ranging between 0.1 and 0.5 μm and matrix grains in the order of 0.5 to 1.5 μm. Strain rate sensitivity values ranged between 0.35 to 0.5, with the higher values seen to occur in the alloys with higher carbon contents. Typical elongations were between 200 to 500% (intermediate strain rates), with the higher elongations also seen in higher carbon containing alloys. Even for a high strain rate, 1.7×10^{-2} sec^{-1}, a 1.6% carbon containing alloy elongated 170% at 800°C.

Wadsworth and Sherby[10] found that the addition of chromium in small amounts greatly enhances the superplastic properties of ultra-high carbon steels. They discovered that the chromium enters the cementite stabilizing it and thereby minimizing ferrite grain growth. Experimentally, they found that at a strain rate of 1.7×10^{-4}

sec^{-1}, a 1.6% carbon, 1.5% chromium alloy elongated 1220%, a plain carbon 1.6% steel elongated 470% and a 1.0% carbon 1.5% chromium steel elongated 330%. All three constant strain rate tests were run at 650°C. Grain sizes were in the same order as for plain ultra-high carbon steels. Strain rate sensitivity values were between 0.3 and 0.6. Even at a high strain rate of 1.7×10^{-2} sec^{-1} for a 1.6% C, 1.5% Cr steel at 650°C, an elongation of 330% was achieved. For the same alloy and conditions, but at a strain rate of 0.17 sec^{-1}, an excellent elongation of 131% was seen to occur.

Walser and Sherby[11] carried out more extensive work on ultra-high carbon steels above the A_1 temperature. They theorized that the austenite grains should be fine grained because of the extensive network of fine grained ferrite that provided nuclei for the austenite grains. Furthermore, the undissolved cementite particles should inhibit austenite grain growth. At all temperatures there was the presence of strain hardening caused by grain coarsening. Elongations were less than those seen below the A_1 temperatures, but they were still a very respectable 350 to 750%. The reason they gave was that there is more cementite below the A_1 temperature, i.e. the grains are better stabilized at the lower temperatures. They experimentally determined an activation energy of 170 KJ/mole for superplastic flow. This value is very similar to that for grain boundary self diffusion in α or γ iron. When slip creep was the dominate mechanism (non-superplastic flow) the activation energy was similar to that for lattice diffusion in α or γ iron.

Sherby et al[12] discovered that adding silicon to ultra-high carbon steels further enhances the stabilization of grains. As a

result, superplasticity was extended to strain rates above 10^{-3} sec^{-1}. At 800°C and a strain rate of 1.7 x 10^{-2} sec^{-1} elongations in the order of 500% were seen for an alloy containing 1.25% carbon, 1.5% chromium, 3% silicon and 0.5% manganese. Silicon stabilizes ferrite which has the effect of raising the A_1 temperature, thus increasing the quantity of proeutectoid cementite.

Daehn, Kum and Sherby[13] discovered that cladding superplastic ultra-high carbon steel with a non-superplastic material will enable the non- superplastic material to behave in a superplastic fashion. They used a ferritic 26 Cr-1 Mo stainless steel as the cladding material and a 1.25% C, 3% Si ultra-high carbon steel as the base superplastic material. The clad material attained an elongation of 850% at 825°C with a constant crosshead speed and an initial strain rate of 1.67 x 10^{-3} sec^{-1}. This result compares with a value of 250% obtained from a similar test performed on the cladding material alone. The fine grained structure in the ultra-high carbon steel allowed excellent solid state bonding to occur. An abundance of grain boundaries act as sinks for vacancy, and impurity atoms during deformation. The predicted elongations were not achieved however, and this was due to the cladding material cracking prematurely.

Ruano, Eiselstein and Sherby[14] showed that the higher carbon white cast irons could also be made to behave superplasticly. Fine ferrite grains of 1 to 2 μm were realized by the consolidation of rapidly solidified powders. The following elongations were seen at a temperature of 700°C and a strain rate of 1.7 x 10^{-4} sec^{-1}; 1410% for a 3.0% C, 1.5% Cr white cast iron, 940% for a 3.0% C white cast iron

and 480% for a 2.4% C white cast iron. Strain rate sensitivity values of 0.5 were achieved. Activation energies were similar to those for grain boundary self diffusion. Even with up to 45 vol% carbides there was almost no cavitation.

Kim et al[15] demonstrated the existence of superplasticity in iron carbide. They tested an alloy containing 5.25% C, 1.5% Cr, which translates into 80 vol% iron carbide and 20 vol % ferrite or austenite. Samples were obtained from extruded powders that produced average ferrite grain sizes of 2 to 3 μm and average iron carbide grain sizes of 3 to 4 μm. There was almost no grain growth evident during deformation. Elongations and strain rate sensitivity values are given in Table 2 . At a strain rate of 1 x 10^{-4} sec^{-1} a maximum elongation of 610% was seen.

T (°C)	m	$\dot{\epsilon}$ (s^{-1})	Elongation (%)
725	0.62	0.0005	52
725	0.61	0.0001	100
800	0.60	0.0002	150
900	0.62	0.0015	130
900	0.62	0.0005	180**
950	0.68	0.0009	200**
1000*	0.72	0.0009	250
1000*	0.72	0.0002	310
1000*	0.72	0.0001	400

*Obtained from strain-rate-change tests in tension.

**Tested in air.

Table 2 Elongation-to-failure results (tested in forming gas).

3.2.3 Segregation Stabilized

The iron alloys that make up segregation stabilized alloys include, C-Mn steels, microduplex stainless steels that are essentially free of carbon and medium carbon low alloy steels. The fine grained microstructure essential for superplastic materials is obtained by either thermal cycling or by conventional hot and cold rolling. These alloys generally consist of approximately equal volume fractions of ferrite and austenite at the deformation temperature. Alloy additions preferentially segregate either phase, hence the term segregation stabilized. Various alloys used to accomplish this include chromium, titanium and molybdenum (ferrite stabilizers), and nickel, manganese and nitrogen (austenite stabilizers).

3.3 Ductile Cast Iron

3.3.1 General

Little research has been completed thus far to determine if ductile cast iron can be made superplastic. Much of the work that has been completed was done by Tanaka and Ikawa.[16-18] Before their work is discussed, some of the results on the workability of ductile cast iron is presented.

3.3.2 Workability

Otoguro et al[19] examined the properties of hot-rolled ductile cast iron. They found that satisfactory plates of hot-rolled cast iron could be produced at a reduction ratio of 50 to 60% per heat between 850 to 1000°C. For the optimum results, the cast iron should possess a carbon and silicon content that is as low as possible, while graphite spheroidization should be higher than 90%. Keeping these two

factors in mind, they found that the best rolling temperatures were between 950 and 1050°C. It was discovered that a fully ferritized structure would enable the hot-rolled specimen to undergo a considerable amount of bending.

Zhang and Bennett[20] also found that the optimum temperature range for hot rolling was 950 to 1050°C. They achieved 84 to 93% reduction of area at 950°C in more than 10 passes. In somewhat of a contrast to the findings of Otoguro et al, Zhang and Bennett found that lower carbon, manganese and aluminum contents and higher silicon contents would improve the amount of reduction produced by hot rolling.

3.3.3 Superplastic Ductile Cast Iron

In 1974 Tanaka and Ikawa tested three ductile cast irons with compositions shown in Table 3. They refined the microstructures by up-quenching in an aluminum bath. Strain rate sensitivity for the three castings are seen in Figure 8 which represents flow stress vs. strain rate. The highest strain rate sensitivity is seen to be 0.5 at 748°C for the M15 casting. Elongations varied between 10 and 100% for the three alloys. This is small when compared with most superplastic alloys which exhibit elongations of many hundred percent. They discovered that void formation on either sides of the spheroidal graphite caused this occurrence of premature failure. Higher levels of manganese seem to increase strain rate sensitivity values.

	C	Si	Mn	P	S	Mg
M 03	3.35	1.82	0.28	0.023	0.008	0.044
M 10	3.08	1.84	0.92	0.024	0.009	0.036
M 15	3.20	1.95	1.42	0.022	0.009	0.049

Table 3 Chemical Compositions of Specimens (wt%)

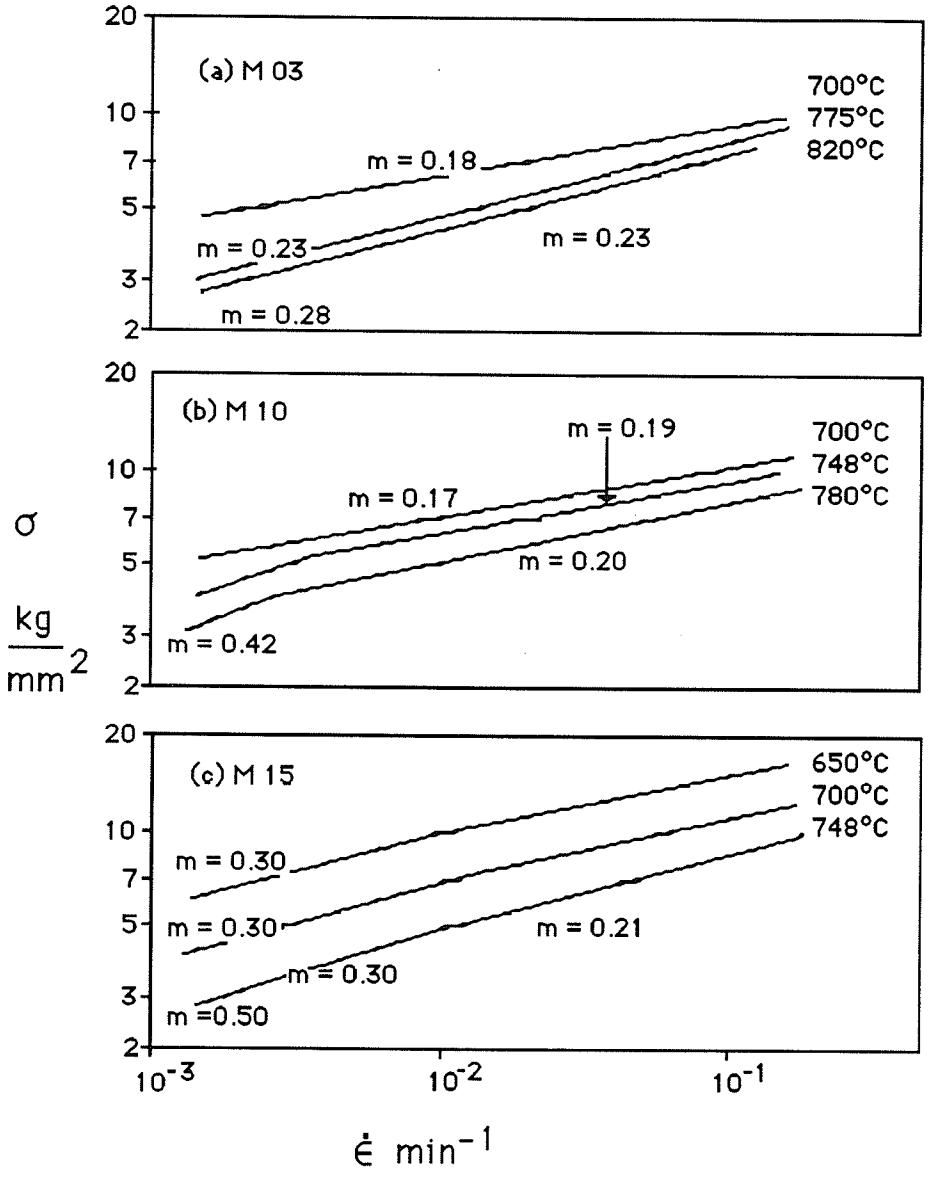

Figure 8 Logarithmic Plot of Flow Stress versus Strain Rate.

In 1976, Tanaka and Ikawa studied transformation superplasticity in ductile cast iron. They deformed samples of low

carbon ductile cast iron with two different structures, one pearlitic the other ferritic. They ran constant load tests between 700 and 850°C and back to 700°C at a temperature cycling rate of 5°C/min. Similar tests were run between 500 and 950°C at a cycling rate of 225°C/min. Strain rate sensitivity values were as high as 0.8 and uniform elongations greater than 200% during the repeated thermal cycling. Flow stress vs. strain rate is seen in Figure 9. They found that larger deformations occurred during the heating portion than during the cooling portion of the cycle. Furthermore the pearlitic iron was seen to deform more than the ferritic iron. They proposed that the plasticity was incurred by excess vacancies during volume changes throughout the cycle. They found that voids formed on either side of the spheroidal graphite, but unlike in their earlier work these voids filled up successively with matrix structure.

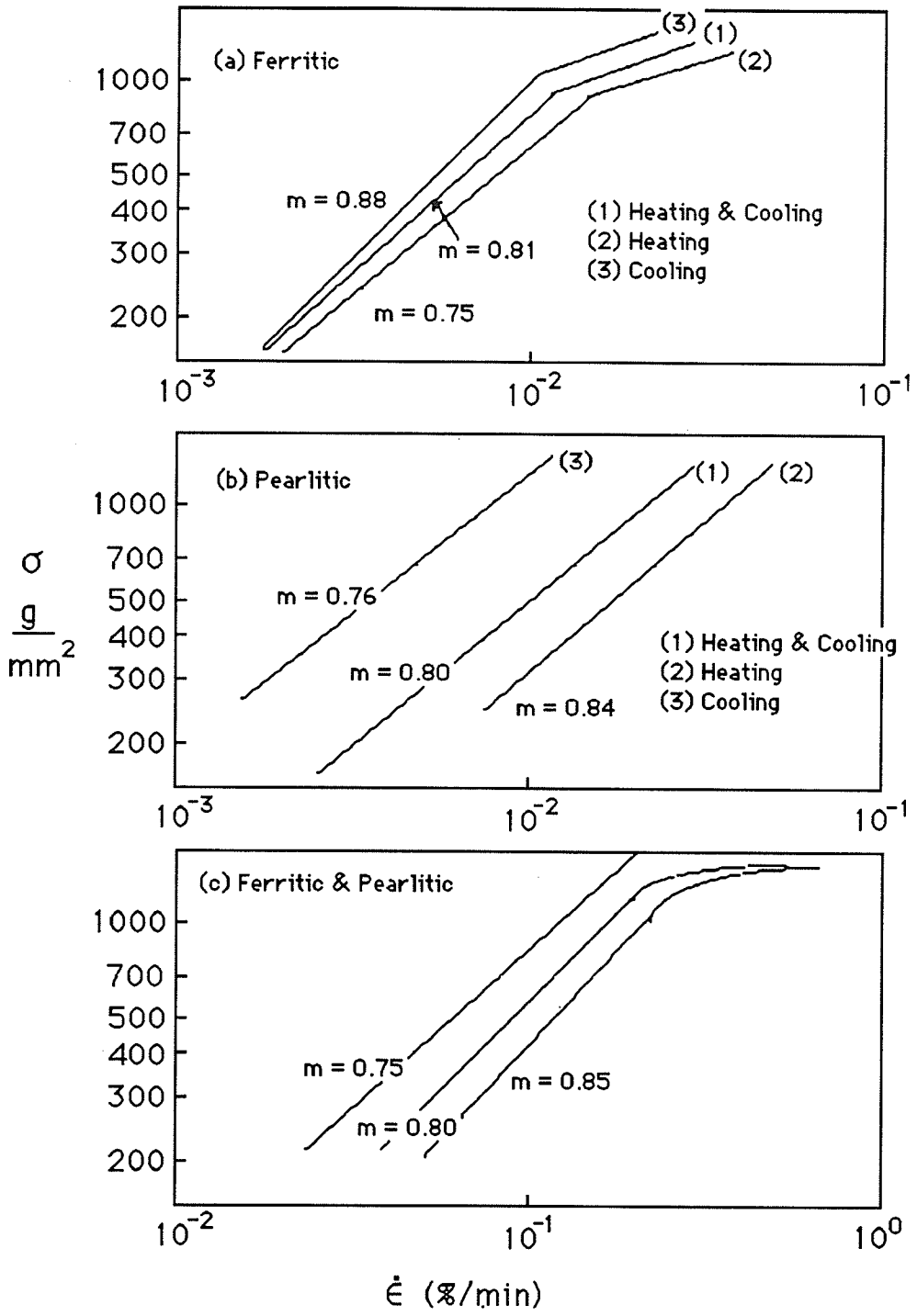

Figure 9 Logarithmic Plot of Flow Stress versus Strain Rate

In 1977, Tanaka and Ikawa presented their findings on grain refinement of ductile cast iron. They found that a fine duplex ferritic and pearlitic matrix structure with a grain size of 4 to 6 μm was

possible by thermal treatment. Copper or nickel additions were necessary to make this structure homogeneous throughout.

Chijiiwa and Hayashi[21-22] completed a study on the mechanical properties of ductile cast iron over a wide range of temperatures (room temperature to liquidus). They ran tension tests at strain rates between 10^{-4} to 10^{-1} sec^{-1} over this entire range of temperatures. They found that elongations generally increased as the temperature increased except for brittle behavior at 180°C, 400°C, throughout the eutectoid transformation temperature range, 1000°C and above 1120°C. Flow stress versus strain rate is seen in Figure 10 over the range of temperatures between 870 to 1110°C.

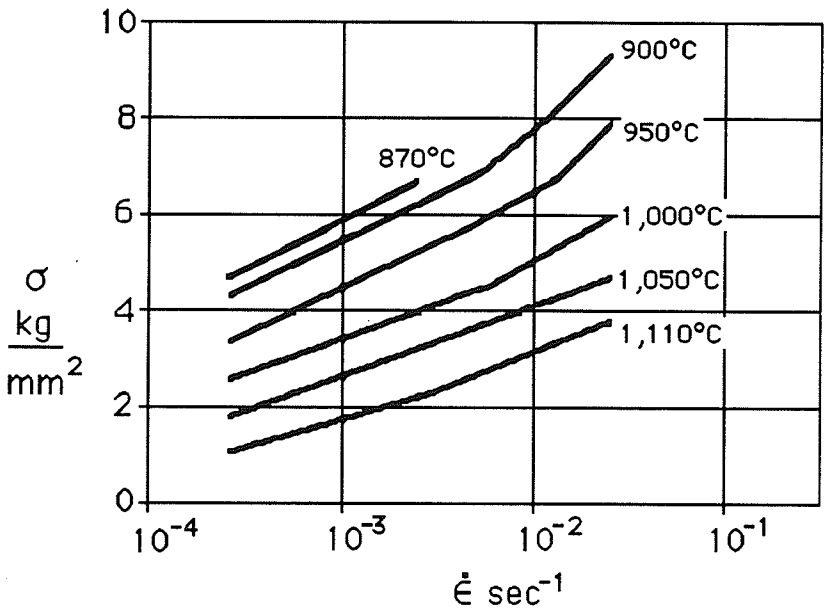

Figure 10 Logarithmic Plot of Flow Stress versus Strain Rate

4 EXPERIMENTAL

4.1 Castings

Castings used for this work were made from commercial ductile iron acquired from Ancast Industries Ltd. These castings were Ductile 65 y-blocks which Ancast uses extensively for mechanical testing of their iron in order to determine some of the qualitative parameters necessary for their daily production.

A quantitative elemental analysis of these Ductile 65 y-blocks is shown in Table 4.

ELEMENT	WEIGHT PERCENTAGE
CARBON	3.35 - 3.65
SILICON	2.40 - 2.70
MAGNESIUM	0.040 - 0.065
MANGANESE	0.45 MAXIMUM
PHOSPHORUS	0.02 MAXIMUM
CHROMIUM	0.018 } SHOULD BE
VANADIUM	0.018 } KEPT TO A
SULFUR	0.018 } MINIMUM

Table 4 Compositional makeup of ductile 65 y blocks used in this thesis.

4.2 Machining

The castings were turned down to the appropriate size and shape (in preparation for swaging, compression testing, or tensile testing) on a Southbend lathe, ensuring that there was not excessive heat generation.

4.3 Swaging

Specimens for compression testing were first hot swaged at 850°C from 0.5 inches in diameter down to 0.2 inches in diameter.

Specimens for tensile testing were first hot swaged at 850°C from 0.625 inches in diameter down to 0.4 inches in diameter. These specimens were subsequently machined down to the appropriate size for tension (1.1 cm gauge length and 5.0 mm gauge diameter).

Each rod of ductile cast iron was brought to temperature (850°C) swaged down to the next size and returned to the furnace for 5 minute intervals to ensure homogeneity of temperature for the next pass. The rods were air cooled after swaging was complete. All swaged specimens were annealed at 1000°C for 1 hour prior to further testing.

As received specimens were not swaged but machined down to the appropriate size and shape.

Further swaging was performed on two bars of ductile cast iron in an attempt to break up and refine the microstructure. The first bar was hot swaged at 934°C from a diameter of 0.560 inches down to 0.322 inches. This sample was allowed to air cool whereupon it was cold swaged at room temperature from 0.322 inches down to 0.200 inches. The sample was finally annealed at 1000°C for 1 hour in the hopes that recrystallization would occur. The second sample was also hot swaged at 934°C but it was only swaged down to 0.448 inches in diameter. At this point it was allowed to cool and was consequently cold swaged at room temperature from 0.448 inches down to 0.258 inches in diameter. This sample was also annealed at 1000°C for 1 hour.

4.4 Compression Tests

Compression testing was carried out on an Instron testing machine. The specimens (swaged and as received) were mounted individually in a sealed chamber, exposed to a steady flow of argon and brought to the desired test temperature. Five test temperatures were used: 750°C, 800°C, 850°C, 900°C and 950°C. Temperature steady state was reached anywhere from 1/2 hour to 1 hour after the chamber was enclosed by the furnace. Upon attaining steady state, strain rate change compression tests were carried out at various increments of strain rate between $1X10^{-6}$ sec^{-1} to $2X10^{-3}$ sec^{-1}. The experiments were monitored by a computer which recorded load via the load cell, deformation via the Direct Current Differential Transformer (DCDT) and time. After the completion of each experiment the specimens were allowed to cool in the chamber upon removal of the furnace.

4.5 Tensile Tests

Tensile tests (swaged and as received) were performed in a similar manner to the compression tests on a comparable screw driven Instron machine. The notable differences were, strain rate change tensile tests were performed at 800°C, 850°C, 900°C and 950°C, and the strain rate increments varied between $1X10^{-5}$ sec^{-1} to $2X10^{-3}$ sec^{-1}.

Constant strain rate tensile tests were also performed in a similar manner. Each test was conducted at an individual constant

strain rate at a constant temperature for the duration of the experiment (either $5X10^{-5}$, $1X10^{-4}$, $5X10^{-4}$ or $1X10^{-3}$ sec^{-1}).

All tension samples were approximately 0.5 cm in diameter with a 2.0 cm gauge length.

4.6 Metallography

Selected as received samples (untested), swaged samples (untested), compression samples (swaged and as received), tension samples (swaged and as received) were cut, mounted, polished and etched using appropriate metallographic techniques. An abrasive cutoff saw and a slow speed saw were used for cutting, while polishing was completed on a 1 micron diamond abrasive wheel. Etching was carried out using 2% nital (2 percent nitric acid in ethanol).

Grain size measurement was not performed since the high temperature microstructure was very difficult to etch properly to reveal grain boundaries. It was also not done because it was determined that other evidence obtained through experimental results was sufficient to explain and theorize how the ductile cast iron reacted to the testing.

4.7 Hardness Testing

Hardness tests were performed using a Leitz Microhardness Tester to determine the hardness of the graphite, the pearlite and the ferrite present in the matrix.

5 RESULTS

5.1 Swaging

All swaged specimens used for compression and tension testing were relatively free of surface cracks. This was not the case for the specimens hot swaged and subsequently cold swaged at room temperature however. These samples exhibited severe cracking, even complete torsional fracture and failure. This was seen to occur only on the final pass down to 0.200 inches in diameter for the first sample. The second sample demonstrated severe cracking in several places on the second last pass and complete failure during the final pass down to 0.258 inches in diameter.

5.2 Compression Tests

A summary of compression tests performed along with strain rate sensitivity results derived from these tests are seen in Tables 5 and 6. Typical differential strain rate change, true stress versus true plastic strain curves for as received and swaged material compressed at constant temperatures between 750°C and 950°C are shown in Figures 11 through 22. A similar curve for swaged material tested at 950°C was unavailable as the data was not properly monitored by the computer. The following sample calculations demonstrate the method that was used to determine strain rate sensitivity values in compression.

Swaged sample 1) tested in compression at 800°C. Strain rate sensitivity values are calculated from the load versus time curve using equation 2:

$$m = \frac{\ln \frac{P_2}{P_1}}{\ln \frac{\varepsilon_2}{\varepsilon_1}} \quad \text{.....(2)}$$

where P_2 and P_1 are the extrapolated loads from the load versus time curve corresponding to ε_2 and ε_1 which are the strain rates.

{1} Strain rate change from 1 x 10^{-5} to 2 x 10^{-5}:

P_2 = 26 Kg and P_1 = 23 Kg

$$m = \frac{\ln \frac{26}{23}}{\ln 2} = 0.177$$

{2} Strain rate change from 2 x 10^{-5} to 1 x 10^{-4}:

P_2 = 40 Kg and P_1 = 26 Kg

$$m = \frac{\ln \frac{46}{30}}{\ln 5} = 0.266$$

{3} Strain rate change from 1 x 10^{-4} to 2 x 10^{-4}:

P_2 = 57 Kg and P_1 = 48 Kg

$$m = \frac{\ln \frac{57}{48}}{\ln 2} = 0.248$$

{4} Strain rate change from 2 x 10^{-4} to 4 x 10^{-4}:

P_2 = 67.5 Kg and P_1 = 59 Kg

$$m = \frac{\ln \frac{67.5}{59}}{\ln 2} = 0.194$$

{5} Strain rate change from 4 x 10^{-4} to 2 x 10^{-3}:

P_2 = 89 Kg and P_1 = 68 Kg

$$m = \frac{\ln \frac{89}{68}}{\ln 2} = 0.167$$

Optical micrographs of select specimens are shown in Figures 23, 24, 25 and 26.

Table 5 Summary of swaged material compression tests along with calculated strain rate sensitivity values.

$\dot{\epsilon}$ by increment	1×10^{-5} to 2×10^{-5}	5×10^{-5} to 1×10^{-4}	2×10^{-5} to 1×10^{-4}	1×10^{-4} to 2×10^{-4}	2×10^{-4} to 4×10^{-4}	2×10^{-4} to 5×10^{-4}	2×10^{-4} to 1×10^{-3}	4×10^{-4} to 1×10^{-3}	5×10^{-4} to 1×10^{-3}	4×10^{-4} to 2×10^{-3}	1×10^{-3} to 2×10^{-3}
Test Temperature											
750°C 1)		0.151		0.188		0.091			0.068		
2)*	0.073		0.102	0.120			0.167				
3)*	0.077		0.046								
800°C 1)*	0.177		0.266	0.248	0.194					0.167	
2)*	0.102		0.161	0.154			0.167				0.128
850°C 1)	0.170		0.263	0.173							
2)*	0.170		0.195	0.196	0.174			0.143			
3)*	0.275		0.247	0.161			0.148				
900°C 1)*			0.196	0.217			0.172				
2)*	0.152		0.217	0.202			0.139				0.161
3)	0.138		0.225	0.188							
950°C 1)*	0.233		0.128								
2)*			0.271	0.238			0.209				0.172

*Strain rate sensitivity values extracted from load time curves. All other values extracted from true stress versus true plastic strain curves.

$\dot{\epsilon}$ by increment	1×10^{-5} to 2×10^{-5}	2×10^{-5} to 1×10^{-4}	1×10^{-4} to 2×10^{-4}	2×10^{-4} to 1×10^{-3}	1×10^{-3} to 2×10^{-3}
Test Temperature					
750°C 1)	0.113	0.169	0.185		
800°C 1)			0.138	0.120	
2)	0.103	0.173	0.217	0.157	0.147
850°C 1)	0.290	0.193			0.246
2)	0.194	0.184		0.112	
3)*	0.129	0.202	0.164	0.149	
900°C 1)*	0.073	0.201	0.148	0.107	
2)	0.189	0.195	0.269		
950°C 1)*	0.129	0.167	0.138		
2)	0.135	0.178	0.197	0.179	

*Strain rate sensitivity values extracted from load time curves. All other values extracted from true stress versus true plastic strain curves.

Table 6 Summary of as received material compression tests with calculated strain rate sensitivity values.

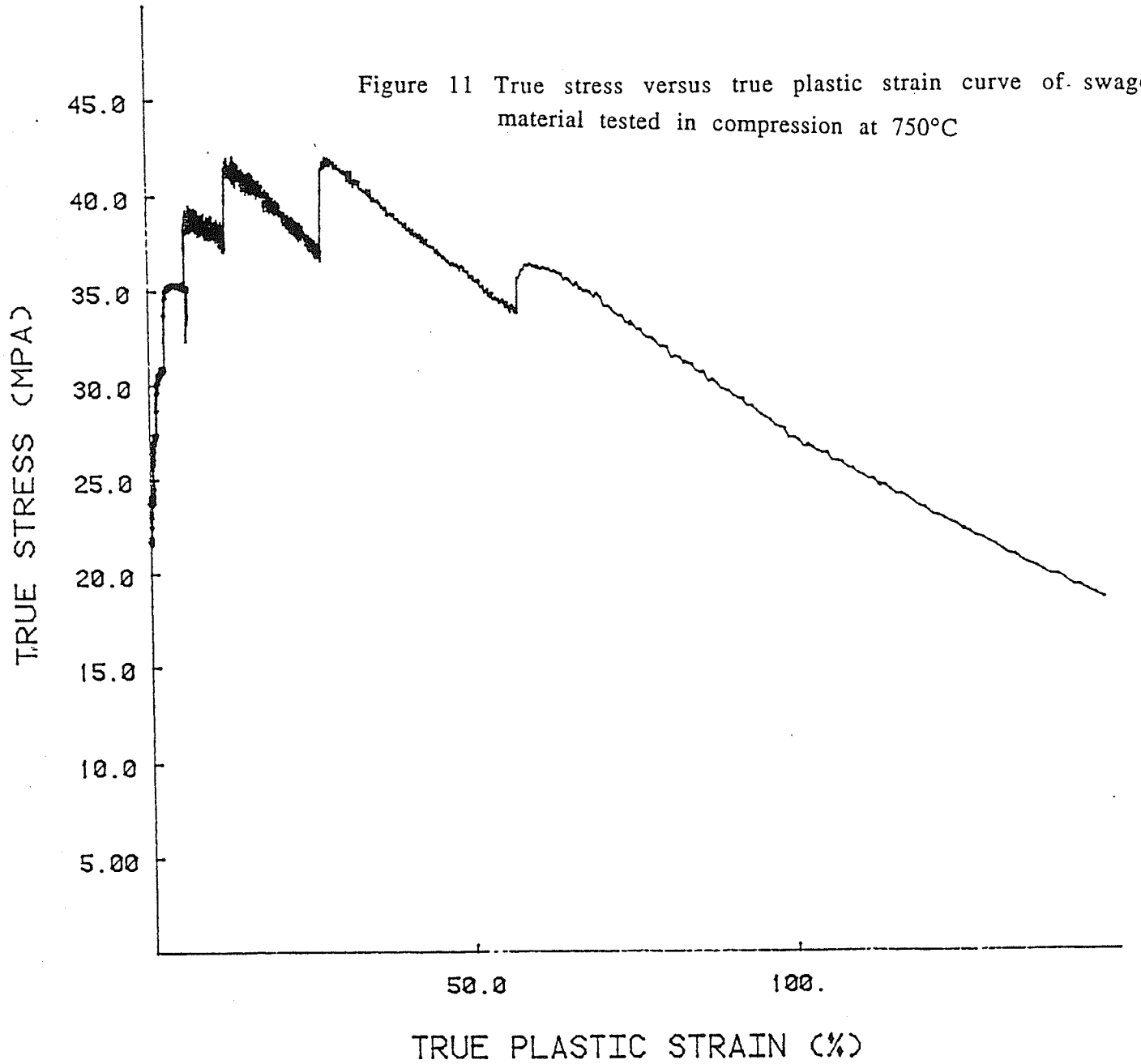

Figure 11 True stress versus true plastic strain curve of swaged material tested in compression at 750°C

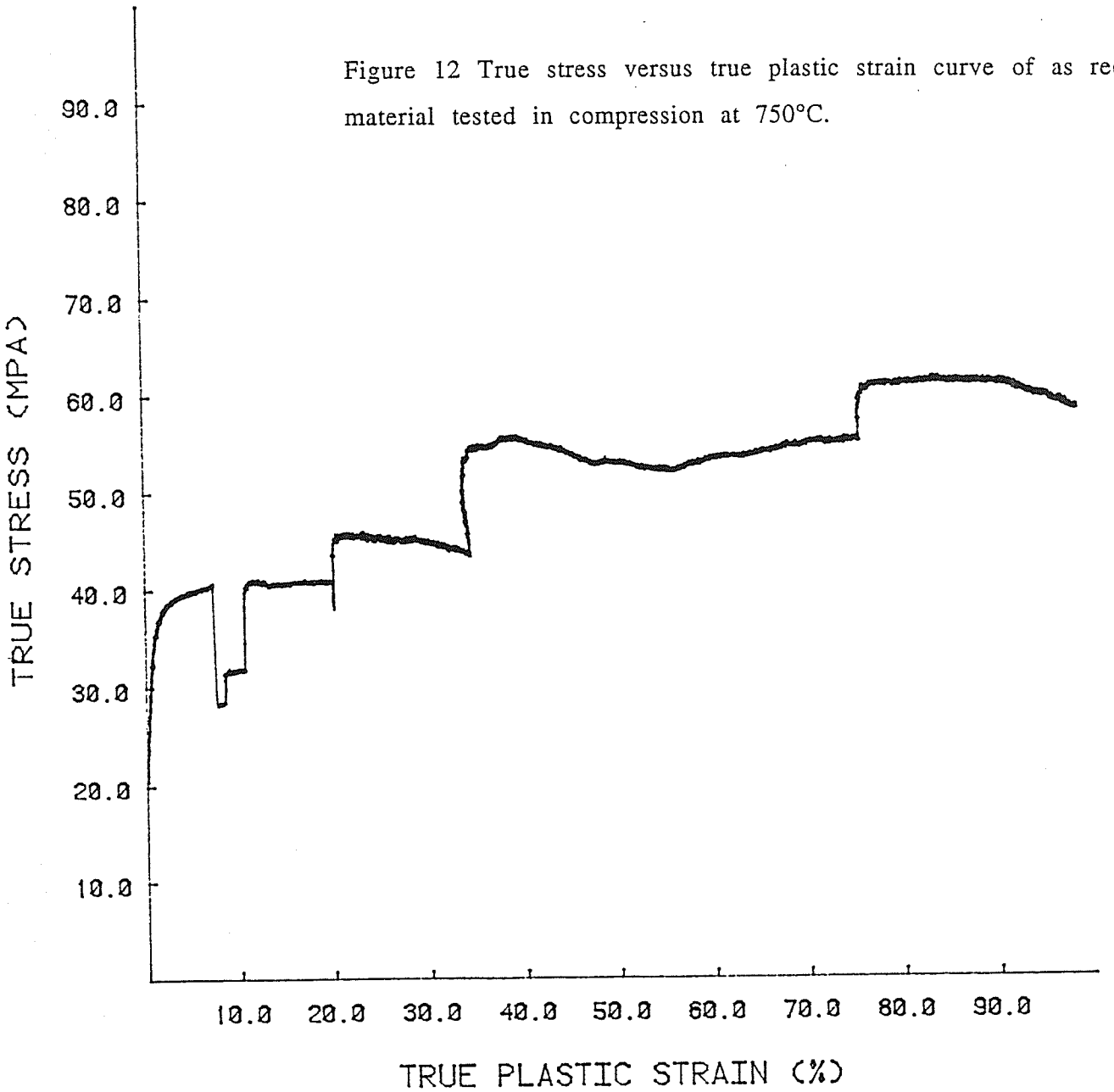

Figure 12 True stress versus true plastic strain curve of as received material tested in compression at 750°C.

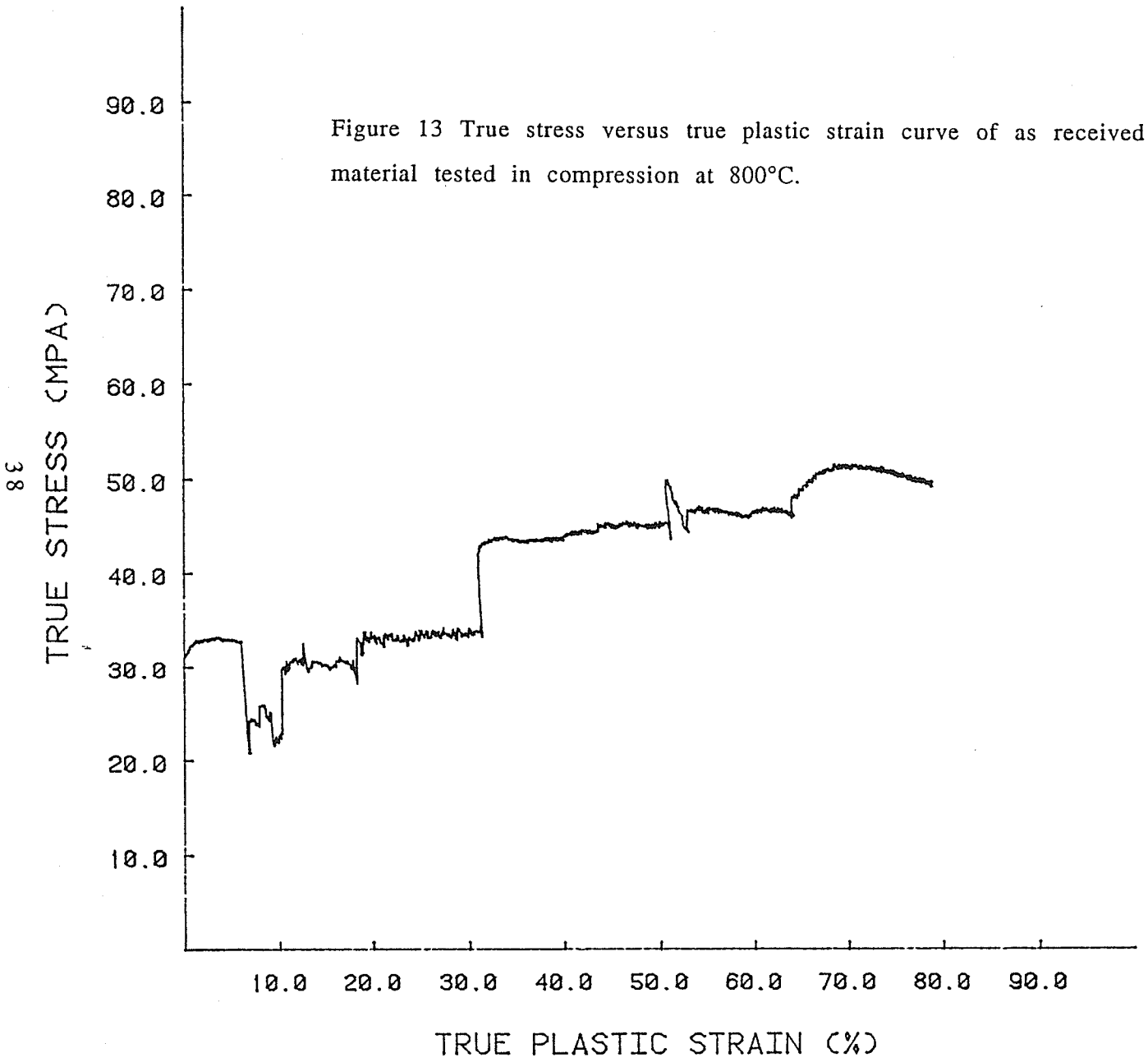

Figure 13 True stress versus true plastic strain curve of as received material tested in compression at 800°C.

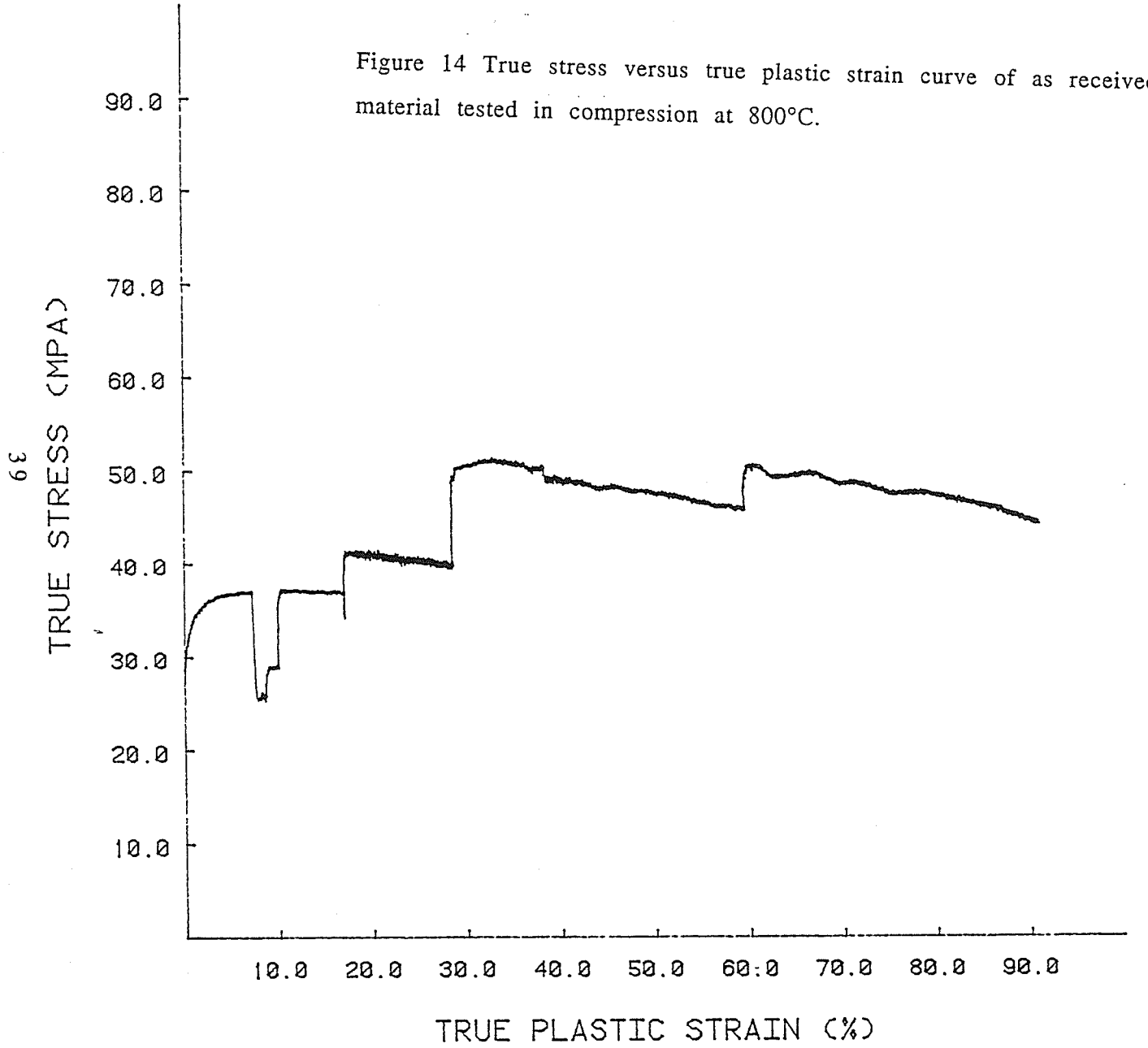

Figure 14 True stress versus true plastic strain curve of as received material tested in compression at 800°C.

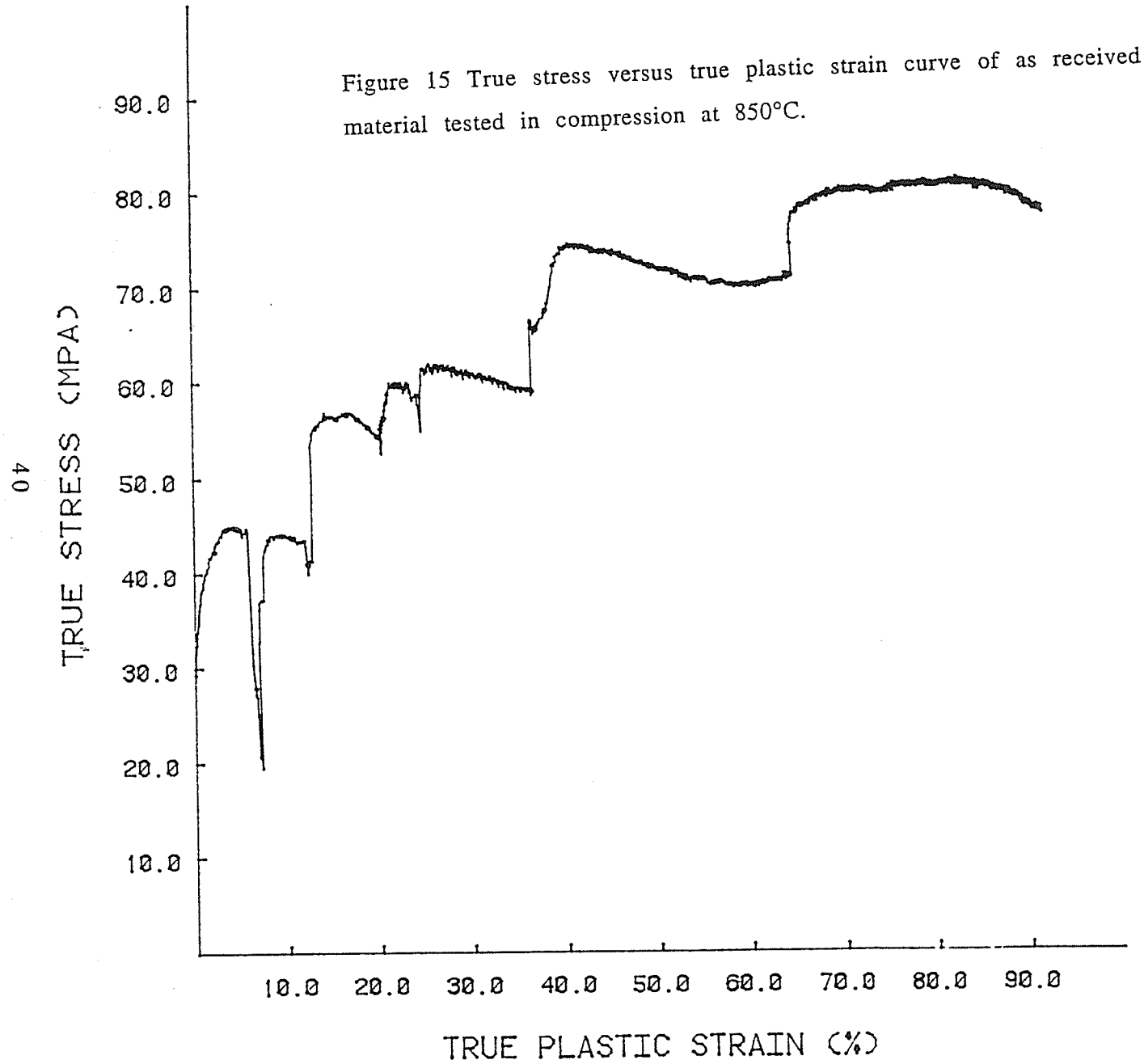

Figure 15 True stress versus true plastic strain curve of as received material tested in compression at 850°C.

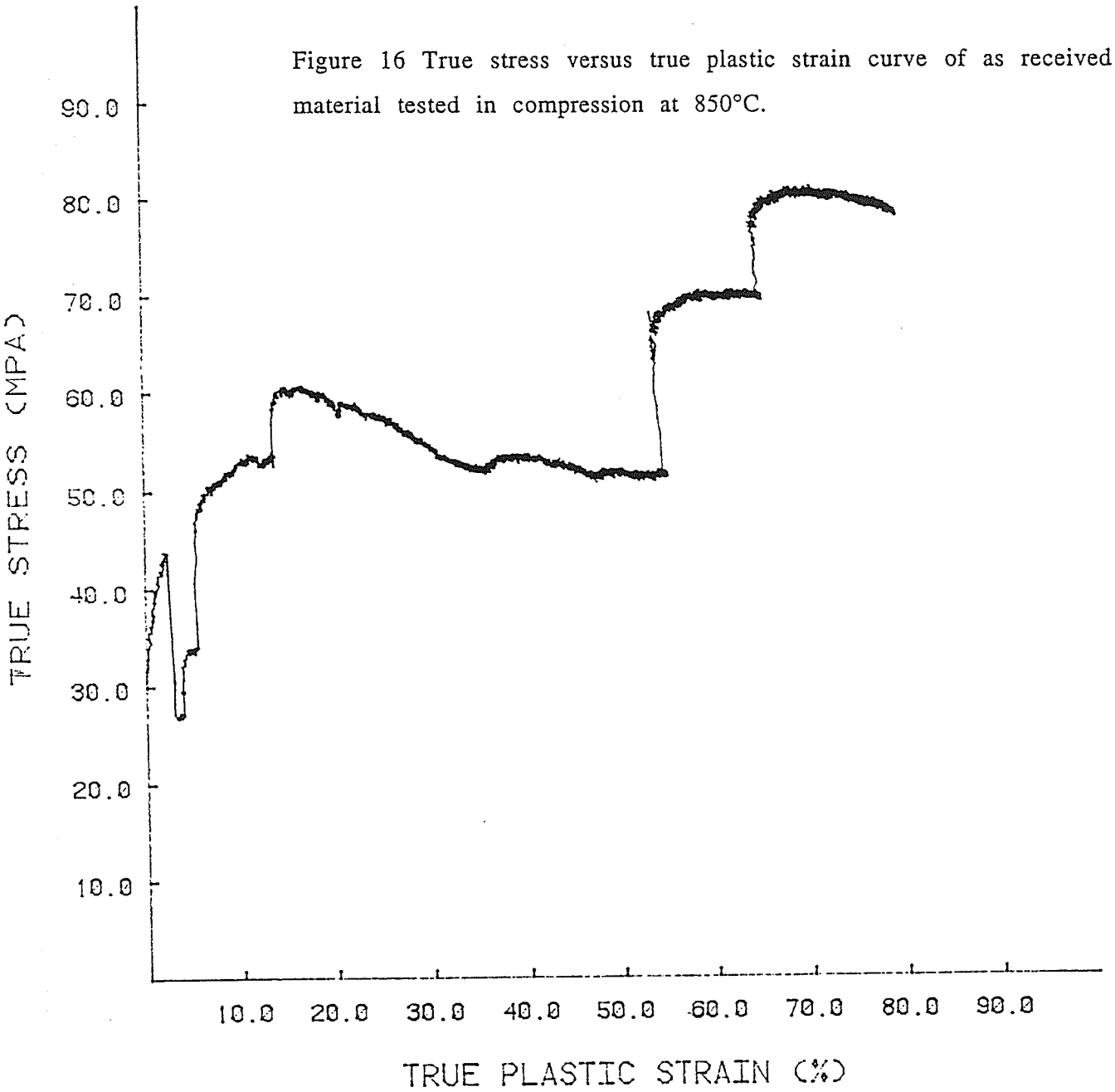

Figure 16 True stress versus true plastic strain curve of as received material tested in compression at 850°C.

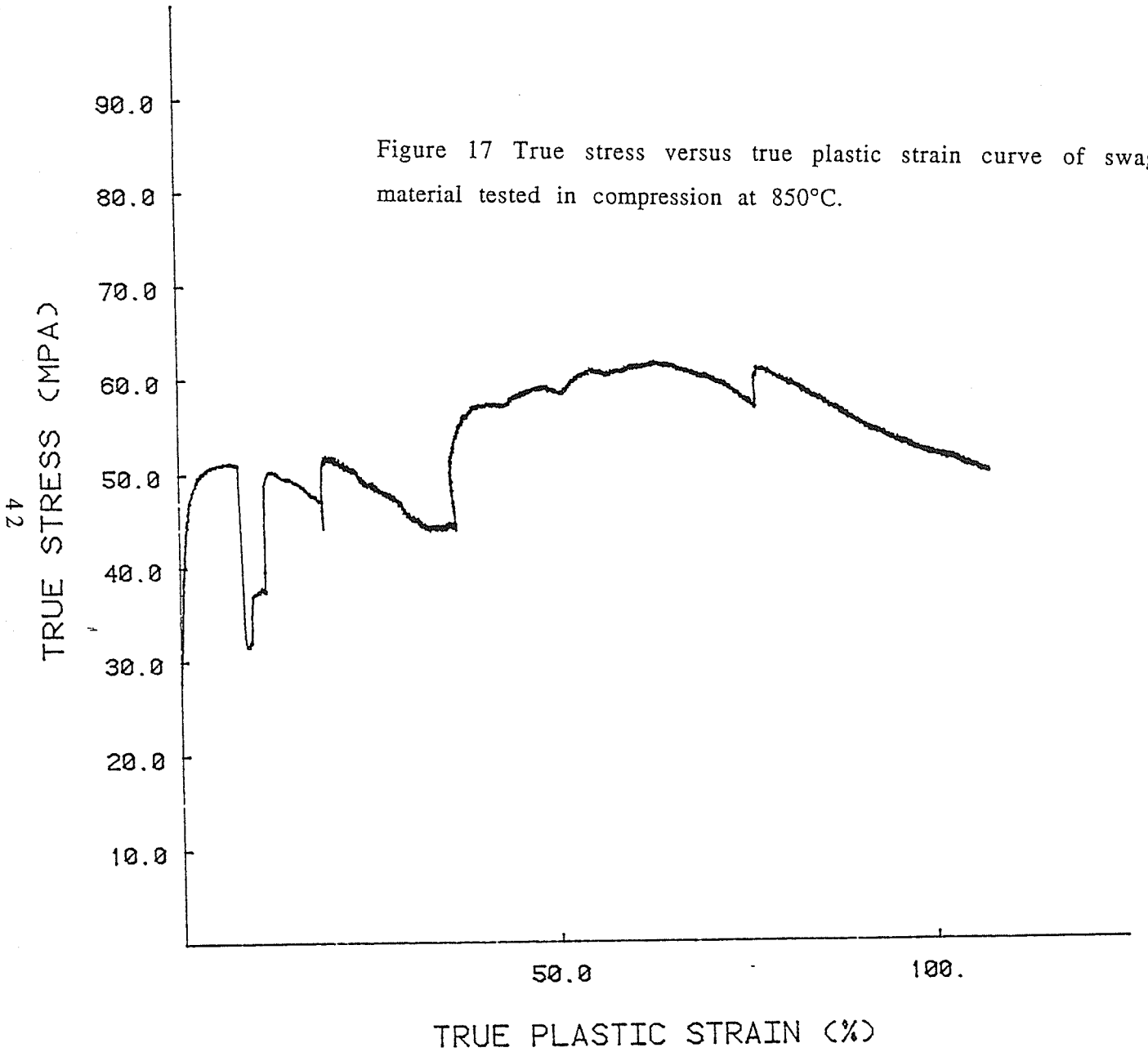

Figure 17 True stress versus true plastic strain curve of swaged material tested in compression at 850°C.

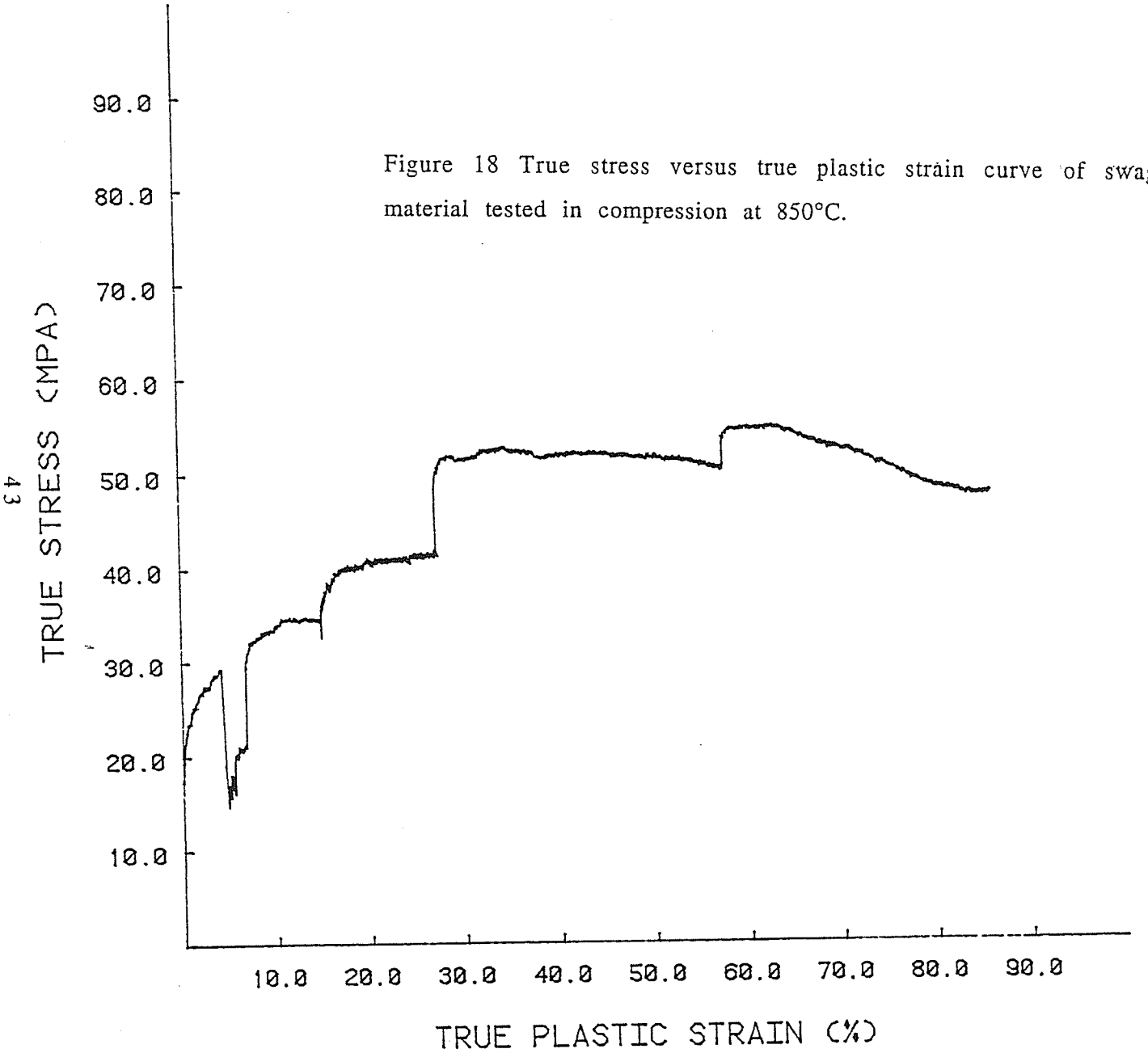

Figure 18 True stress versus true plastic strain curve of swaged material tested in compression at 850°C.

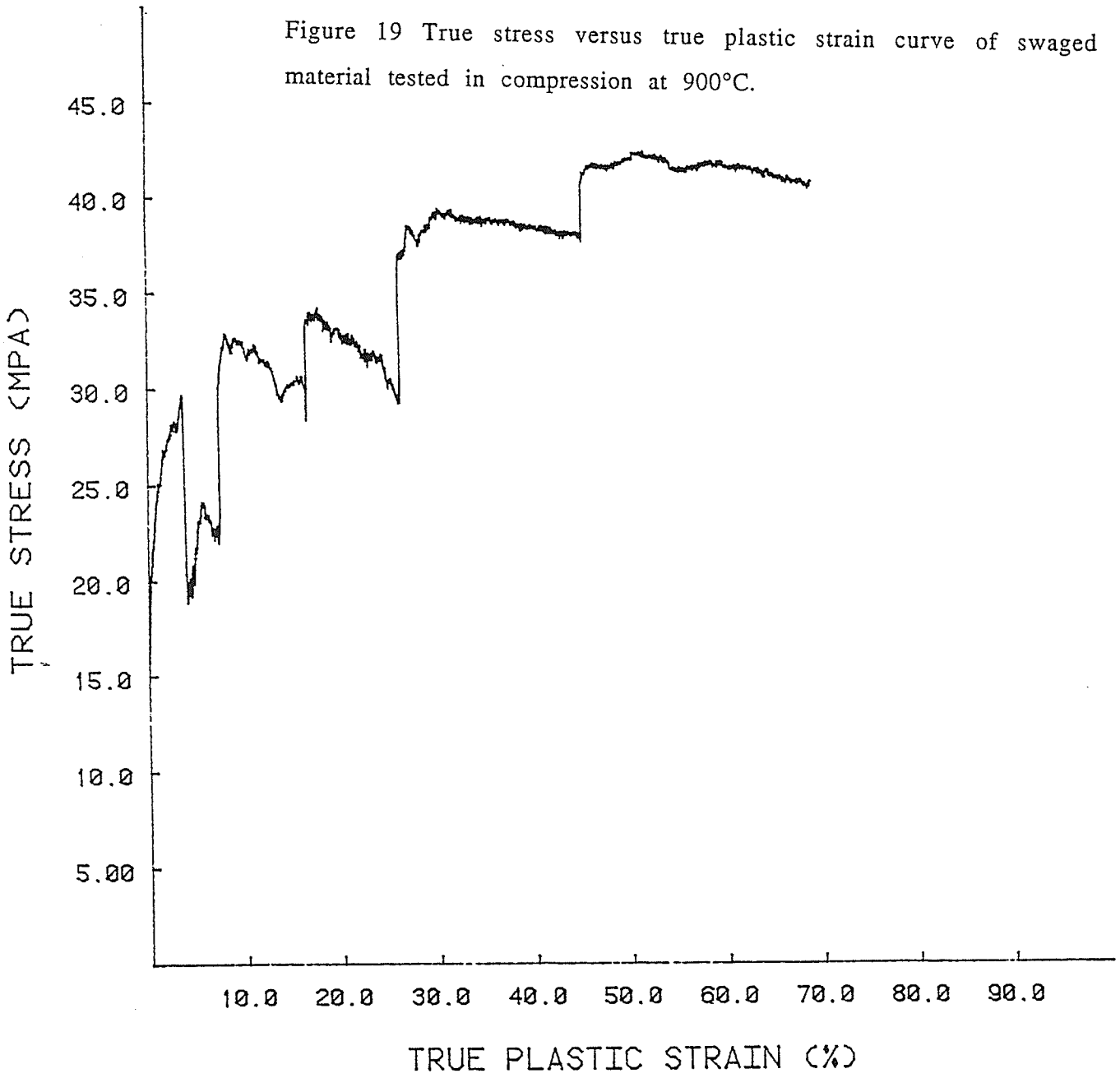

Figure 19 True stress versus true plastic strain curve of swaged material tested in compression at 900°C.

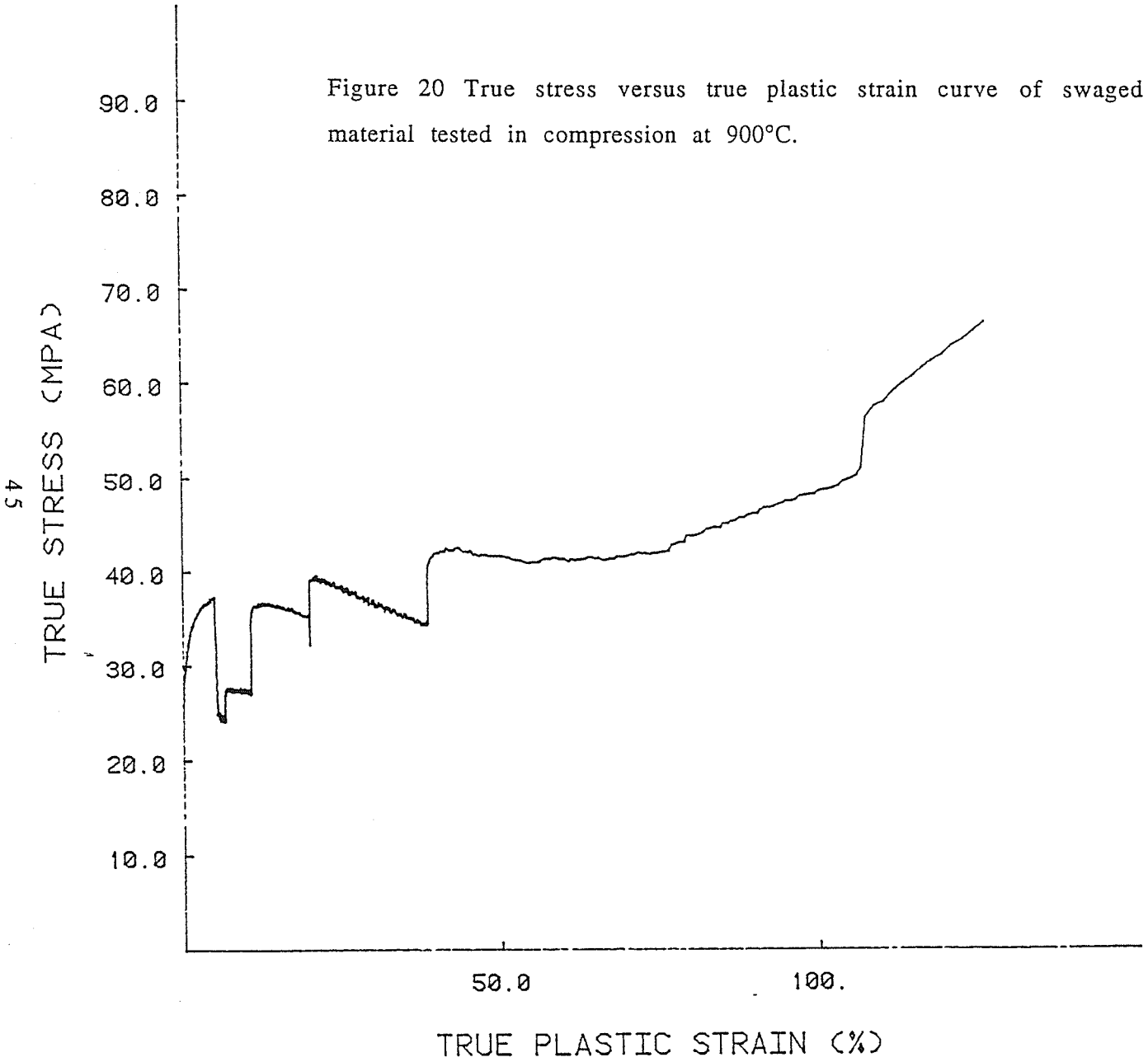

Figure 20 True stress versus true plastic strain curve of swaged material tested in compression at 900°C.

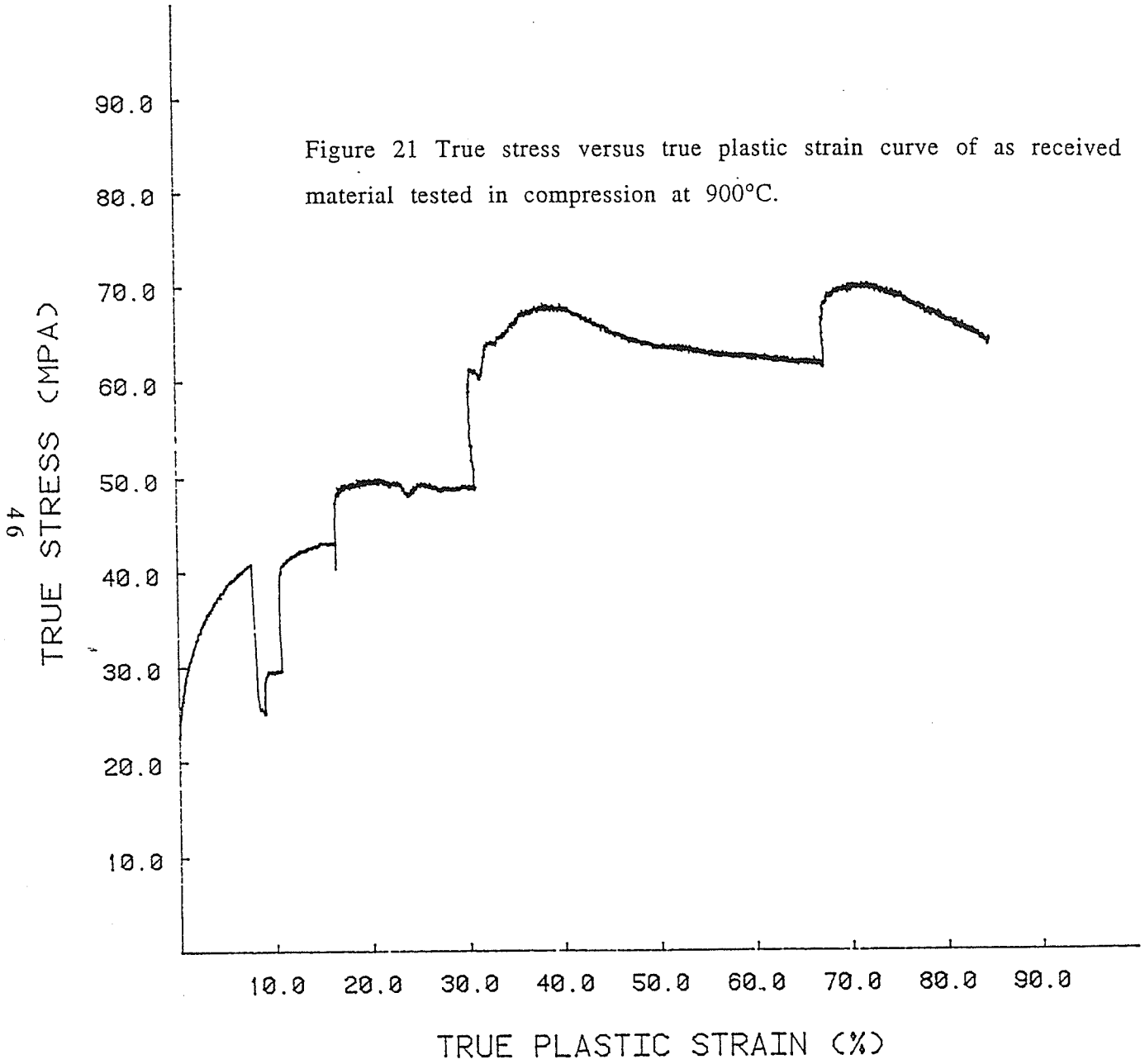

Figure 21 True stress versus true plastic strain curve of as received material tested in compression at 900°C.

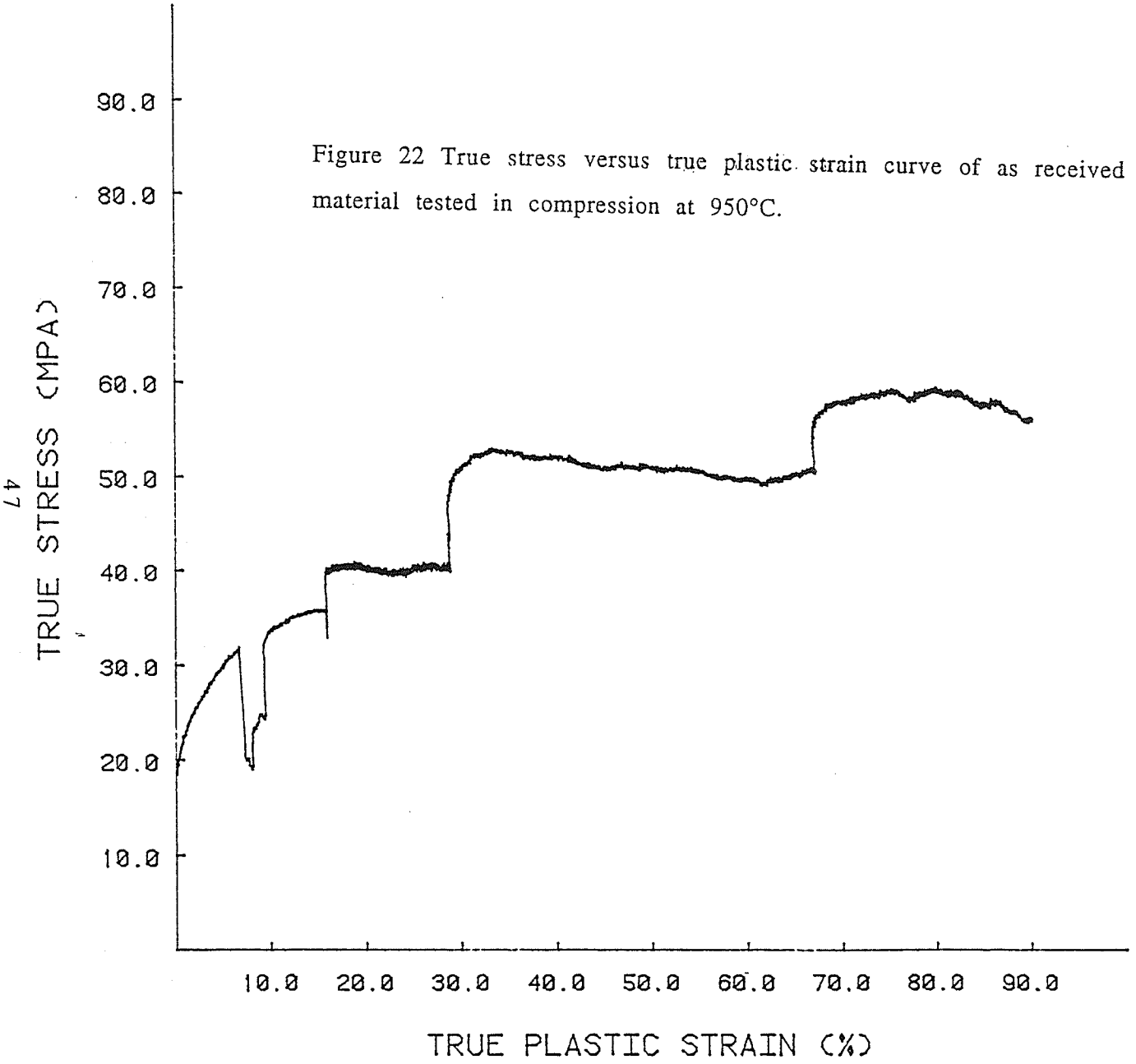

Figure 22 True stress versus true plastic strain curve of as received material tested in compression at 950°C.

Figure 23 Optical micrograph of a longitudinal section of as received material tested in compression at 750°C. 210X, etchant 2% nital.

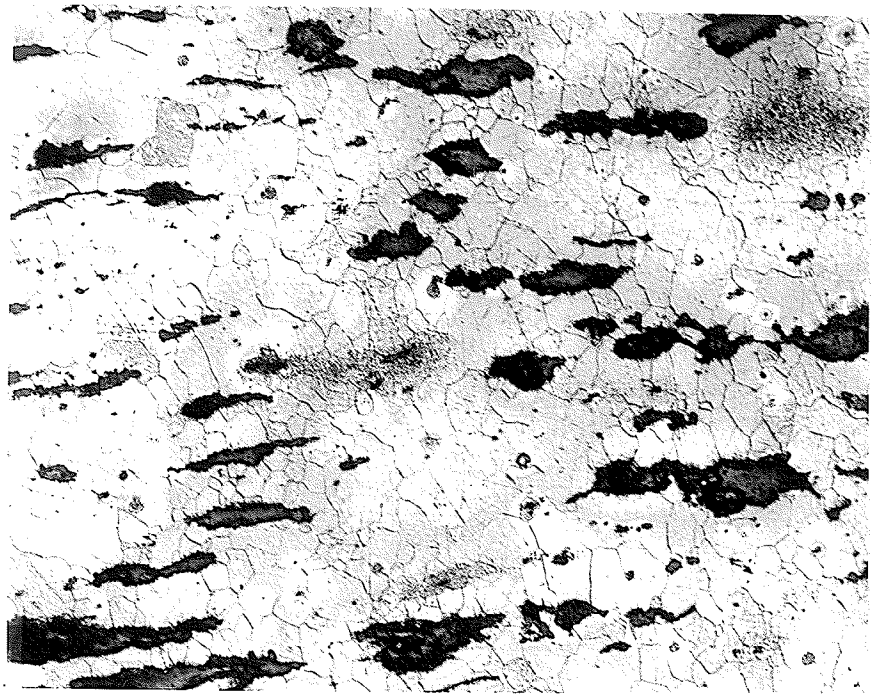

Figure 24 Optical micrograph of a longitudinal section of swaged material tested in compression at 750°C. 210X, etchant 2% nital.

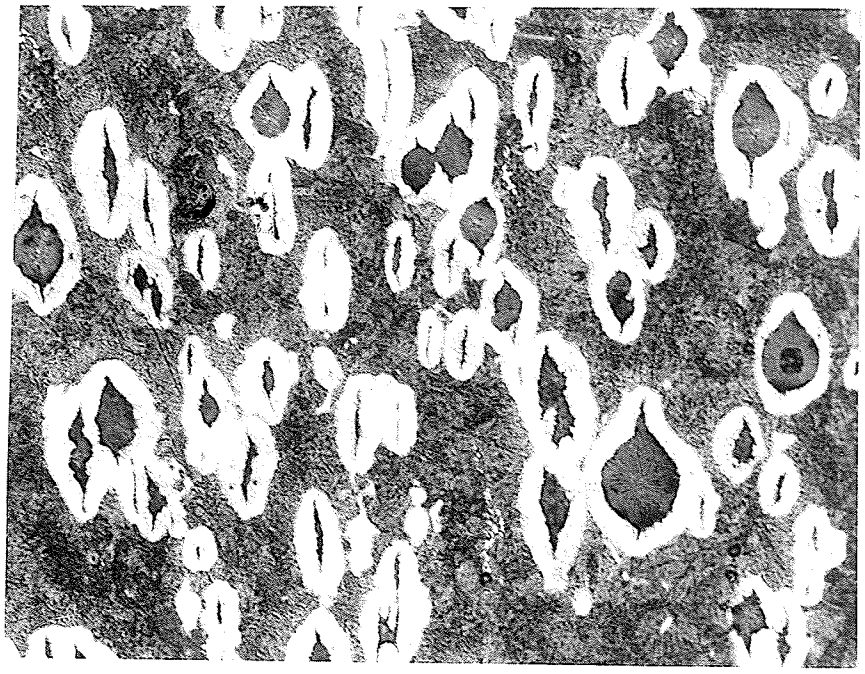

Figure 25 Optical micrograph of a longitudinal section of as received material tested in compression at 950°C. 210X, etchant 2% nital.

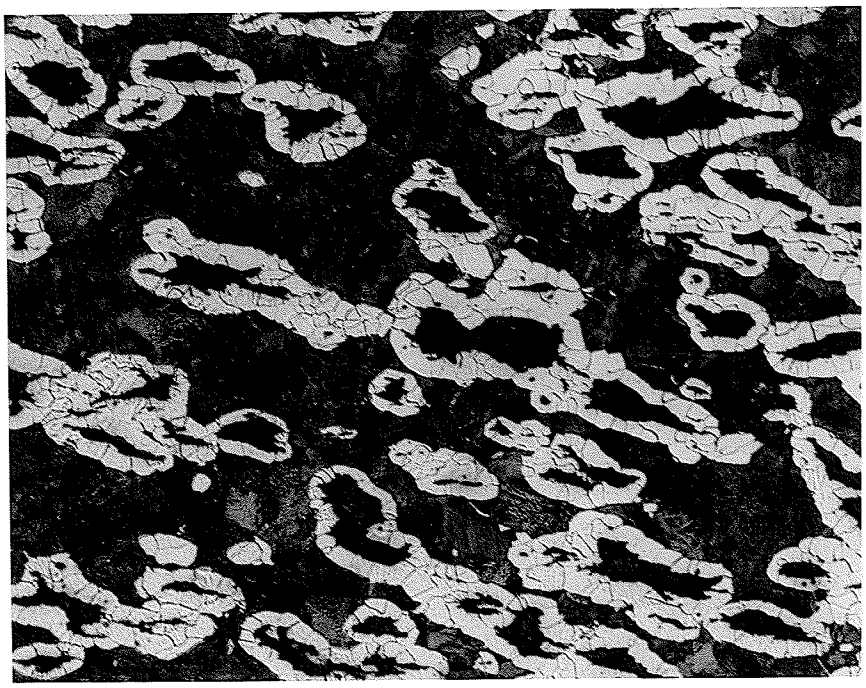

Figure 26 Optical micrograph of a longitudinal section of swaged material tested in compression at 950°C. 210X, etchant 2% nital.

5.3 Tension Tests

A summary of differential strain rate tension tests performed and strain rate sensitivity values derived from these tests are seen in Table 7. Elongation to failure values are shown in Tables 8 and 9. Representative constant strain rate tension test, true stress versus true plastic strain curves are seen in Figures 27 through 37. From the constant strain rate tension tests performed, logarithmic plots of the ultimate tensile flow stress versus strain rate were derived for each test temperature. These are shown in Figures 38, 39, 40 and 41. Differential strain rate change tension tests, true stress versus true plastic strain curves, are seen in Figures 42 through 47 for both swaged and as received material. Derived from these differential strain rate curves are plots of strain rate sensitivity versus strain rate in Figures 48 to 51. The following sample calculations demonstrate the method that was used to determine strain rate sensitivity values in tension.

As received sample 1) tested in tension at 850°C. Strain rate sensitivity values are calculated from the true flow stress versus true plastic strain curve using equation 3:

$$m = \frac{\ln\frac{\sigma_2}{\sigma_1}}{\ln\frac{\varepsilon_2}{\varepsilon_1}} \qquad \text{.....(3)}$$

where σ_2 and σ_1 are the extrapolated true flow stresses from the true stress versus true plastic strain curve corresponding to ε_2 and ε_1 which are the strain rates.

{1} Strain rate change from 5 x 10^{-5} to 1 x 10^{-4}:

σ_2 = 39 Mpa and σ_1 = 30 Mpa

$$m = \ln\frac{39}{30} \Big/ \ln 2 = 0.379$$

{2} Strain rate change from 1 x 10^{-4} to 2 x10^{-4}:

σ_2 = 48.75 Mpa and σ_1 = 39 Mpa

$$m = \ln\frac{48.75}{39} \Big/ \ln 2 = 0.322$$

{3} Strain rate change from 2 x 10^{-4} to 1 x 10^{-3}:

σ_2 = 63.75 Mpa and σ_1 = 48.75 Mpa

$$m = \ln\frac{63.75}{48.75} \Big/ \ln 5 = 0.167$$

{4} Strain rate change from 1 x 10^{-3} to 2 x 10^{-3}:

σ_2 = 75 Mpa and σ_1 = 63.75 Mpa

$$m = \ln\frac{75}{63.75} \Big/ \ln 2 = 0.194$$

Optical micrographs of both swaged material and as received material tested at 800°C and 850°C respectively are shown in Figures 52 through 55.

$\dot{\epsilon}$ by increment	5×10^{-5} to 1×10^{-4}	1×10^{-4} to 2×10^{-4}	2×10^{-4} to 1×10^{-3}	1×10^{-3} to 2×10^{-3}	1×10^{-4} to 5×10^{-4}
Test Temperature					
800°C (A)	0.182	0.117	0.176	0.235	
(S)	0.215	0.317	0.201		
850°C (A)	0.379	0.322	0.167	0.235	
(S)	0.290	0.296	0.161	0.156	
900°C (A)	0.311	0.219	0.185	0.131	
(S)	0.306				0.174

Table 7 Summary of differential strain rate tension tests and calculated strain rate sensitivity values. (A) - As received material, (S) - Swaged material.

STRAIN RATE	TEST TEMPERATURE 800°C	850°C	900°C	950°C
1×10^{-4}	45% 106% (SWAGED)		40%	55%
2×10^{-4}		49%		
5×10^{-4}	55%		74%	
1×10^{-3}	48%	69%	75%	64%

Table 8 Elongation to failure results for constant strain rate tension tests. The majority of these tests were performed on as received material. Percent elongation values were extracted from engineering stress vs. engineering strain curves.

	TEST TEMPERATURE		
	800°C	850°C	900°C
SWAGED	74%	57%	52%
AS REC'D	68%	74%	

Table 9 Elongation to failure results for differential strain rate tension tests. Percent elongation values were extracted from engineering stress vs. engineering strain curves.

Figure 27 True stress versus true plastic strain curve of swaged material tested in tension at 800°C under a constant strain rate of 1 x 10^{-4}.

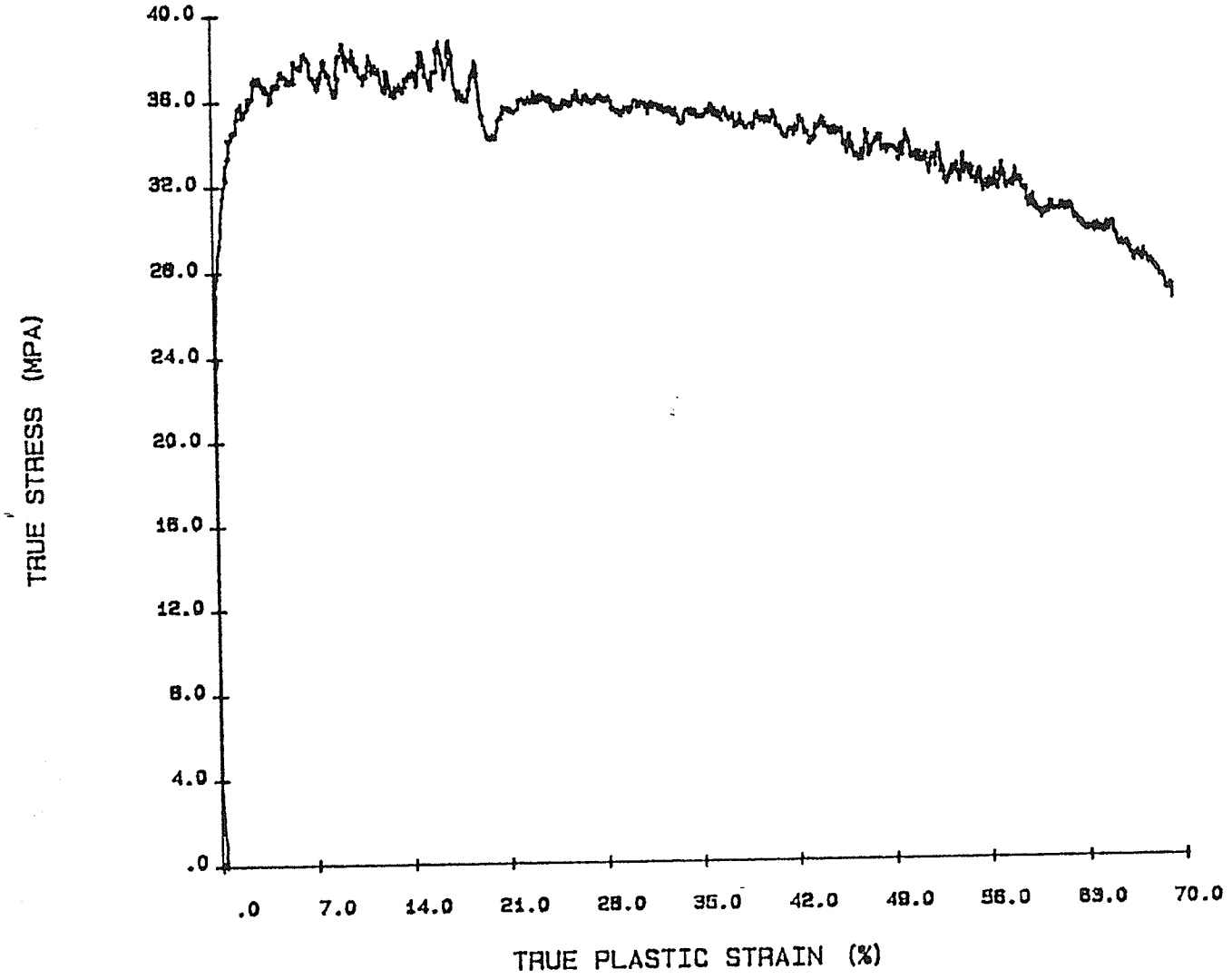

Figure 28 True stress versus true plastic strain curve of as received material tested in tension at 800°C under a constant strain rate of 1 x 10^{-4}.

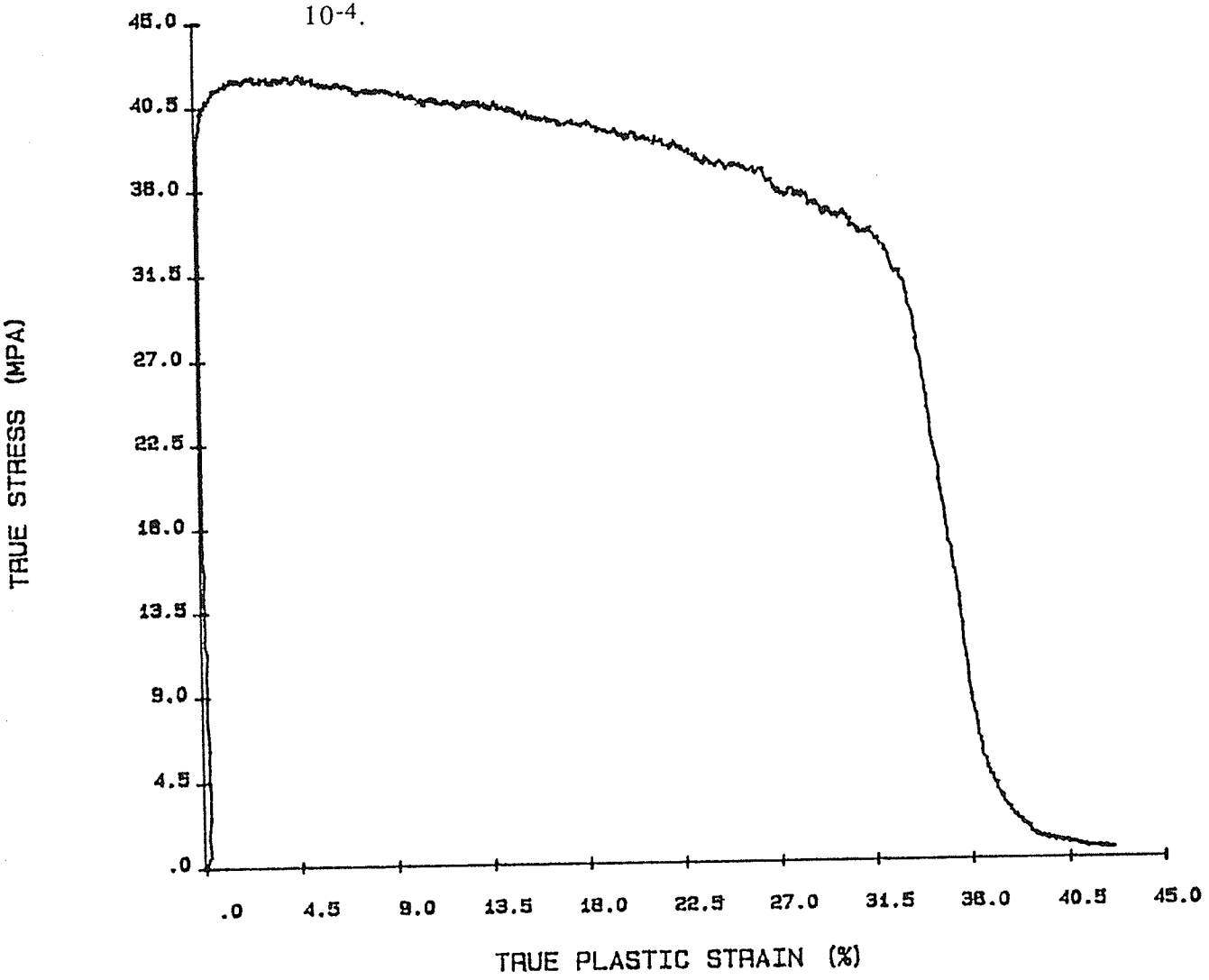

Figure 29 True stress versus true plastic strain curve of as received material tested in tension at 800°C under a constant strain rate of 5 x 10^{-4}.

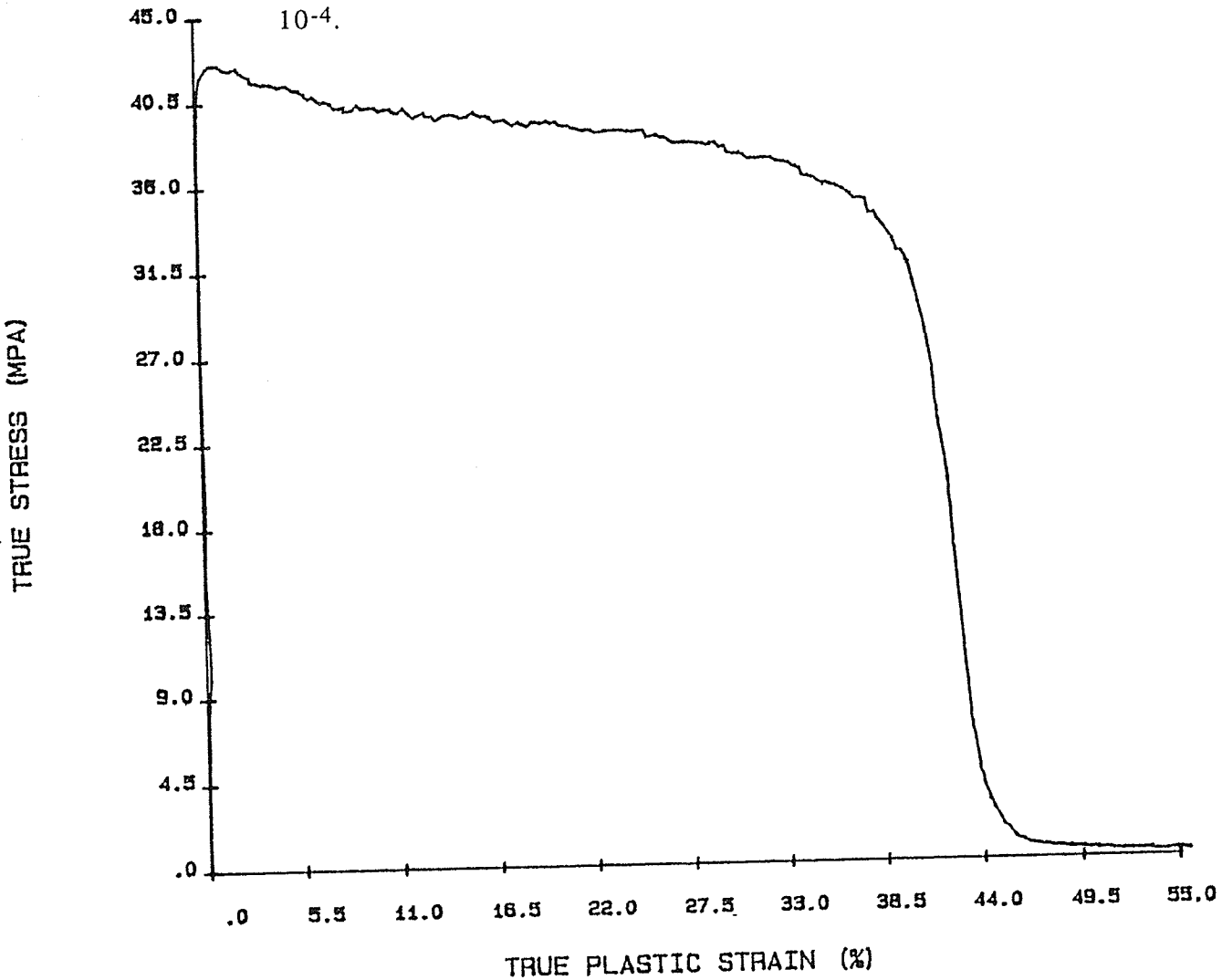

Figure 30 True stress versus true plastic strain curve of as received material tested in tension at 800°C under a constant strain rate of 1 x 10^{-3}.

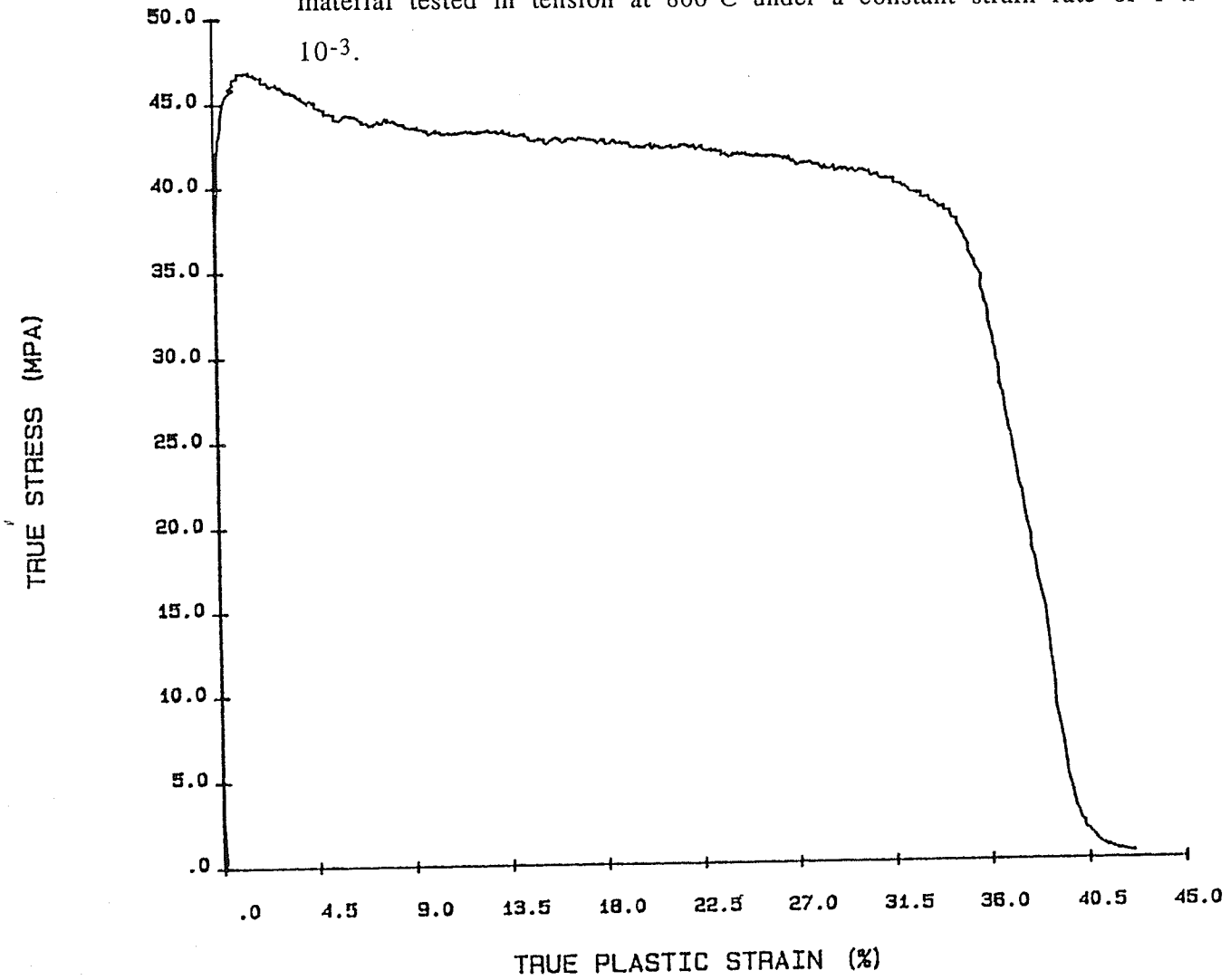

Figure 31 True stress versus true plastic strain curve of as received material tested in tension at 850°C under a constant strain rate of 5 x 10^{-4}.

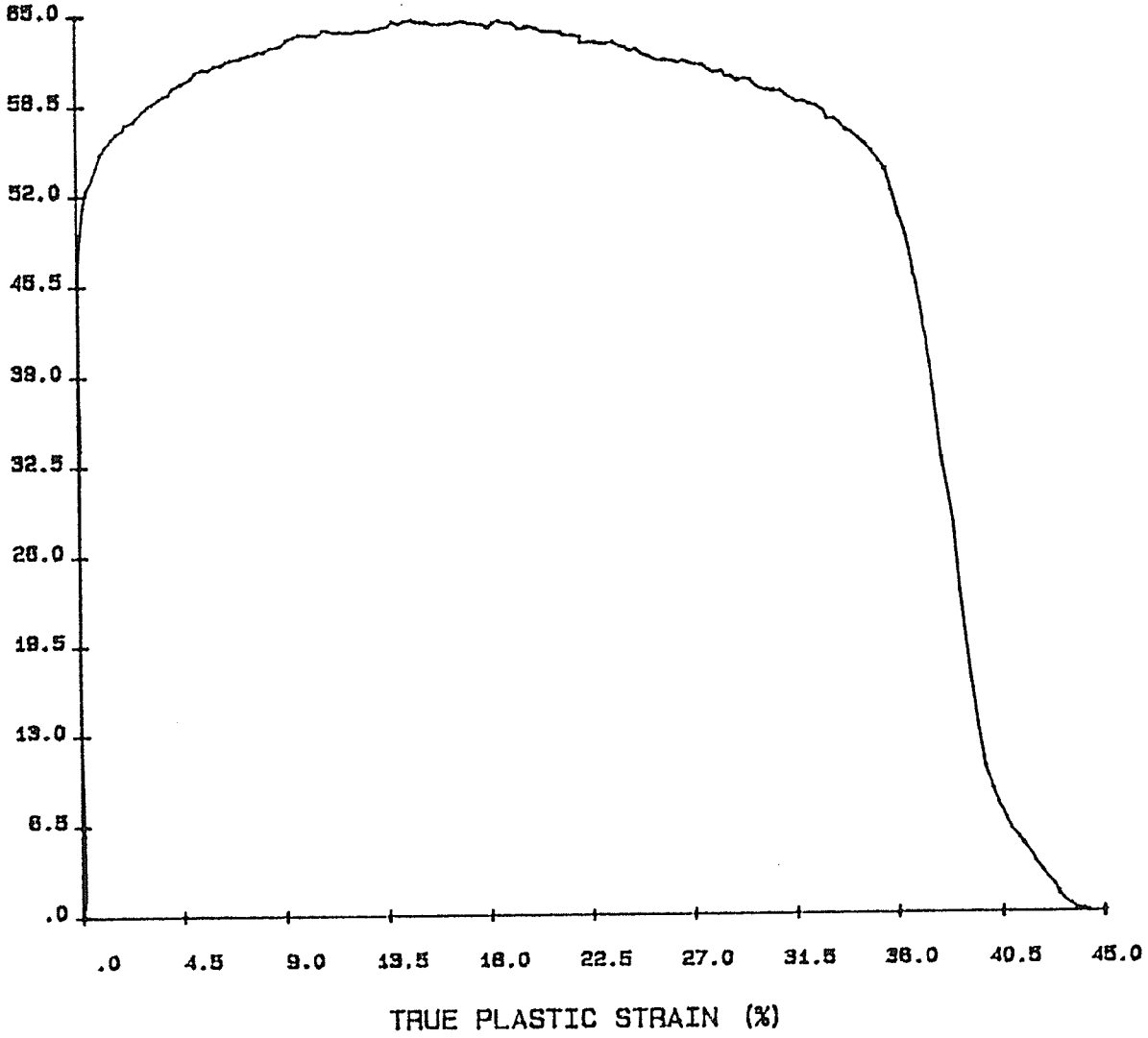

Figure 32 True stress versus true plastic strain curve of as received material tested in tension at 850°C under a constant strain rate of 1 x 10^{-3}.

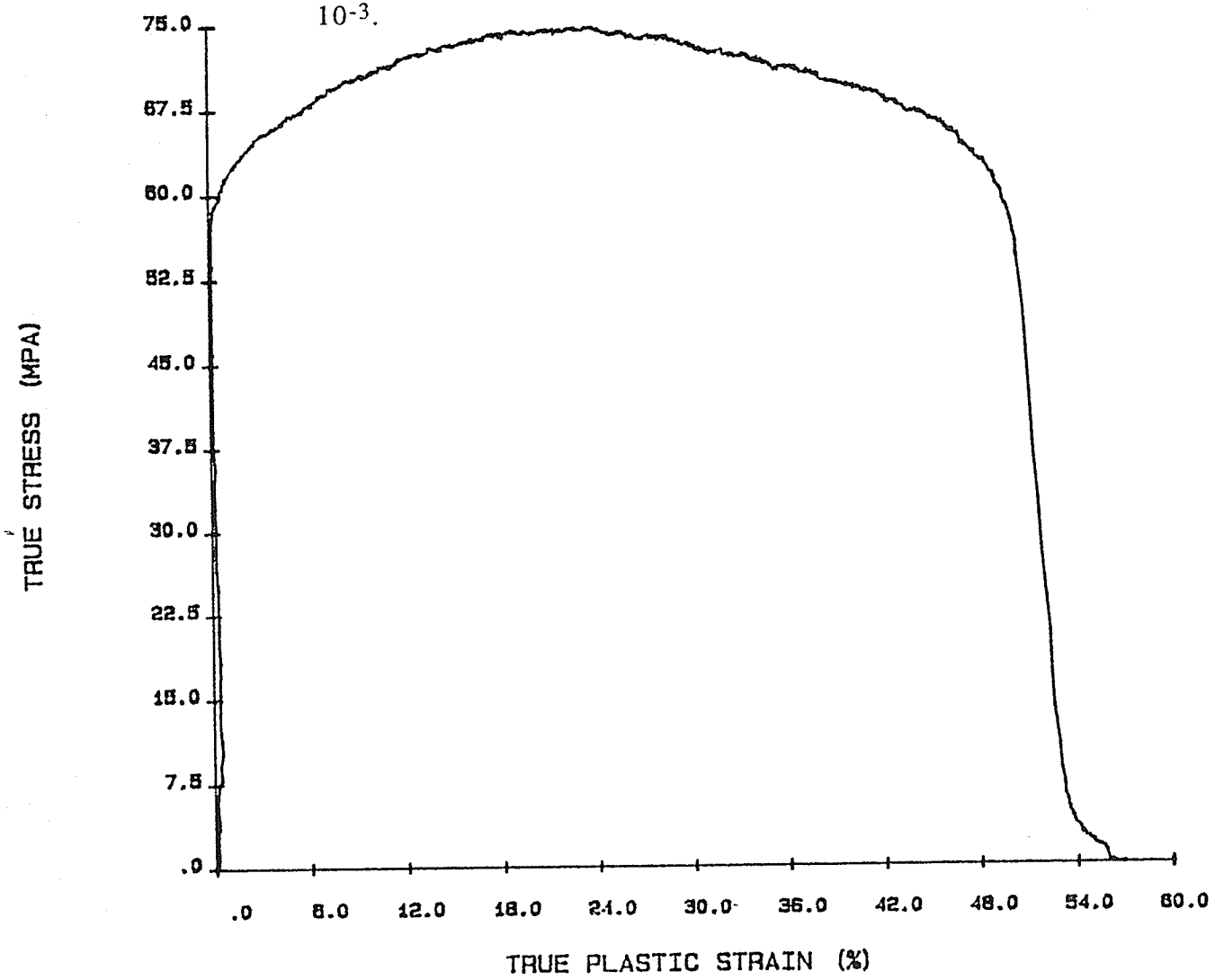

Figure 33 True stress versus true plastic strain curve of as received material tested in tension at 900°C under a constant strain rate of 1 x 10^{-4}.

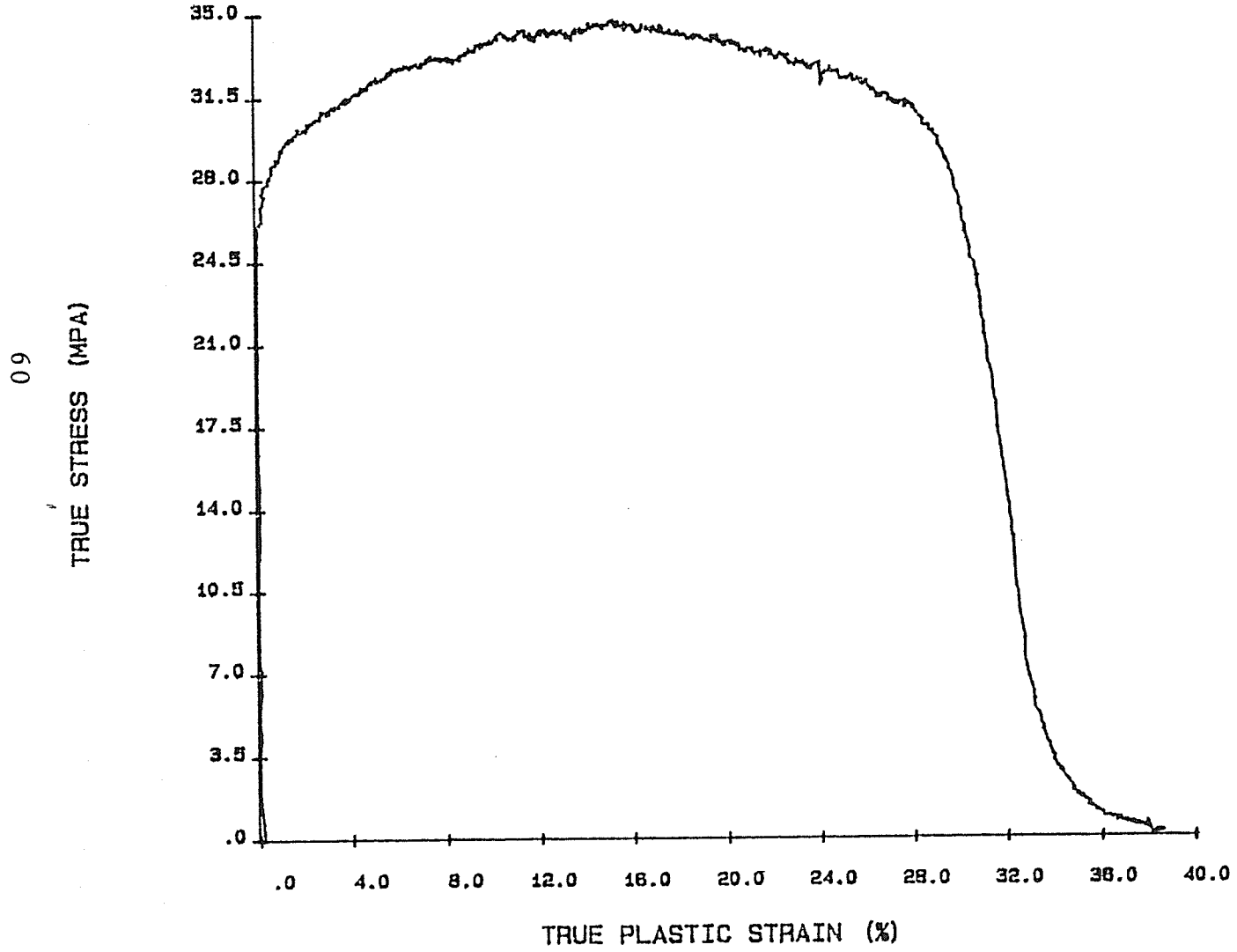

Figure 34 True stress versus true plastic strain curve of as received material tested in tension at 900°C under a constant strain rate of 5 x 10^{-4}.

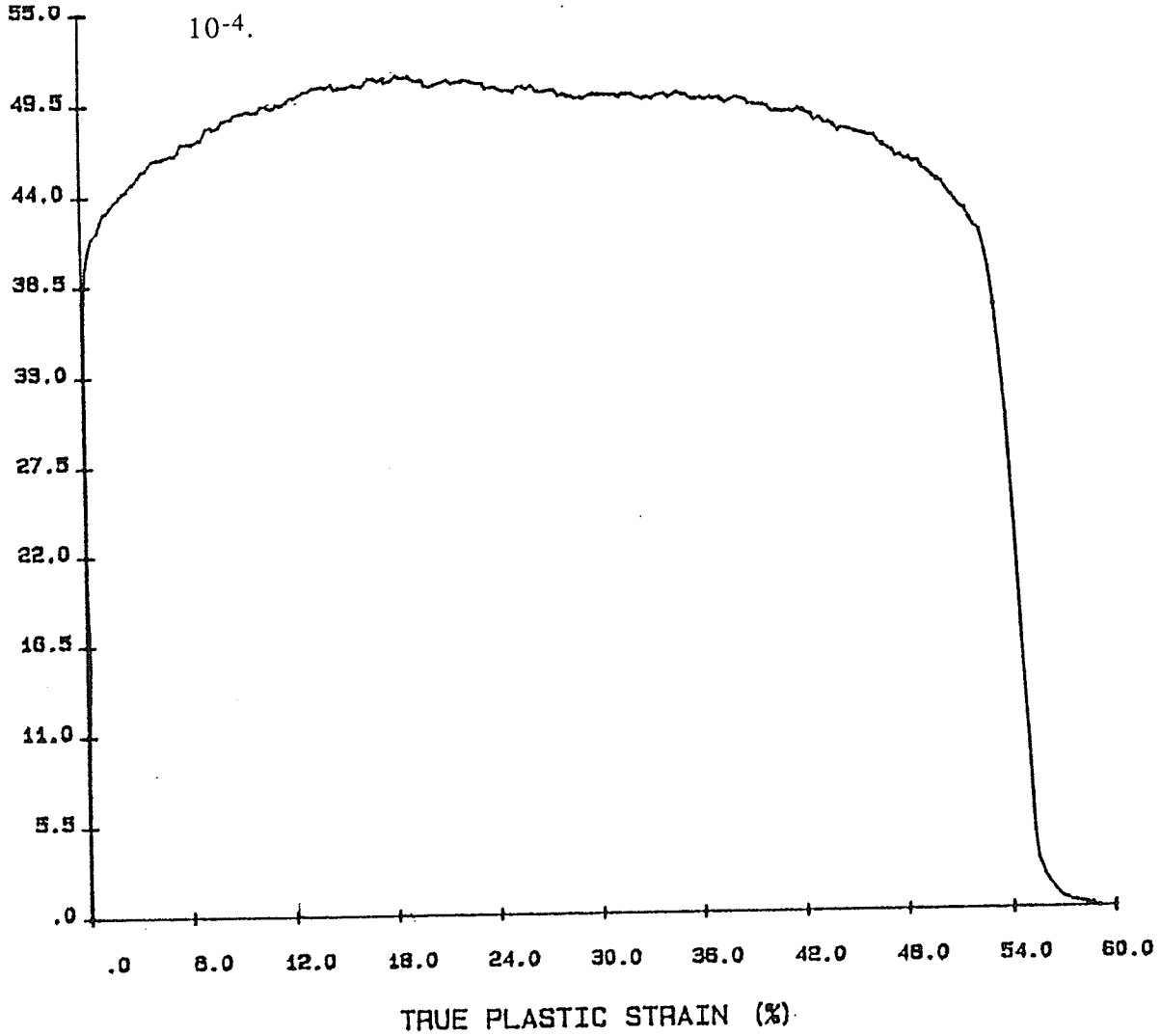

Figure 35 True stress versus true plastic strain curve of as received material tested in tension at 900°C under a constant strain rate of 1 x 10^{-3}.

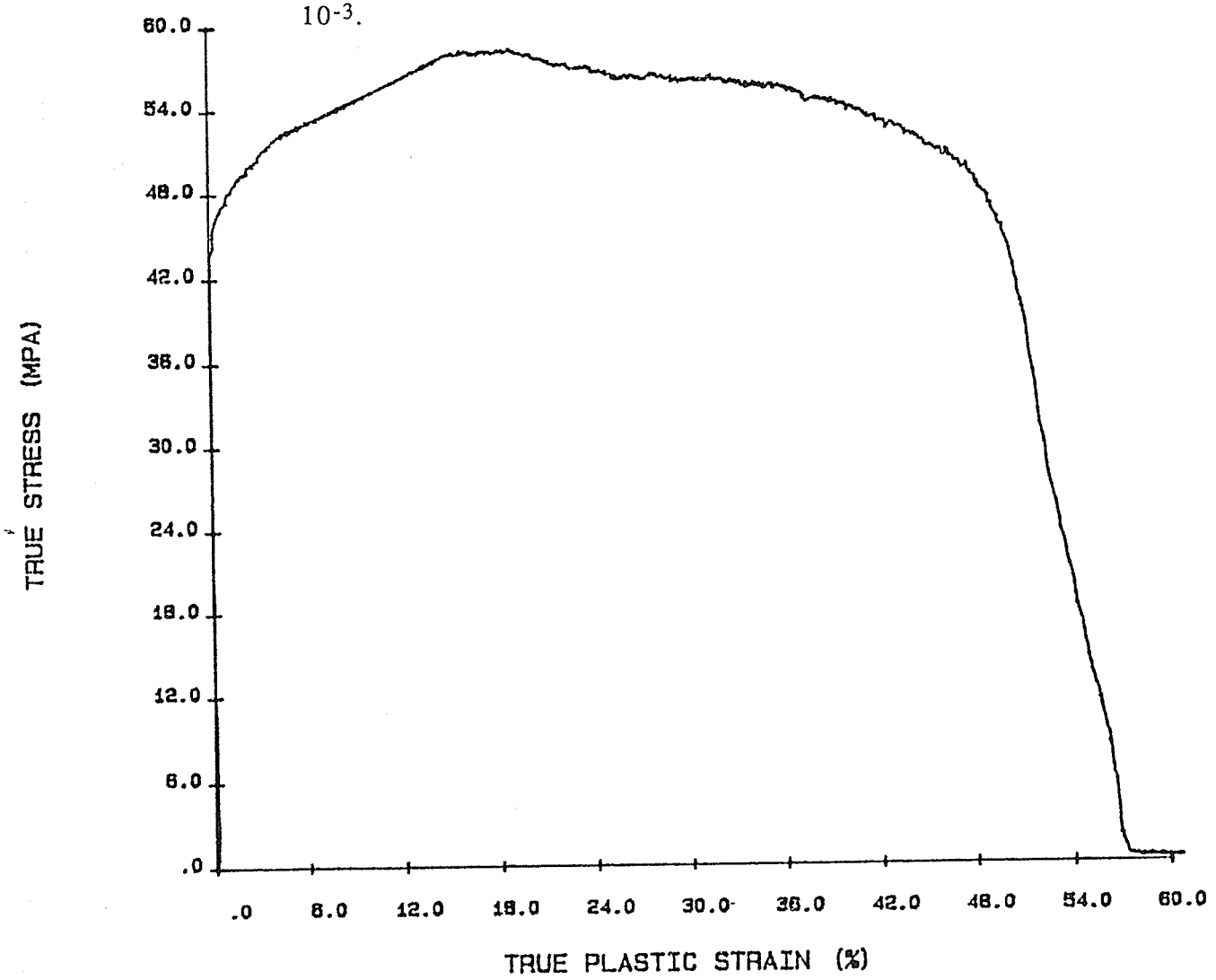

Figure 36 True stress versus true plastic strain curve of as received material tested in tension at 950°C under a constant strain rate of 1 x 10^{-4}.

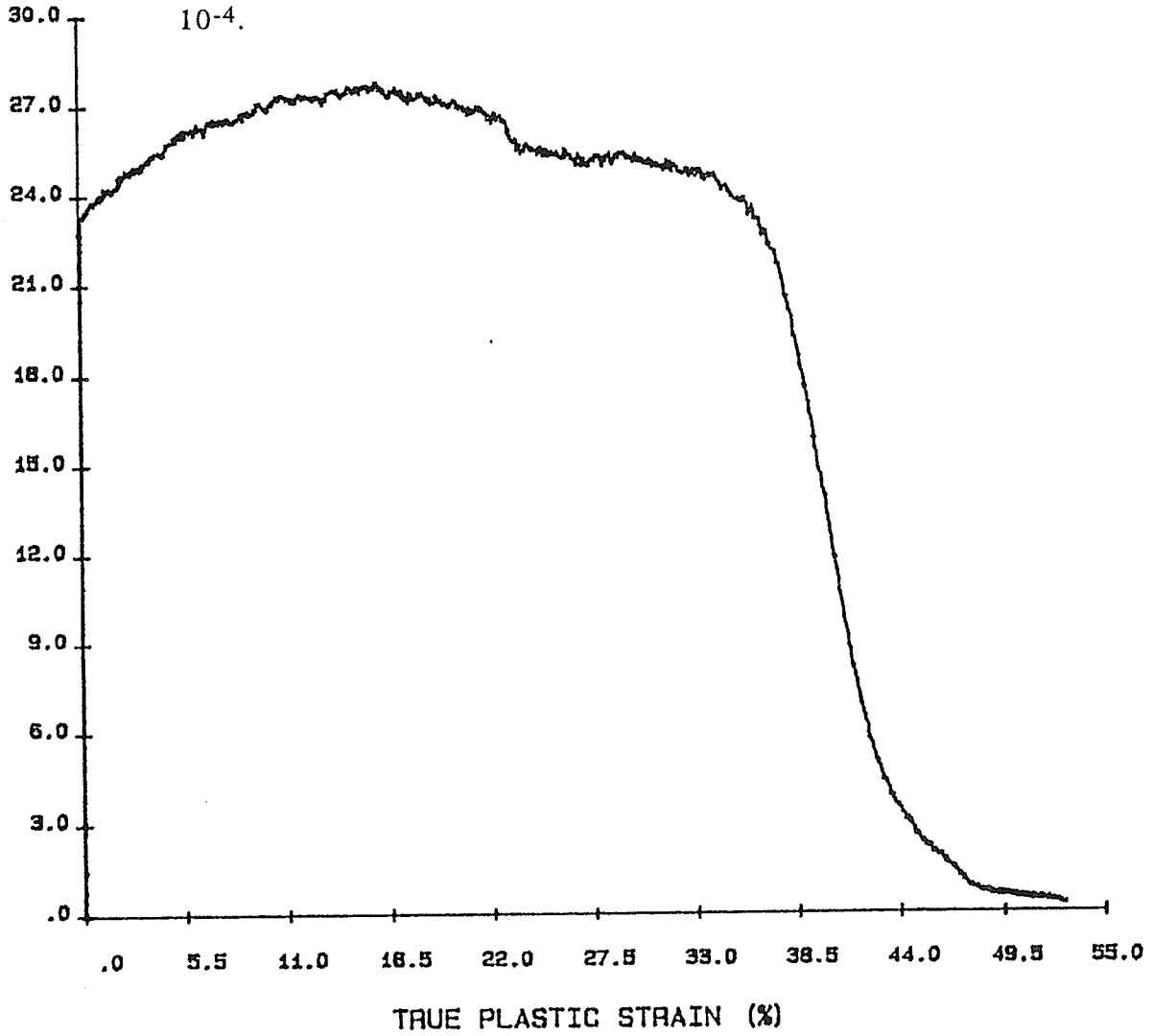

Figure 37 True stress versus true plastic strain curve of as received material tested in tension at 950°C under a constant strain rate of 1 x 10^{-3}.

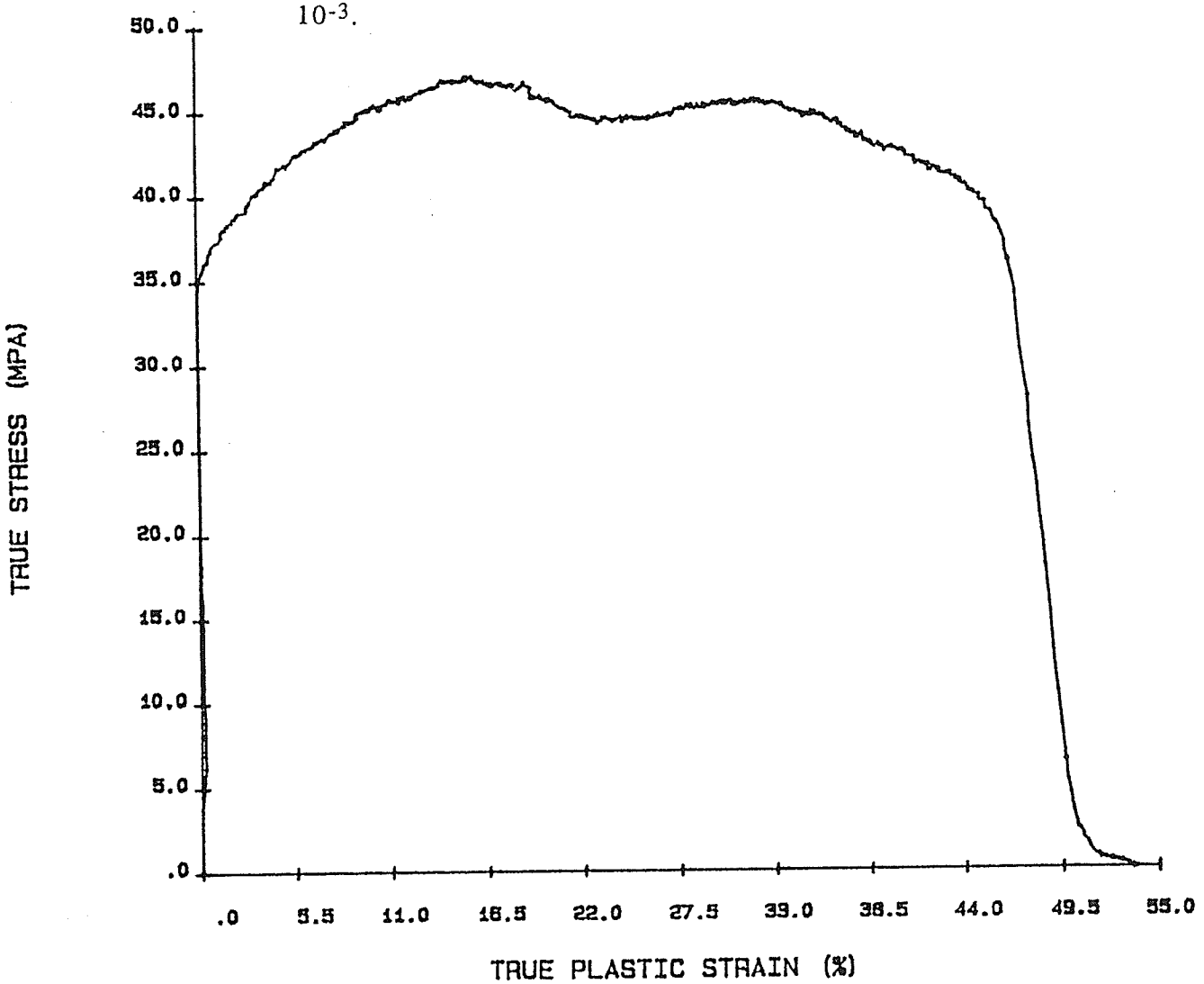

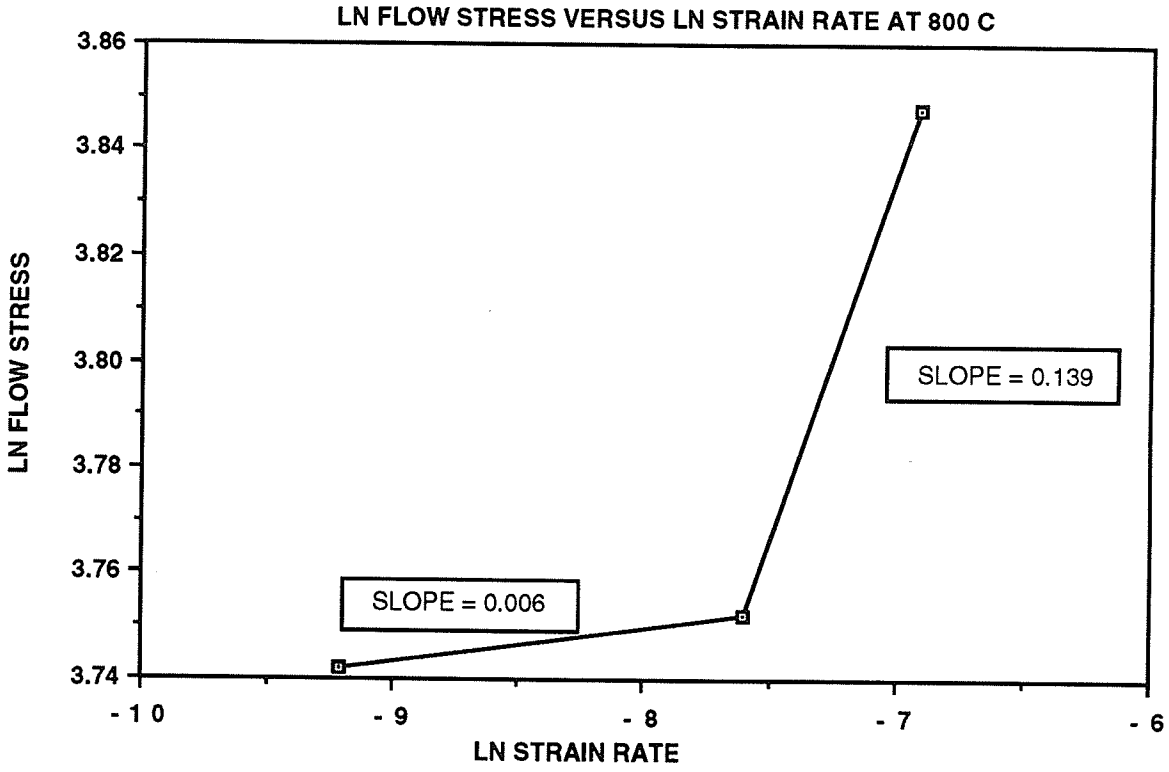

Figure 38 Logarithmic Plot of Flow Stress versus Strain Rate Extrapolated from Constant Strain Rate Tension Tests at 800°C. Flow stresses are ultimate values for the individual tests.

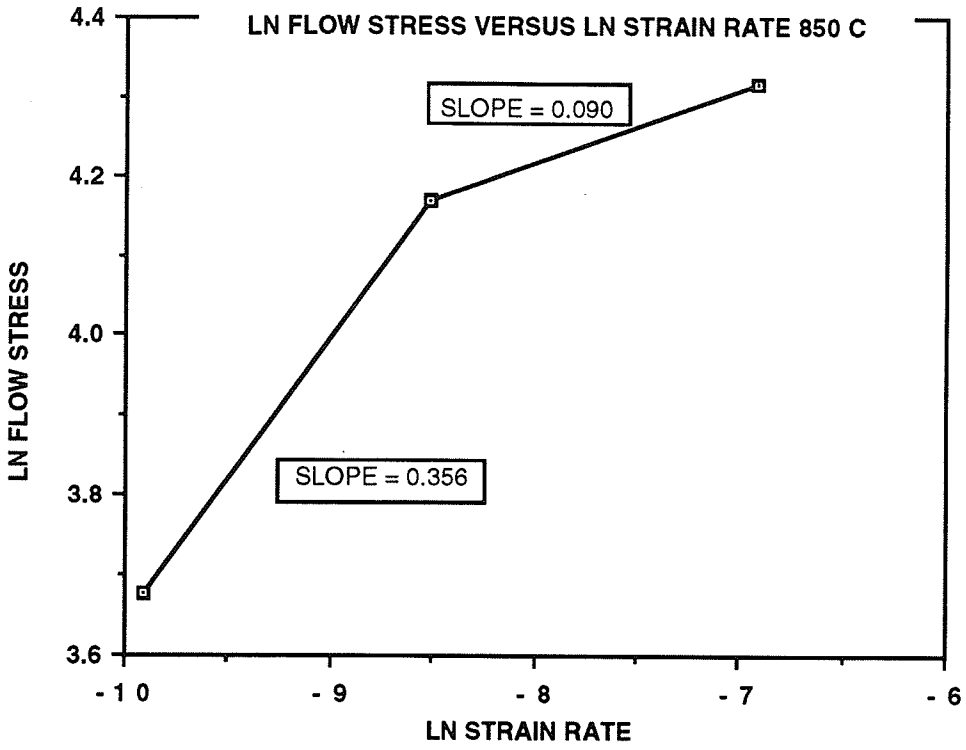

Figure 39 Logarithmic Plot of Flow Stress versus Strain Rate Extrapolated from Constant Strain Rate Tension Tests at 850°C. Flow stresses are ultimate values for the individual tests.

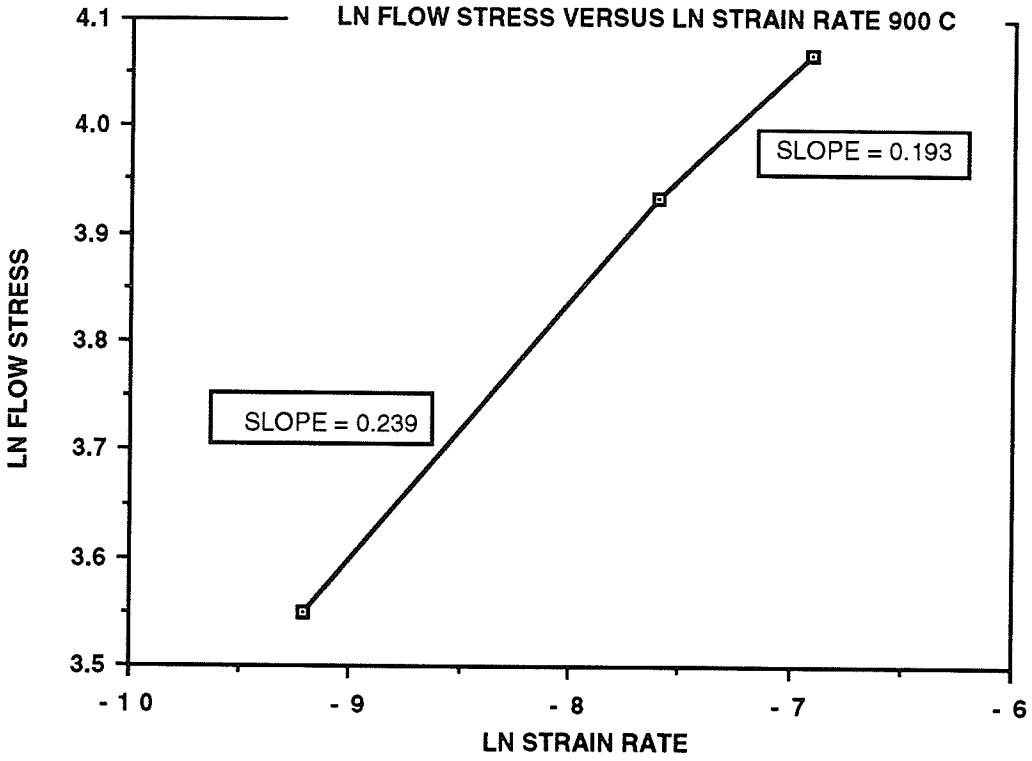

Figure 40 Logarithmic Plot of Flow Stress versus Strain Rate Extrapolated from Constant Strain Rate Tension Tests at 900°C. Flow stresses are ultimate values for the individual tests.

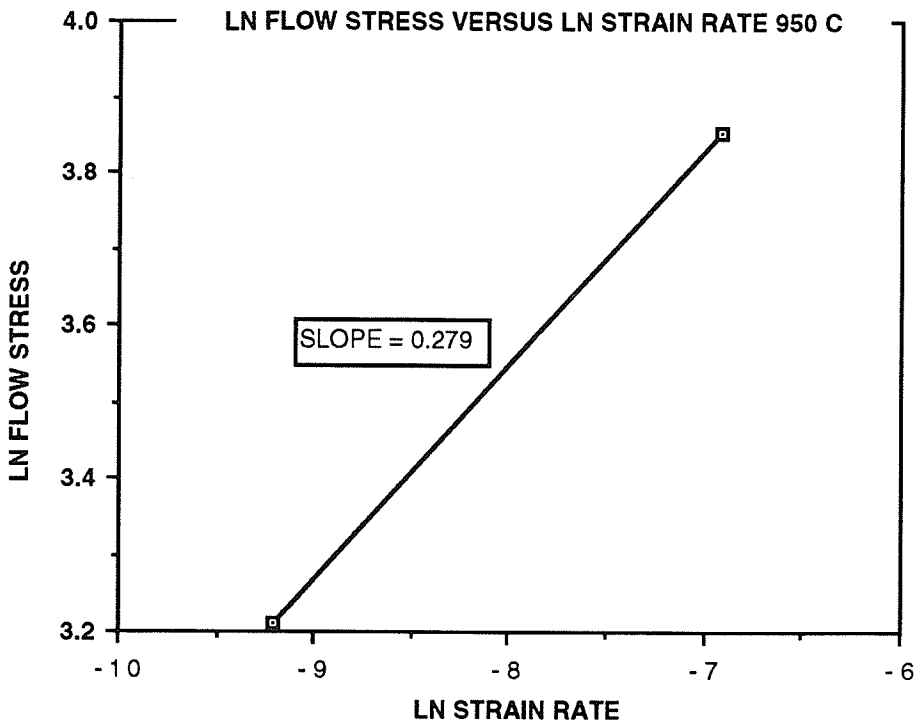

Figure 41 Logarithmic Plot of Flow Stress versus Strain Rate Extrapolated from Constant Strain Rate Tension Tests at 950°C. Flow stresses are ultimate values for the individual tests.

Figure 42 True stress versus true plastic strain curve of as received material tested in tension at 800°C.

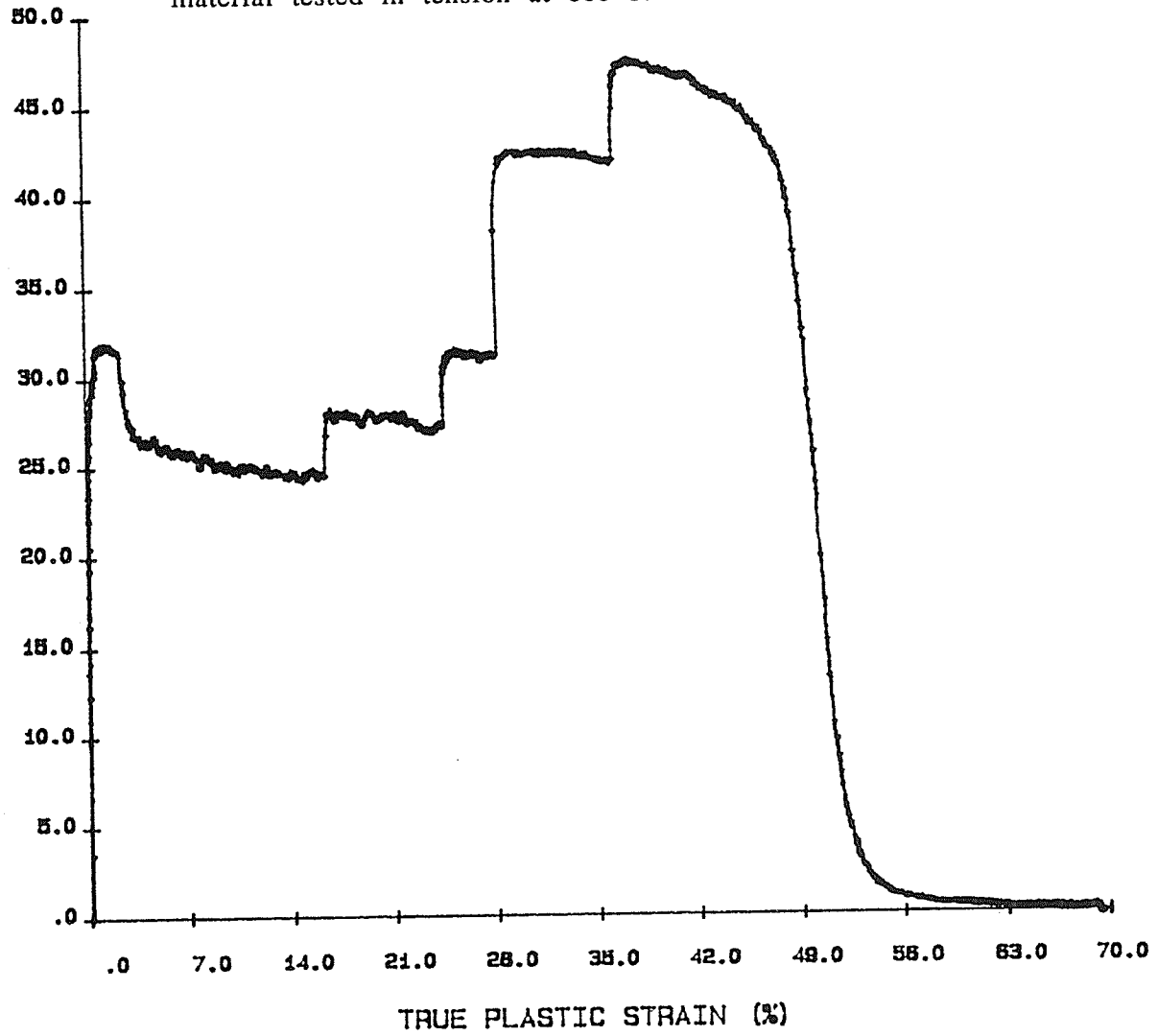

Figure 43 True stress versus true plastic strain curve of swaged material tested in tension at 800°C.

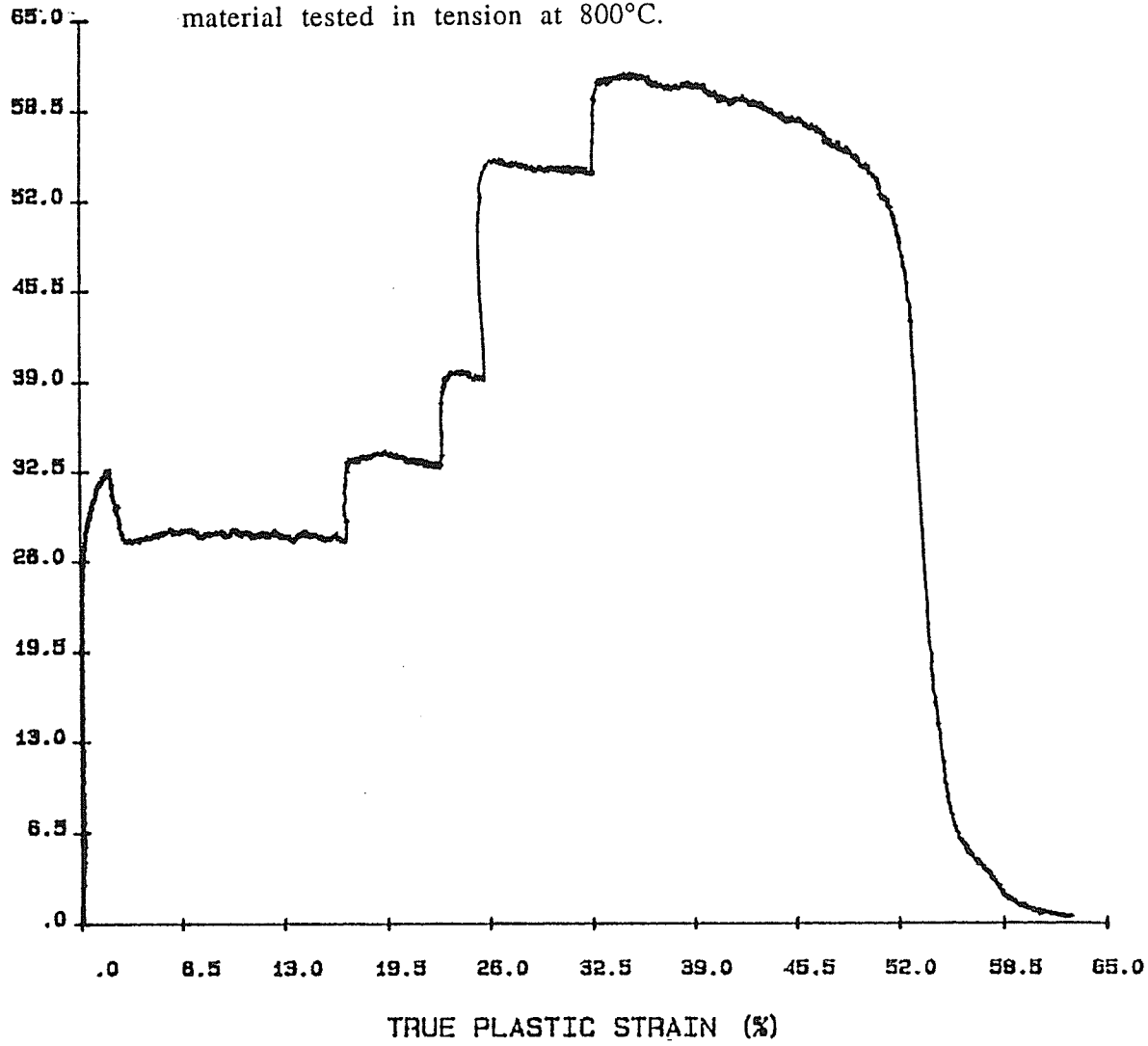

Figure 44 True stress versus true plastic strain curve of as received material tested in tension at 850°C.

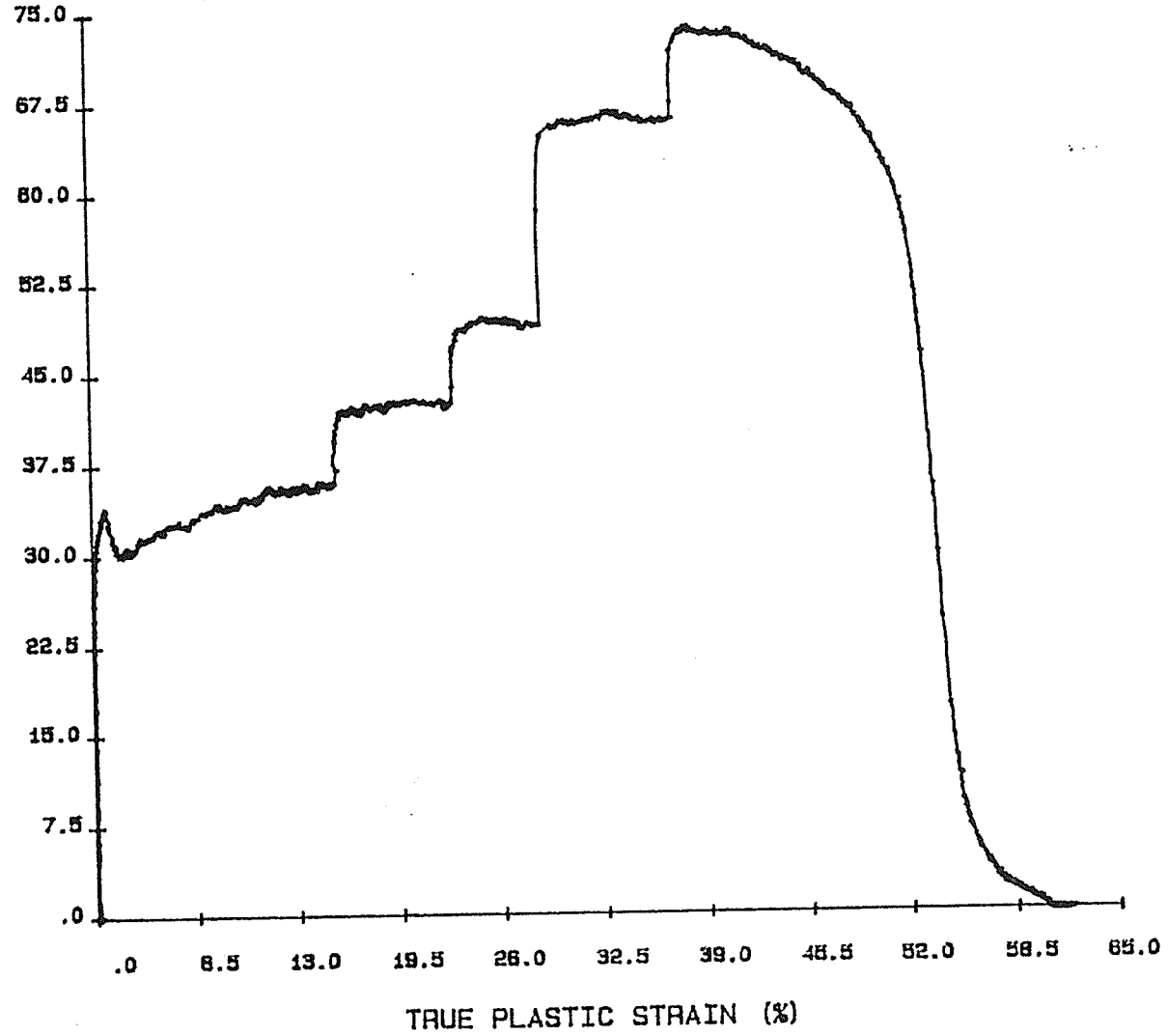

Figure 45 True stress versus true plastic strain curve of swaged material tested in tension at 850°C.

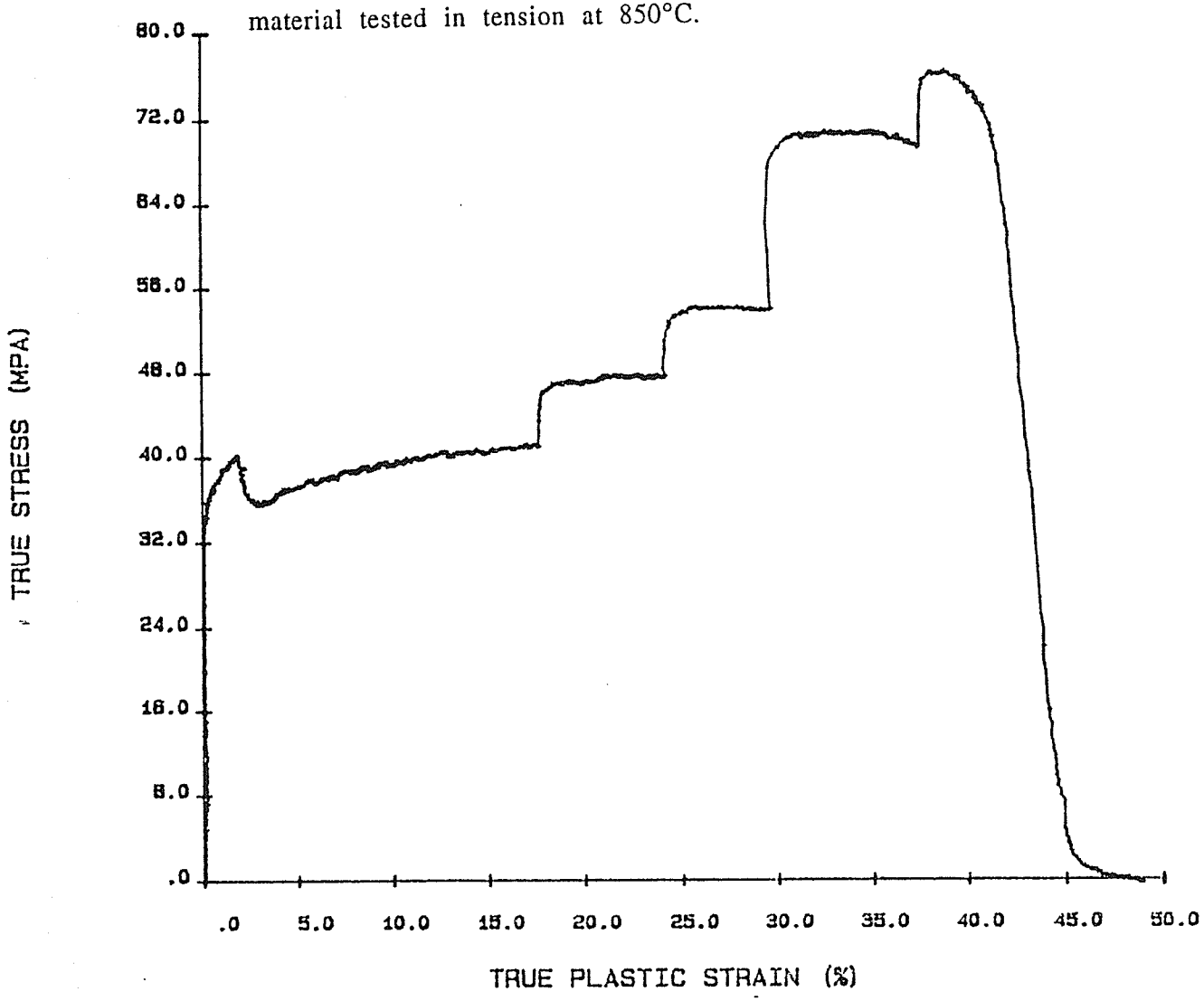

Figure 46 True stress versus true plastic strain curve of as received material tested in tension at 900°C.

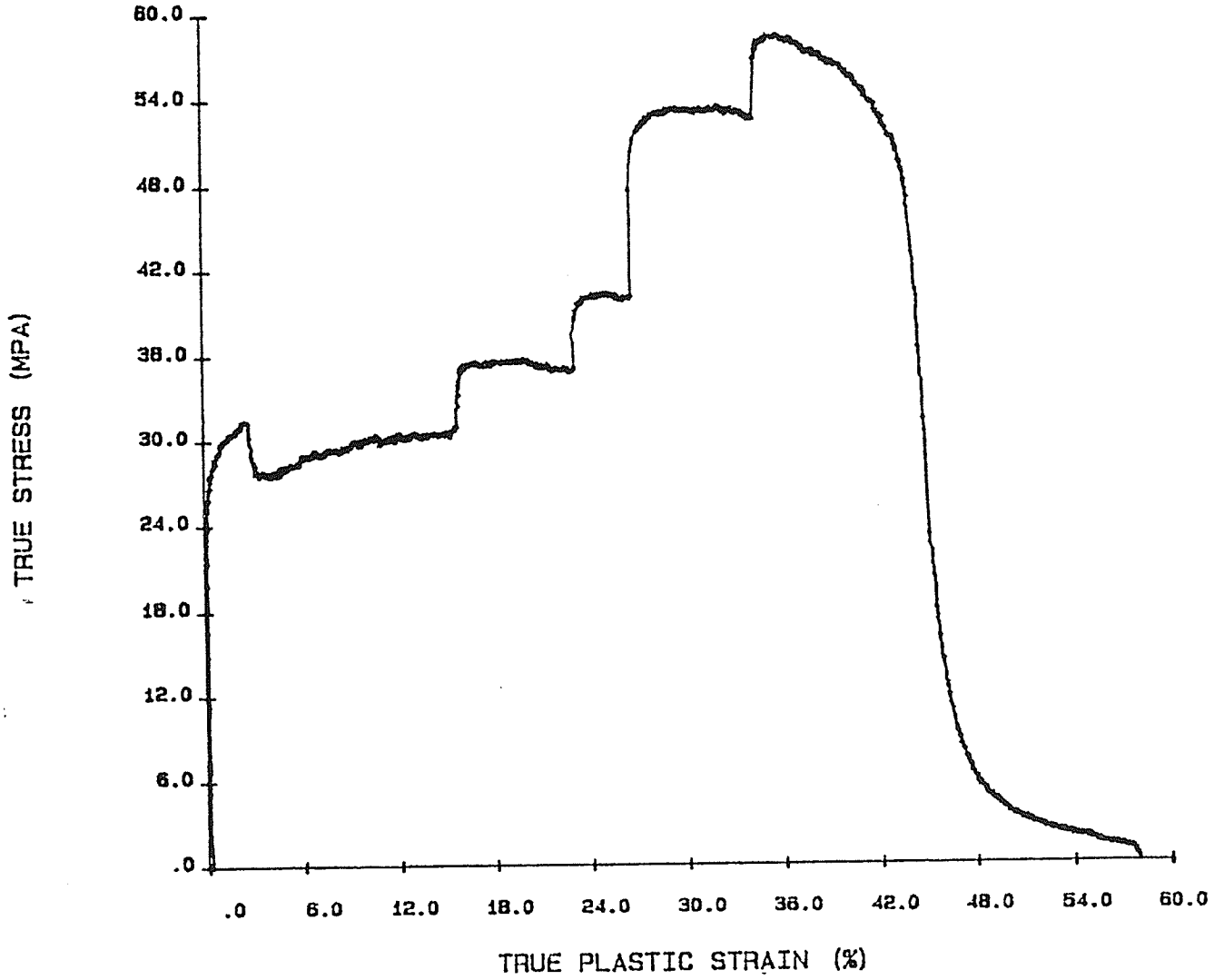

Figure 47 True stress versus true plastic strain curve of swaged material tested in tension at 900°C.

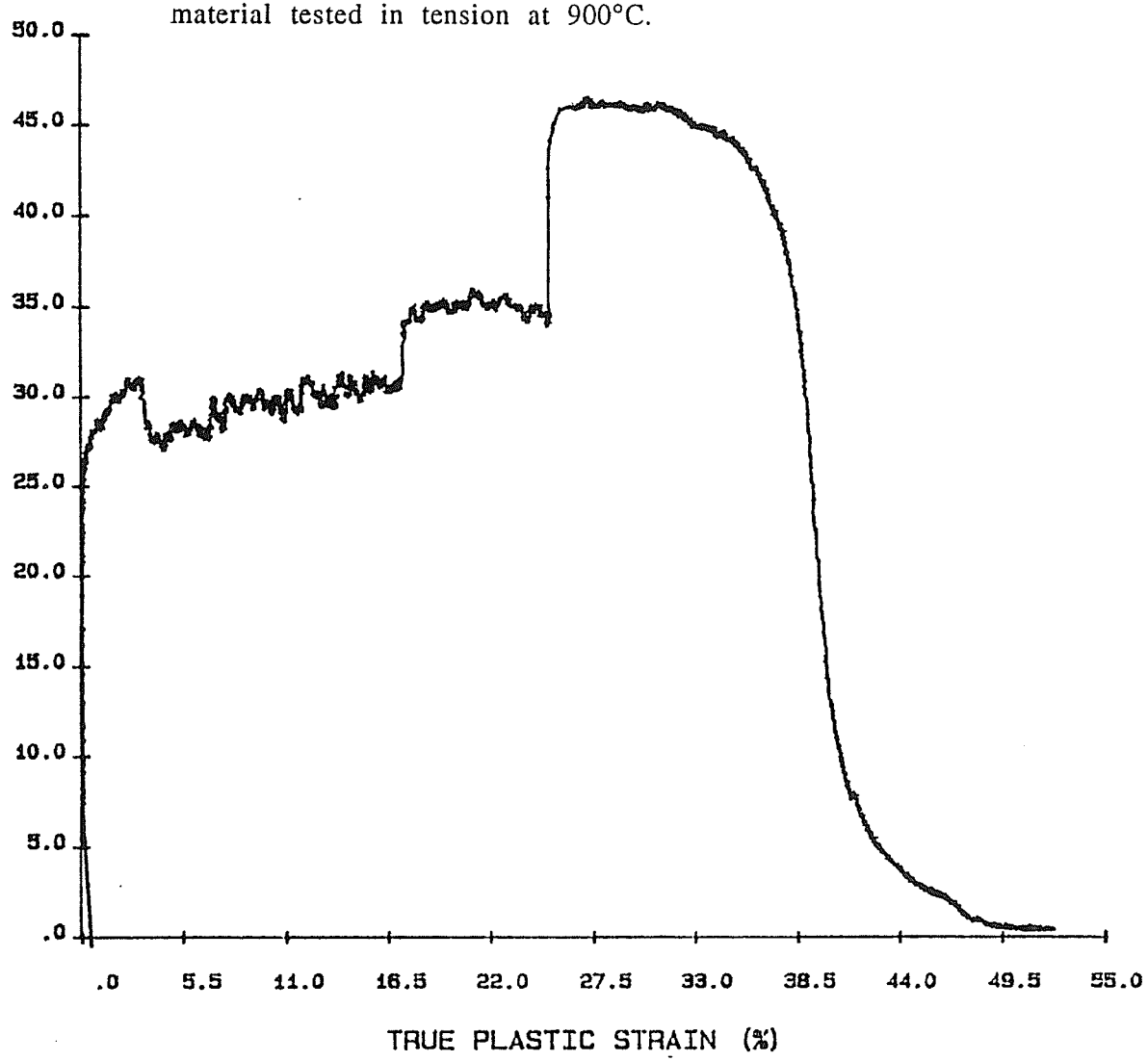

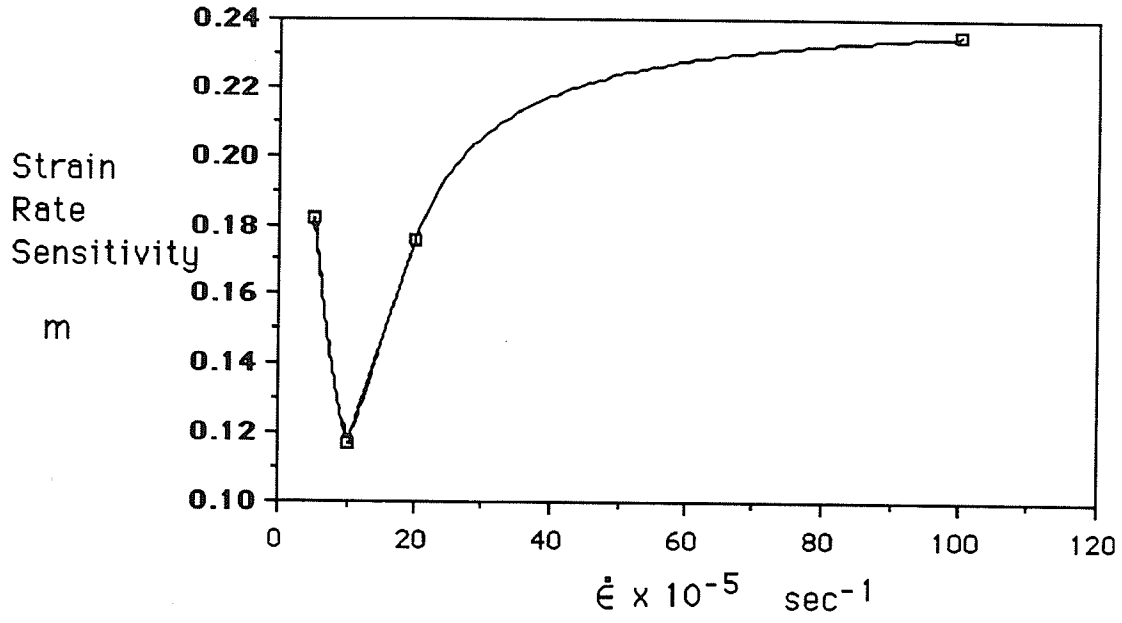

Figure 48 Strain rate sensitivity versus strain rate for as received material tested at 800°C.

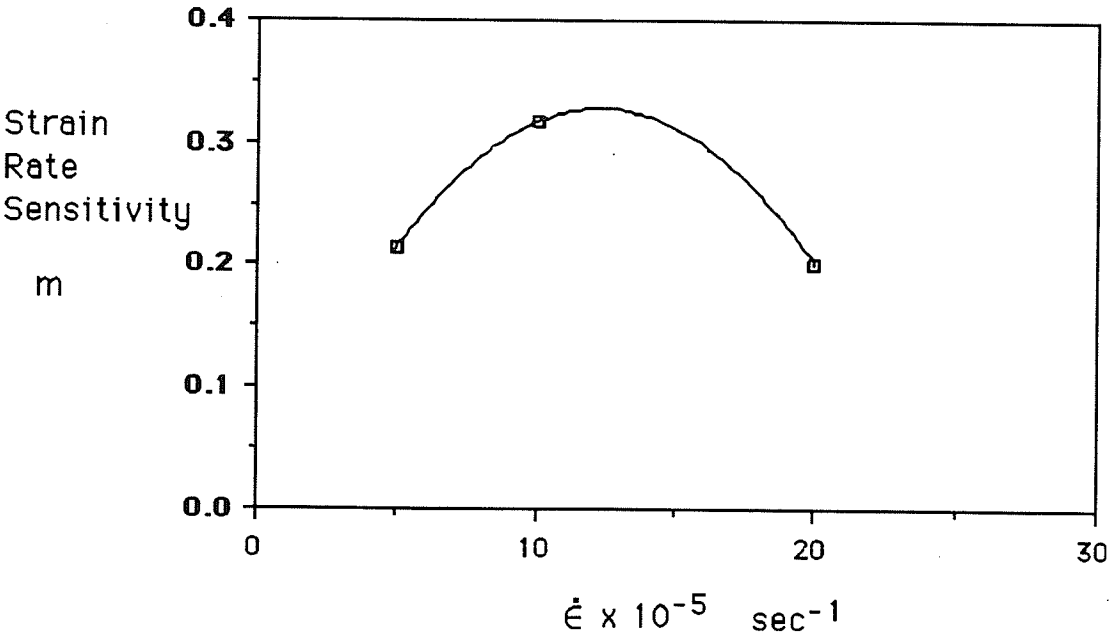

Figure 49 Strain rate sensitivity versus strain rate for swaged material tested at 800°C.

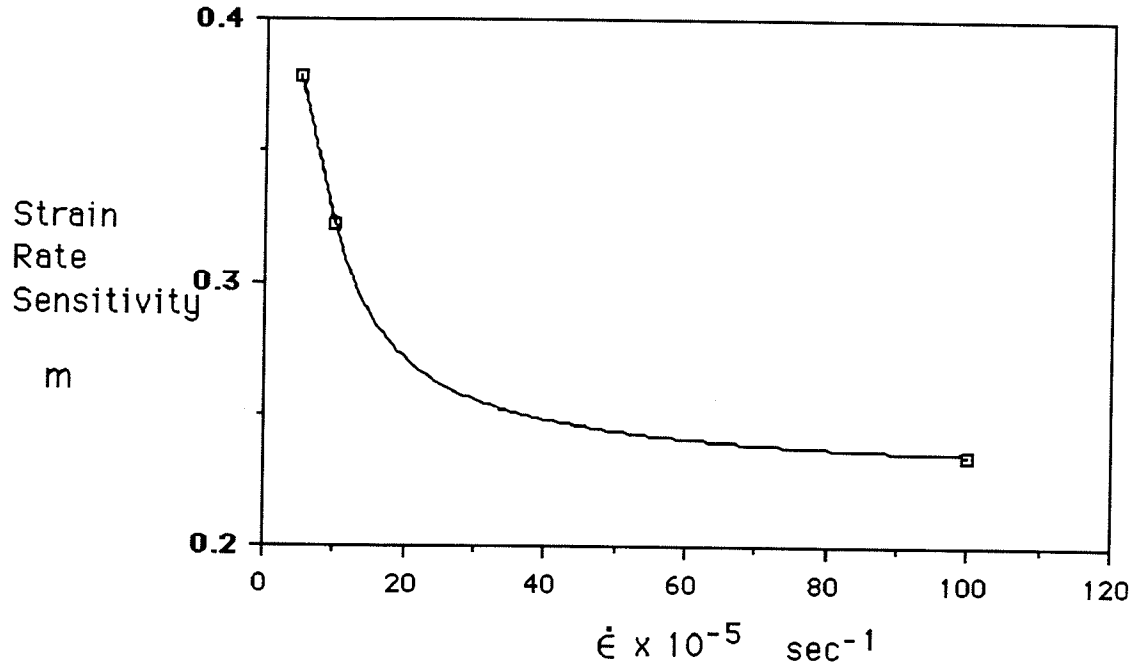

Figure 50 Strain rate sensitivity versus strain rate of as received material tested in tension at 850°C.

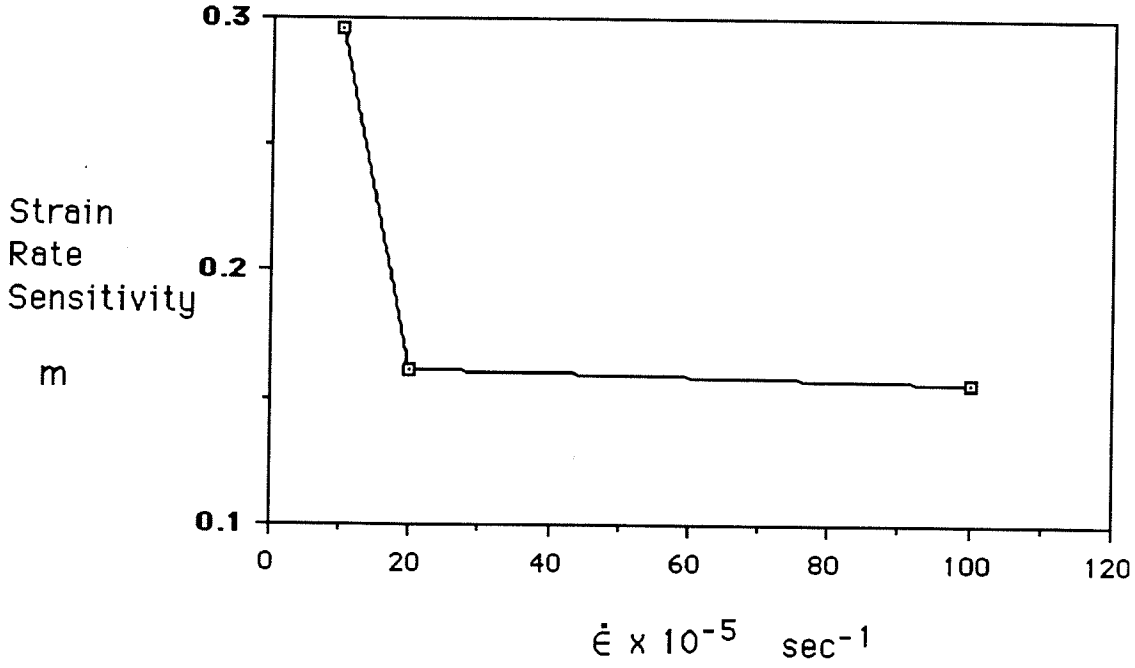

Figure 51 Strain rate sensitivity versus strain rate of swaged material tested in tension at 850°C.

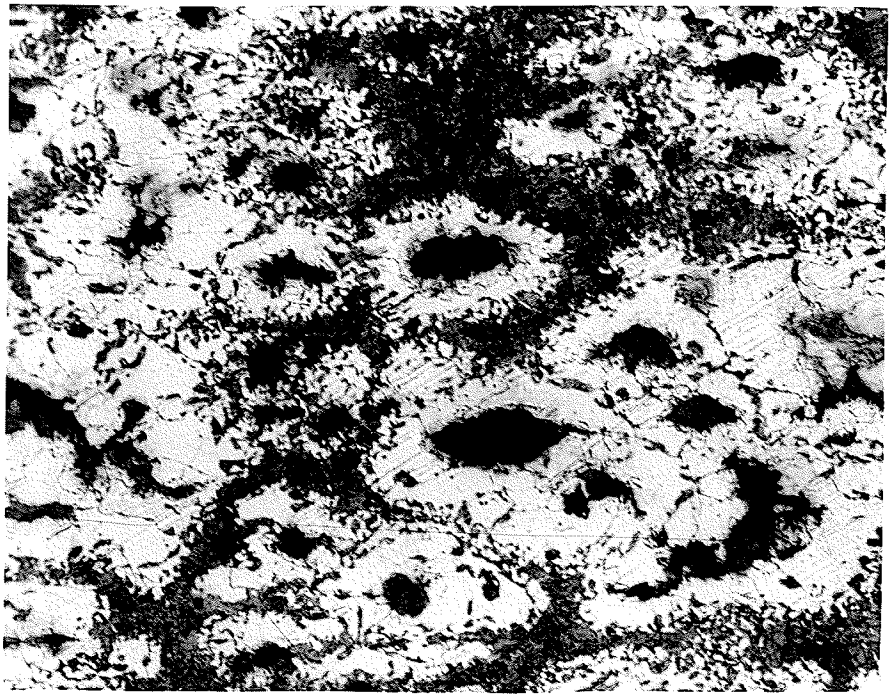

Figure 52 Optical micrograph of a longitudinal section of as received material tested in tension at 800°C. 210X, etchant 2% nital.

Figure 53 Optical micrograph of a longitudinal section of swaged material tested in tension at 800°C. 210X, etchant 2% nital.

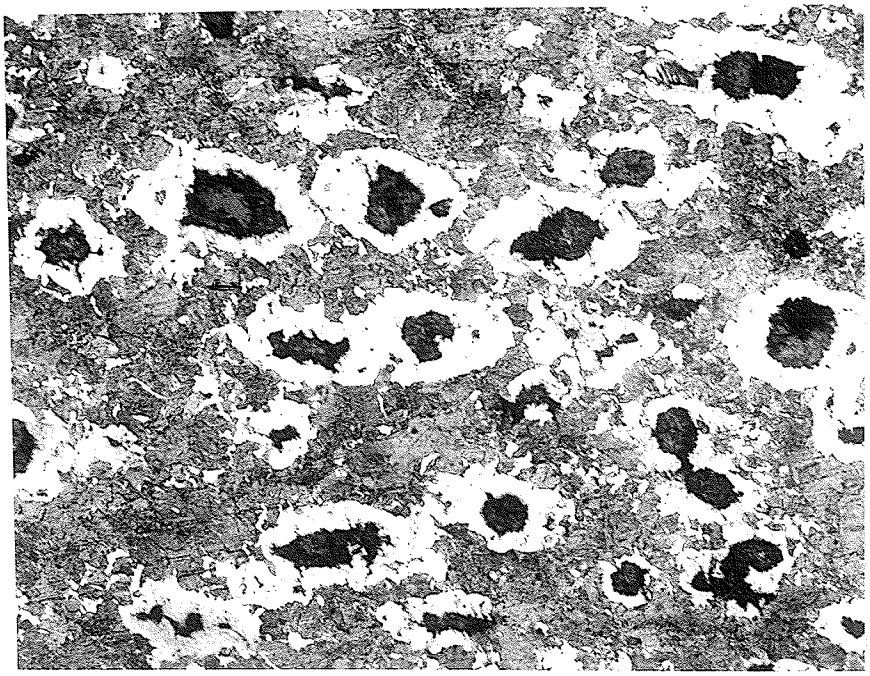

Figure 54 Optical micrograph of a longitudinal section of as received material tested in tension at 850°C. 210X, etchant 2% nital.

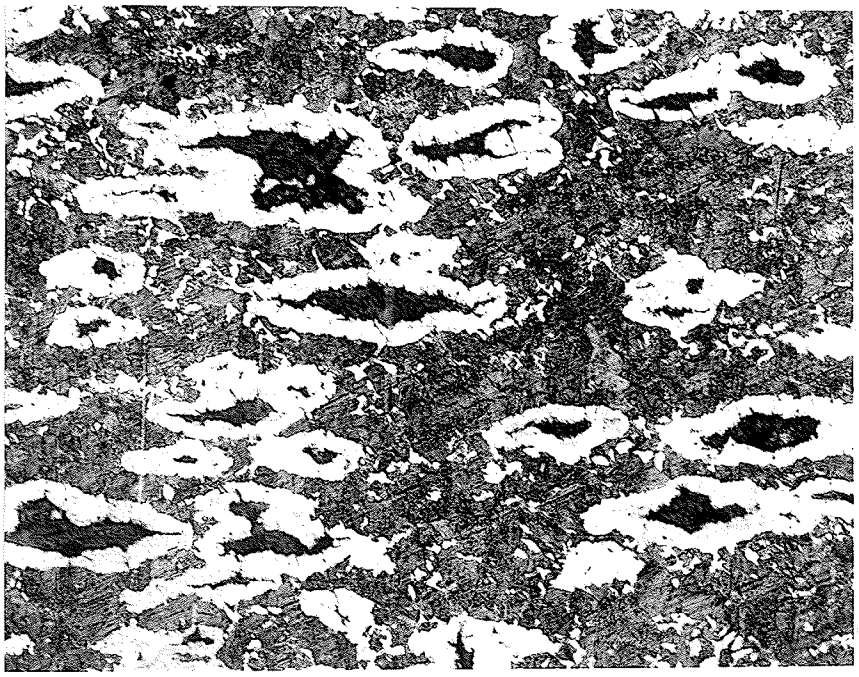

Figure 55 Optical micrograph of a longitudinal section of swaged material tested in tension at 850°C. 210X, etchant 2% nital.

5.4 Hardness Testing

Hardness results are shown in Table 10.

		Ferrite	Pearlite	Graphite
DPH	1)	135.0	350.6	55.1
Hardness	2)	158.5	321.9	61.3
value	3)	134.0	383.1	45.3
	4)	160.4	321.9	57.5
	5)	158.5	321.9	55.1
	Average	149.3	339.9	54.9

Table 10 DPH hardness values for ferrite, pearlite and graphite in ductile cast iron normalized at 950°C for 1 hour.

5.5 Additional Metallography Results

Figures 56, 57, 58 and 59 show as received and swaged material in the untested condition. Figures 60 and 61 show fracture surfaces of both as received and swaged material. Figures 62 and 63 depict the high temperature microstructure of as received material. Figures 64 to 68 demonstrate the shape of graphite at various stages in the cold swaging process.

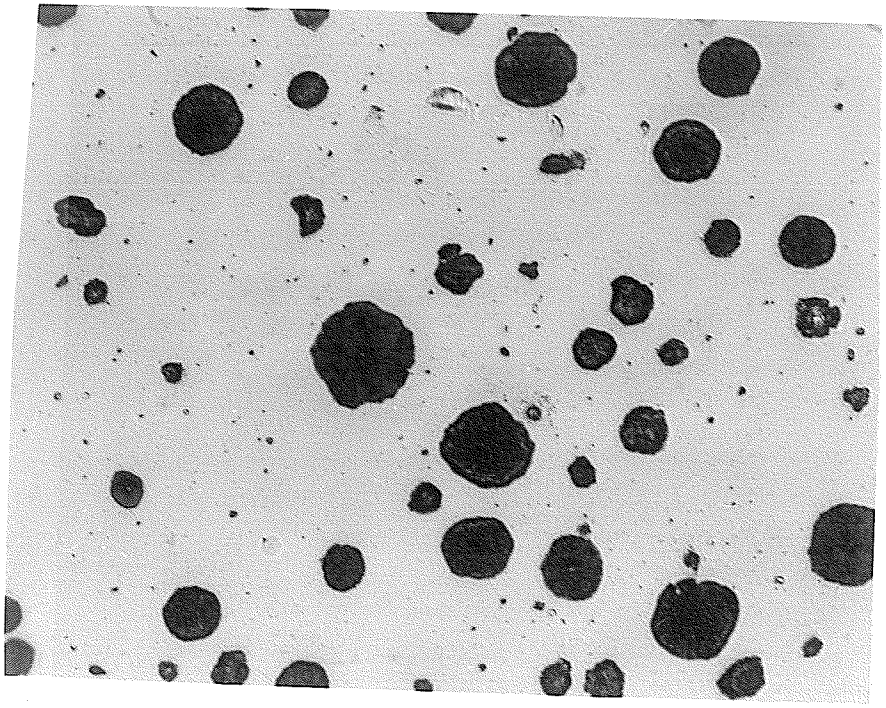

Figure 56 Optical micrograph of a cross section of as received material in the untested condition. 210X, unetched.

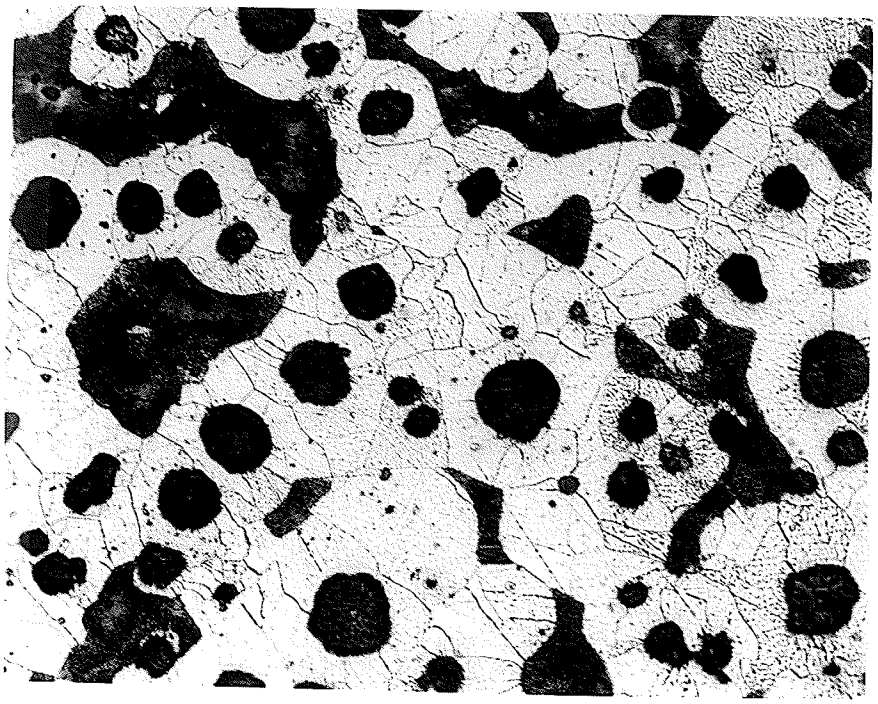

Figure 57 Optical micrograph of a cross section of as received material in the untested condition. 210X, etchant 2% nital.

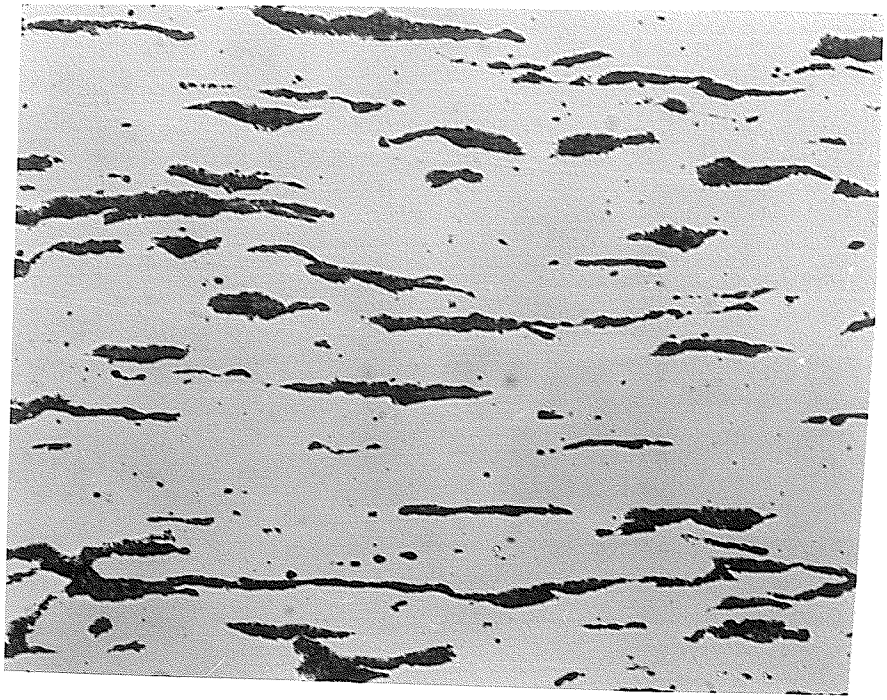

Figure 58 Optical micrograph of a longitudinal section of material swaged at 850°C from 0.5 inches in diameter to 0.2 inches in diameter, in the untested condition. 210X, unetched.

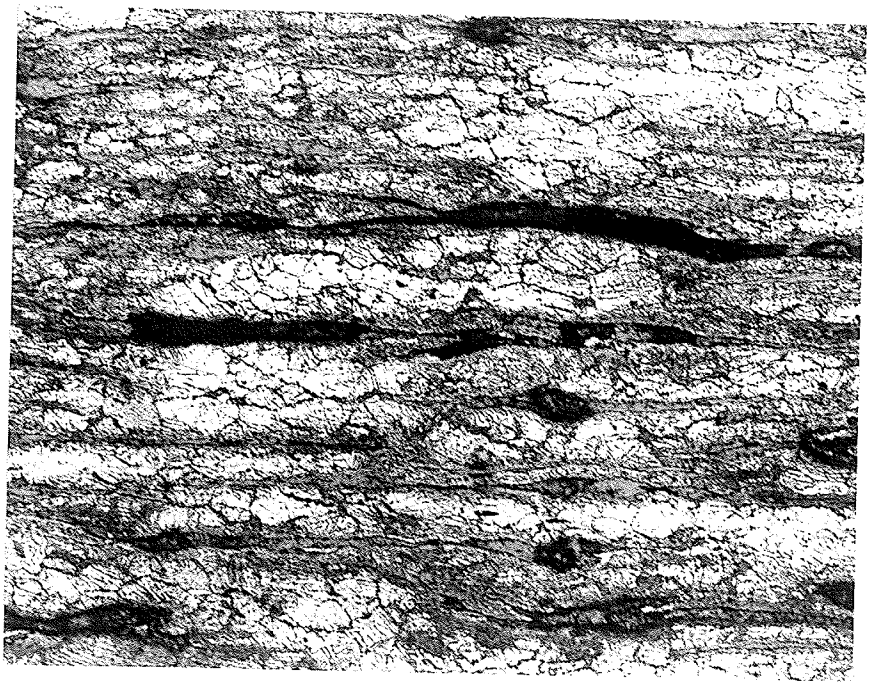

Figure 59 Optical micrograph of a longitudinal section of material swaged at 850°C from 0.5 inches in diameter to 0.2 inches in diameter, in the untested condition. 210X, etchant 2% nital.

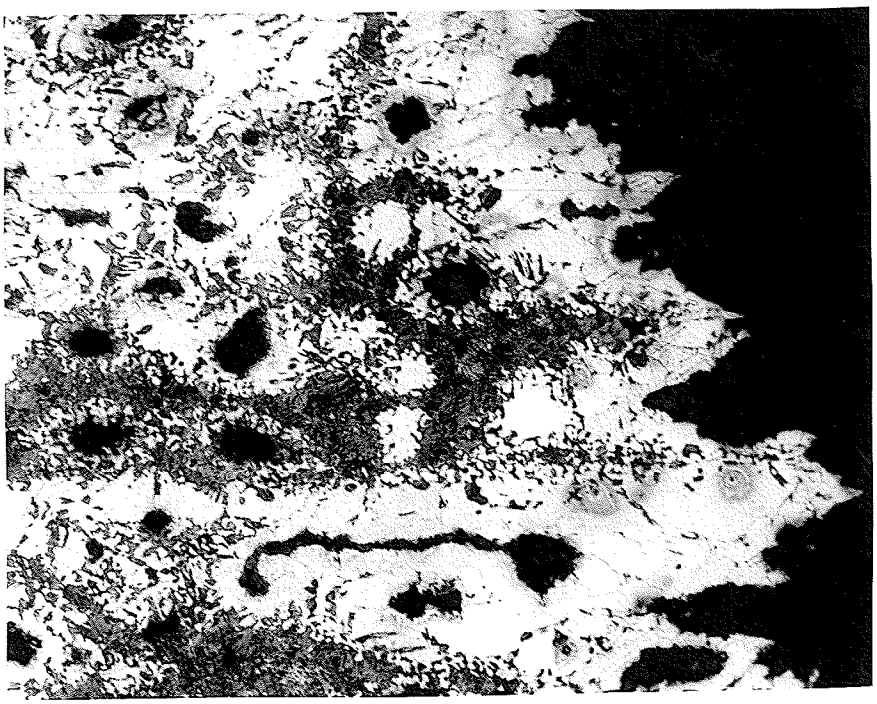

Figure 60 Optical micrograph of a longitudinal section of a fracture surface of as received material tested in tension at 800°C. 210X, etchant 2% nital.

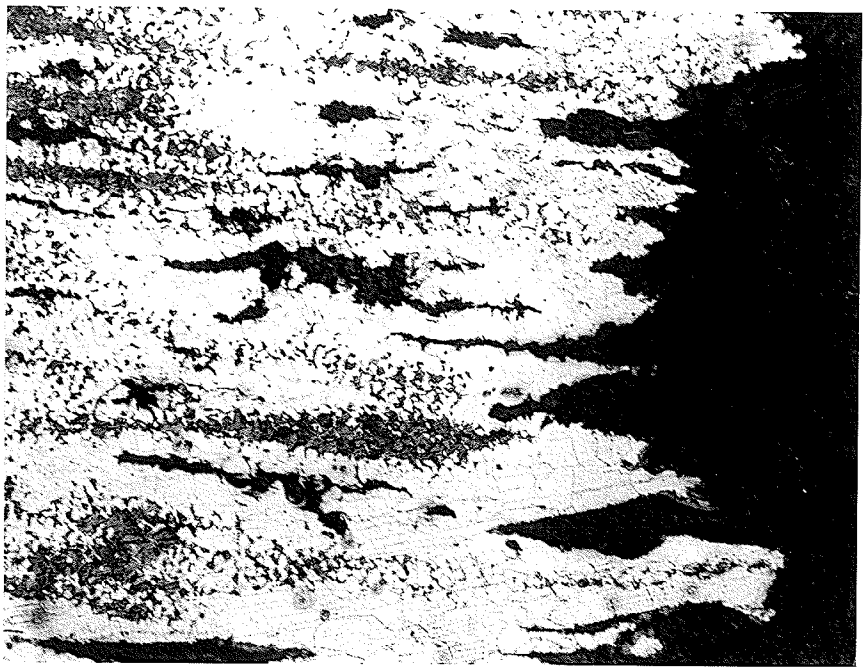

Figure 61 Optical micrograph of a longitudinal section of a fracture surface of swaged material tested in tension at 800°C. 210X, etchant 2% nital.

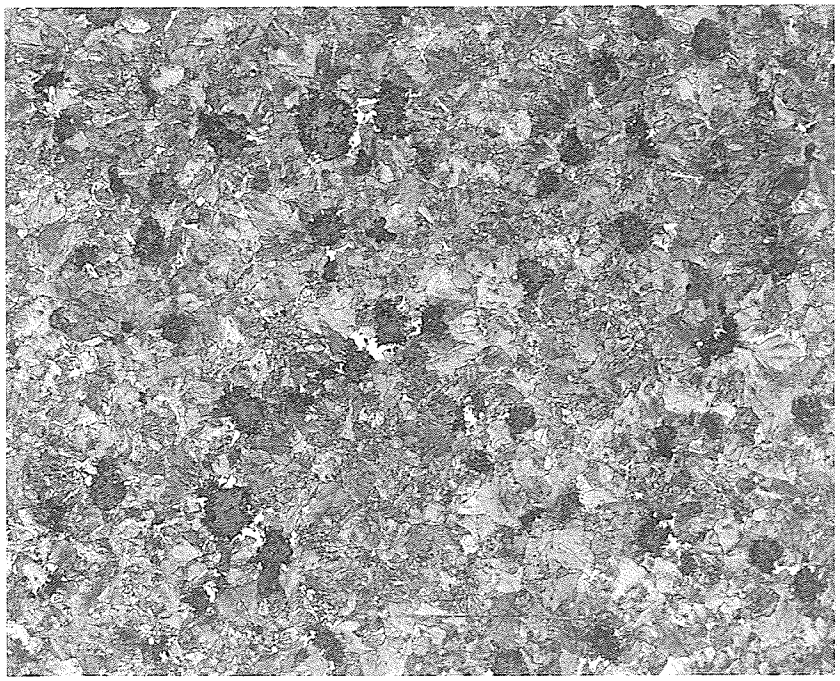

Figure 62 Optical micrograph of a cross section of as received material tested in tension at 800°C. 210X, etchant 2% nital, brightfield image.

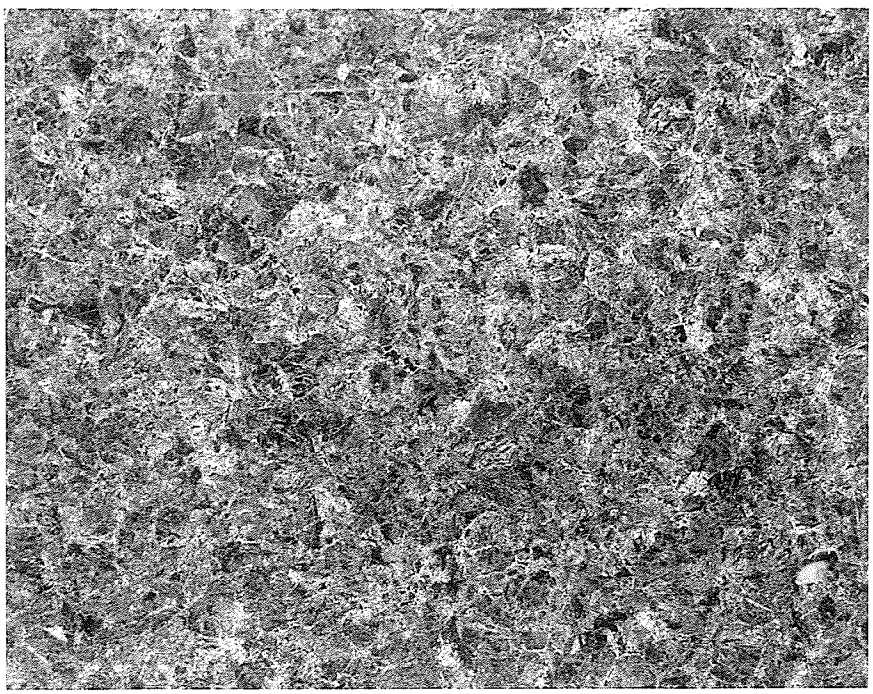

Figure 63 Optical micrograph of a cross section of as received material tested in tension at 800°C. 210X, etchant 2% nital, darkfield image.

Figure 64 Optical micrograph of a longitudinal section of material hot swaged at 934°C from 0.56 inches in diameter to 0.448 inches in diameter and cold swaged at room temperature from 0.448 inches in diameter to 0.322 inches in diameter. 210X, unetched.

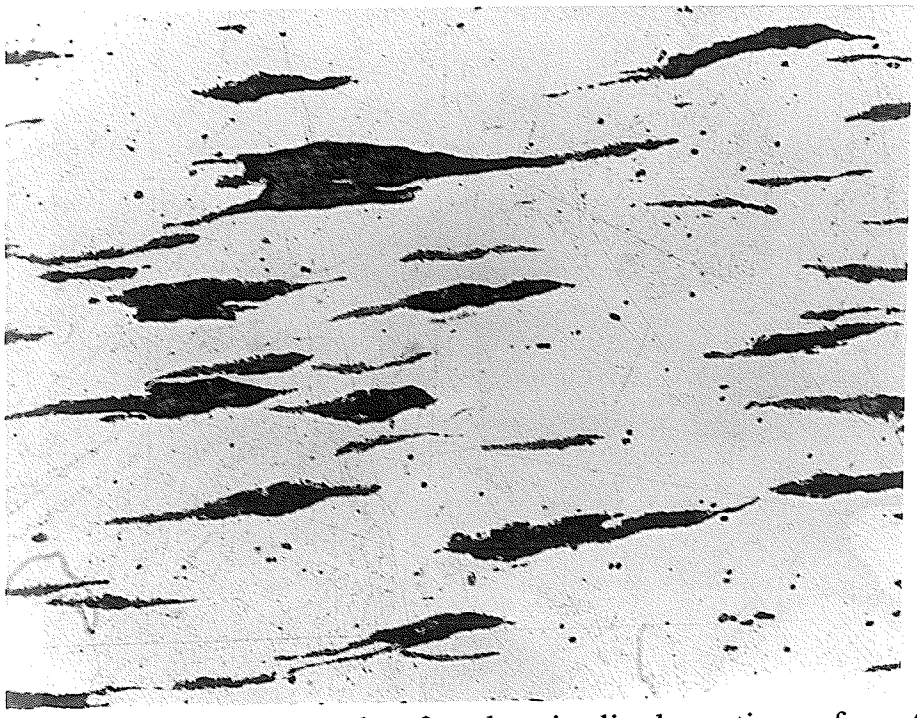

Figure 65 Optical micrograph of a longitudinal section of material hot swaged at 934°C from 0.56 inches in diameter to 0.448 inches in diameter and cold swaged at room temperature from 0.448 inches in diameter to 0.258 inches in diameter. 210X, unetched.

Figure 66 Optical micrograph of a longitudinal section of material hot swaged at 934°C from 0.56 inches in diameter to 0.322 inches in diameter and cold swaged at room temperature from 0.322 inches in diameter to 0.258 inches in diameter. 210X, unetched.

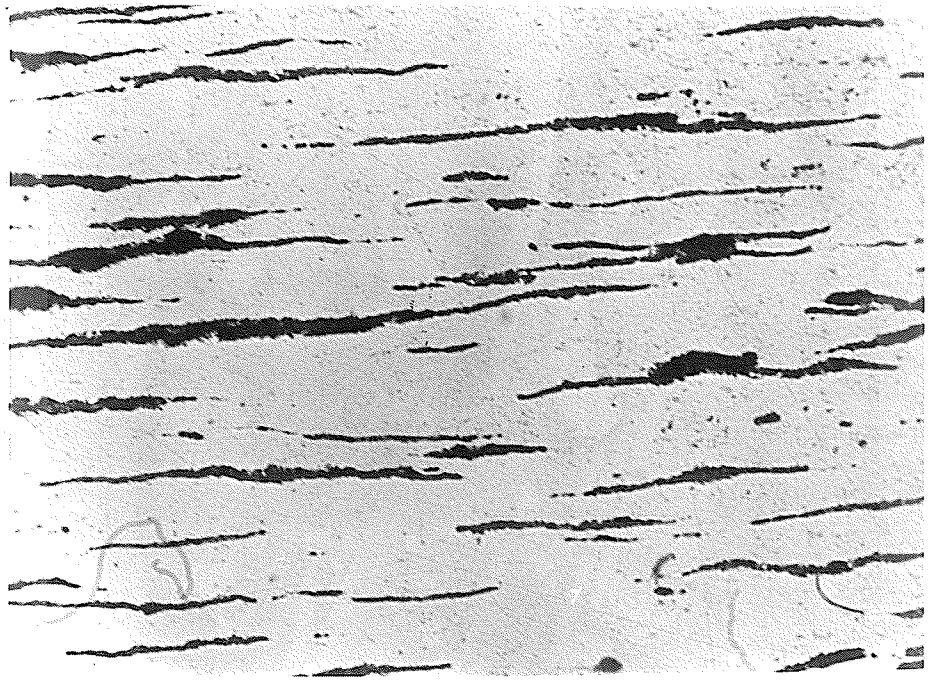

Figure 67 Optical micrograph of a longitudinal section of material hot swaged at 934°C from 0.56 inches in diameter to 0.332 inches in diameter and cold swaged at room temperature from 0.332 inches in diameter to 0.20 inches in diameter. 210X, unetched.

Figure 68 Optical micrograph of a longitudinal section of material hot swaged at 934°C from 0.56 inches in diameter to 0.332 inches in diameter and cold swaged at room temperature from 0.332 inches in diameter to 0.20 inches in diameter. 52.2X, unetched.

6 DISCUSSION OF RESULTS

6.1 Introduction

This chapter is broken up into 3 major sections. Detailed discussion is presented in the following areas; compression test results, tension test results, and optical microscopy results. Emphasis will be placed on what can be inferred from the strain rate sensitivity results, and from the general nature and appearance of the microstructure.

Prior to the commencement of mechanical testing there was little cause for optimism since neither the swaged or the as received material exhibited the characteristic microstructure inherent in typical superplastic materials. After analyzing these results it becomes very clear that the ductile cast iron tested, both the swaged and the as received material, is not superplastic at elevated temperatures although some fairly large deformations were evident.

6.2 Compression Test Results

During the preliminary compression tests some very interesting results for both the as received and swaged material were witnessed. Initially it seemed that the sharp jumps recorded by the Instron machine may have indicated that strain rate sensitivity values were quite high, possibly in the range of superplastic forming. This was surprising since the as received material had not been subjected to any grain refining processes and the swaged material did not appear to exhibit the ideal superplastic microstructure. It will be subsequently shown that the strain rate sensitivity values were not within the range of superplastic forming.

Upon removing the specimens from the furnace it seemed that the results were promising indeed for the as received material at least. Several samples of the as received material evinced substantial deformation, that on a macroscopic level was free of surface cracks. Numerous samples were essentially flattened to such an extent that they resembled in size and shape small coins. In many cases the samples were compressed as much as 70%. As far as the swaged material is concerned the results were quite different; in fact, they were quite the opposite.

The swaged material was profoundly scarred with gaping surface cracks that were highly visible to the naked eye, even though in a number of cases there was a relatively small amount of deformation when compared to the as received material. The flow of as received material is obviously accommodated by some internal processes, while accommodation in the swaged material is through catastrophic failure, ie the formation of gaping surface cracks.

Figures 11 to 22 show the true flow stress plotted versus the true plastic strain for differential strain rate compression tests run at constant temperatures between 750°C and 950°C. These plots show that the material tested, whether it was swaged or as received material, was, on numerous occasions, highly strained. By comparing swaged and as received tests conducted at the same constant temperature it is evident that some differences exist. First of all, the flow stress appears to be higher for the as received material. This fact could be considered beneficial for the swaged material as a low flow stress is a primary characteristic of superplasticity. In this case however, the apparent advantage of lower flow stress the swaged

material exhibits is not due to superplasticity. This result is most likely caused by different accommodation processes prevalent in the two materials. As was mentioned, accommodation in the swaged material appears to occur by the formation of large surface cracks. This should result in a smaller load necessary to maintain the constant strain rate since there is less resistance due to this mechanism of failure and thus a lower flow stress. The surface cracking effectively relieves stress, whereas the increased stress in the as received material is accommodated for by an internal process; possibly by grain boundary sliding or some sort of diffusional mechanism.

The sharp jumps associated with the changes in strain rate in Figures 11 to 22, translate into relatively small strain rate sensitivity values that are less than those characteristic of superplasticity. These strain rate sensitivity values, as shown in Tables 5 and 6, are below the generally accepted minimum of 0.30 for superplastic materials. In fact, many of the experts in the field consider a superplastic material to be effective only if it exhibits a strain rate sensitivity value of 0.5 or greater, amongst other criteria.

6.3 Tension Test Results

As with the compression tests there was a certain amount of optimism during the running of the initial tension tests. Again, the sharp jumps recorded by the chart recorder upon a change in strain rate looked somewhat promising. As the tests progressed the elongations were beginning to look encouraging as there was no indication that failure was about to occur. When failure did occur it was very abrupt. As a result elongation to failure values, Tables 8

and 9, for both the as received and swaged specimens were in many cases satisfactory but not overly remarkable. The greatest elongation to failure, 106%, occurred in a swaged specimen subjected to a constant strain rate of 1 x 10^{-4} sec^{-1} at 800°C. Generally, there seems to be slightly larger elongations at higher strain rates and higher temperatures. This is not always the case, as is evident in the swaged differential strain rate tension tests where the elongations are greater at lower temperatures.

The differential strain rate change tension tests provide contrasting results in comparison to the same tests performed in compression. In tension the flow stress for the swaged material is higher than it was for the as received material (Figures 42 to 47). As mentioned in the last section the lower flow stress in compression for the swaged material was most likely due to the formation of surface cracks. In tension the appearance of surface cracking was not apparent in either material. The reason for this is not entirely known. It can be surmised that the difference in shape of the graphite nodules between swaged and as received material is probably the prime factor both in tension and in compression.

As mentioned a material's ability to exhibit a lower flow stress is a characteristic of superplasticity. Swaging was performed in an attempt to improve the material's ability to become superplastic. The swaged materials flow stress properties were improved relative to the as received material in compression but not in tension. This can again be attributed to the difference in nature of the stress relief in the swaged material during the two types of deformation processes.

In tension the strain rate sensitivity values were determined in two ways. Firstly, graphical representations (Figures 38 to 41 as received material) of the logarithm of ultimate flow stress vs. the logarithm of strain rate were plotted using the results from the constant strain rate tension tests (Figures 28 to 37). The slopes of these plots are equal to the strain rate sensitivity. As is evident from these figures the strain rate sensitivity values are not very high. The most promising result is 0.356 at 850°C; all other values are below 0.30. The second method is seen in the sample calculation in section 2.5.3. These results came from the differential strain rate tension tests (Figures 42 to 45). Again these results are not remarkably high. Strain rate sensitivity versus strain rate, was plotted for different tests, in Figures 48 to 51. These plots should demonstrate the range of strain rates over which the optimum superplastic conditions will result. Figure 49 demonstrates that a range in the neighbourhood of $1x\ 10^{-4}\ sec^{-1}$ should produce the best results at 800°C for swaged material. These ranges are not necessarily conclusive since the materials are not superplastic.

6.4 Optical Microscopy Results

In hindsight, when the microstructures of both the as received material and the swaged material are considered, it is evident that the likelihood of superplasticity occurring is not very encouraging.

Upon considering the fracture surfaces of both the swaged material and the as received material (Figures 60 and 61), tested in tension, it is obvious that failure was of a ductile nature. It appears that upon crack initiation, propagation took place choosing the path of least resistance. It is evident from these figures that when a crack

propagated it did so by travelling around rather than through graphite nodules that were in its path. This can be explained in the following way; voids most likely appeared on both sides of the graphite nodules, normal to the direction of loading, resulting in the existence of weak areas in the matrix. This void creation, which also occurs in compression, appears to have occurred on numerous occasions throughout the entire matrix and is particularly apparent in Figures 23 and 25 where it seems that the voids have subsequently been filled up by graphite. Void creation was only catastrophic when there was crack initiation and propagation. The crack responsible for failure was naturally attracted to the weak nature of these voids. The responsible crack will not be suppressed since it propagates faster than the rate at which voids in the vicinity fill up. When there was no crack initiation, the voids simply filled up with graphite via some sort of diffusional mechanism. Prior work supports these conclusions. Chijiiwa and Hayashi pointed out that "In ductile cast iron, the fractograph at temperatures below 1,080°C in the austenitic matrix range shows a ductile fracture in which dimples are nucleated by spheroidal graphite inclusions."[23] Tanaka and Ikawa in their work on "Transformation Superplasticity in Ductile Cast Iron" state "voids are formed at both sides of graphite . . . and the voids become long and slender according to the strain . . . the radius of curvature of the void head becomes smaller. The vicinity of the pointed head in the void will have a higher vacancy concentration than other regions of the matrix. Thus a concentration gradient will be established and a flow of vacancies will occur . . . Conversely a matching flow of atoms will occur in the opposite

direction. This leads to the formation of the fill-up structure."[24] In a sense this mechanism of crack propagation coupled with the appearance of voids implies that the graphite nodules were essentially ripped out of their "sockets". This observation may insinuate that the resistance to tensile separation between the graphite nodules and the austenite grains is quite low. This may suggest that several things did not occur or were not prevalent in the material that would promote a high amount of resistance.

Firstly, the grain boundaries were probably not high angled in nature and that the whole deformation process was not controlled by the grain boundary sliding mechanism. Grain boundary sliding is often the predominant mode of deformation during superplastic flow. Sherby and Wadsworth states that, "Low-angle boundaries do not readily slide under the appropriate shearing stresses."[25] If the boundaries were high angled, grain boundary sliding probably would have occurred more readily and as a result would have been the dominate process suppressing crack initiation and propagation and increasing the resistivity of graphite-austenite separation.

Secondly, the grains were probably not equiaxed to the extent that is necessary for grain boundary sliding to dominate. This is particularly evident in the swaged material and likely does not apply to the as received material. (see Figures 58 and 59). It can be plainly seen in these micrographs that the graphite is no longer in nodular form, rather it is elongated in the direction longitudinal to loading. If these specimens were tested in the transverse direction the probability of grain boundary sliding taking place would be greatly increased as the graphite is closer to the correct shape in this plain.

This is stated by Sherby, "Materials with elongated cylindrical grains, even though fine-grained in a transverse direction, would not be expected to exhibit very much grain boundary sliding when tested longitudinally."[26]

A phenomenon that goes hand in hand with grain boundary sliding during superplastic deformation is the rotation of grains. The elongated graphite nodules in the swaged material when subjected to compressive or tensile forces in the longitudinal direction would have an extremely difficult time rotating even once, let alone the numerous cycles of rotation necessary for superplastic flow. A spherical equiaxed grain however can basically rotate endlessly with a relatively small amount of effort. This is not surprising because any small compact, spherical object should rotate with greater ease than a large elongated cylindrical object that is rotating in the same medium. An elongated object has more surface area in contact with the medium than there is for a spherical object in contact with the same medium. As a result, there is more force required to rotate the elongated object. If the required force does not exist rotation of the elongated object will not occur, whereas the compact spherical object may rotate with ease when subjected to this force. This applies to any medium whether it is a gas, a liquid or a solid. The rotation of an elongated graphite nodule would require a tremendous amount of force as the surrounding austenite does not flow with the relative ease that exists in most gases and liquids. The stresses associated with such a force would be impossible for the material to handle.

Swaging was carried out to refine the grains to the extent necessary to fall within the realm of superplasticity. Swaging was

performed at temperatures close to that at which the tension and compression tests were to be executed. The purpose of swaging was not realized however. The grains were not refined in the desired fashion, in fact, as mentioned previously, they were deformed and elongated, specifically the graphite nodules, in the direction parallel to the direction of swaging. The swaged material resembles closely in structure that of many fibre composite materials rather than the structure of most superplastic materials.

The nonexistence of superplasticity in the swaged material was most likely due to a combination of reasons, reasons that are the same or similar to the reasons for the nonexistence of superplasticity in the as received material. First and foremost, the swaged material was not superplastic because of these elongated graphite nodules. As was mentioned in the Fine Grain Size subsection in the Superplasticity chapter, when a material is mechanically worked to attain an ultra fine grain size, the softer phase has to penetrate through the harder phase as the harder phase is fragmenting. This penetration should cause the elongated grains to become essentially squeezed together and separation should take place resulting in numerous fine grained soft grains in a matrix of ultra fine hard grains. At least half of this process did take place in the swaged ductile cast iron. The austenite appears to have fragmented to some extent and the graphite nodules did elongate and penetrate through these austenite grains. The graphite nodules did not break up as was intended, thus the ideal microstructural arrangement for superplasticity was not realized. Even so it was decided that strain

rate change tests would be performed to determine the outcome of such tests.

The problems of grain boundary sliding and grain rotation not occurring in the as received material, if indeed these processes were not happening, evolve due to an entirely different set of circumstances. The main reason has to do with the size of the grains present in the matrix. Both the graphite nodules and the austenite grains probably possess the sufficient equiaxed shape for grain boundary sliding and grain rotation but not surprisingly, since there was not any grain refinement process applied to this material, both phases are most likely too large. An attempt was made to measure the grain size of the high temperature microstructure of both the as received and the swaged material. In Figures 62 and 63 the high temperature microstructure of as received material is shown under brightfield light and darkfield light respectively. From these micrographs it is quite obvious that the nature and orientation of the austenitic grains makes it very difficult to measure grain size. An attempt was made to trace the microstructure and measure the grains on the image analyzer but there was little confidence in the results obtained. It was decided that it would be pointless to use such results due to their uncertainty. The high temperature austenitic grains observed in the swaged material were just as difficult to measure due to their similar orientations. If grain boundary sliding and grain rotation are already taking place then a further reduction in grain size should cause these mechanisms to continue to dominate but to a greater extent. If the grain size could be refined by an order of magnitude many of the other problems

discussed previously may cease to exist or at least become so minor that their effects are negligible or no longer dominate.

The importance of hardness between the two phases is another factor that can affect superplastic conditions. If a relatively large difference in hardness exists between the two phases (austenite and graphite in the case of ductile cast iron) there will be an increase in the susceptibility to cavitation. This is not always the case if the harder phase is fine enough. Sherby and Wadsworth cited the following example "Chung and Cahoon have shown how hard but fine silicon particles can minimize cavitation during superplastic flow of a fine-grained Al-Si eutectic alloy. Coarse particles, on the other hand, can lead to cavitation."[27] In systems where the phases are relatively similar in strength, cavitation is not normally present. From the hardness testing performed on the phases of Ductile Cast Iron it is apparent that the difference between the hardness of these phases is significant (see Table 8). The hardness of austenite is assumed to fall somewhere between the averages of ferrite and pearlite over the range of test temperatures. The hardness of graphite is assumed to remain stable at these temperatures as well. This difference in hardness is quite likely a contributing factor to cavitation and thus the formation of voids.

An even distribution of austenite and graphite is also an influencing factor for the occurrence of superplasticity. The graphite that exists in the ductile cast iron used in this work is fairly evenly distributed as can be seen in Figure 56. Even distribution is probably not sufficient however. During recrystallization grain growth should be kept to a minimum. This is often realized in most superplastic

materials because the separate well distributed grains are different in composition. Another factor necessary to prevent grain growth is not only a well distributed second phase but also a second phase that is abundant enough and fine enough with respect to the primary phase. Smaller grains will self diffuse into larger grains effectively becoming numerous large grains. With the distribution of an abundant second phase diffusion will be restricted by the solubility of the two phases in each other. The well distributed abundant second phase will also limit self diffusion. The volume percentage of graphite in this ductile cast iron is approximated as follows:

There is approximately 3.5 wt% carbon present in this material.
Using the lever law and the iron carbon phase diagram (see Figure 69) the following equation applies:

$3.5 = f_G \times 100 + f_p \times 0.8$

where f_G is the weight fraction of carbon in the graphite

f_p is the weight fraction of carbon in the pearlite.

From the lever law:

$f_p = 1 - f_G$

$0.035 = f_G + (1 - f_G) \times 0.008$

$f_G = 0.027$ or 2.7 wt% graphite

The density of graphite is 2.2 g/cm^3. The density of 0.8 % carbon steel is approximately 7.82 g/cm^3 derived from Figure 70.
Therefore if there was a sample of ductile cast iron containing 2.7 grams of graphite and 97.3 grams of 0.8% carbon steel, the volumes of each would be:

Volume of graphite $= \frac{2.7}{2.2} = 1.23$ cm^3

Volume of Fe $= \frac{97.3}{7.82} = 12.44\ cm^3$

The volume percent of graphite $= \frac{1.23}{12.44 + 1} \times 100 = 9.2$ vol%

It is likely that ductile cast iron would have to contain as much as 3 times the amount of graphite by volume[28] refined sufficiently and distributed evenly to prevent grain growth and promote superplasticity.

Swaging is limited by the size and number of dies. For this reason, the the initial size of the iron bar was fixed along with the amount of deformation during each subsequent pass. Hot rolling will provide greater degrees of freedom since the initial size and the amount of deformation are not fixed. This greater freedom may produce better thermomechanical results if studied further.

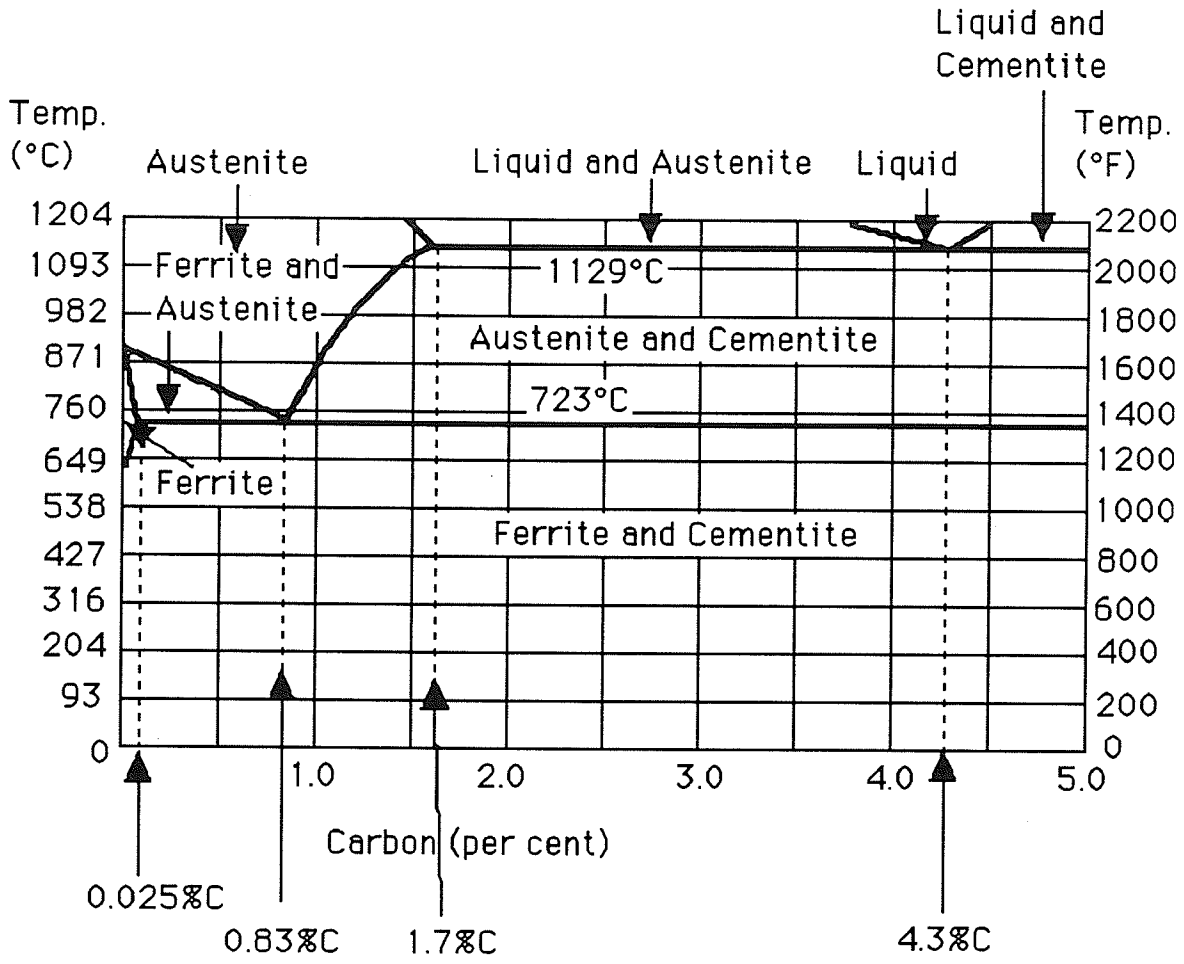

Figure 69 A portion of the iron carbon phase diagram.

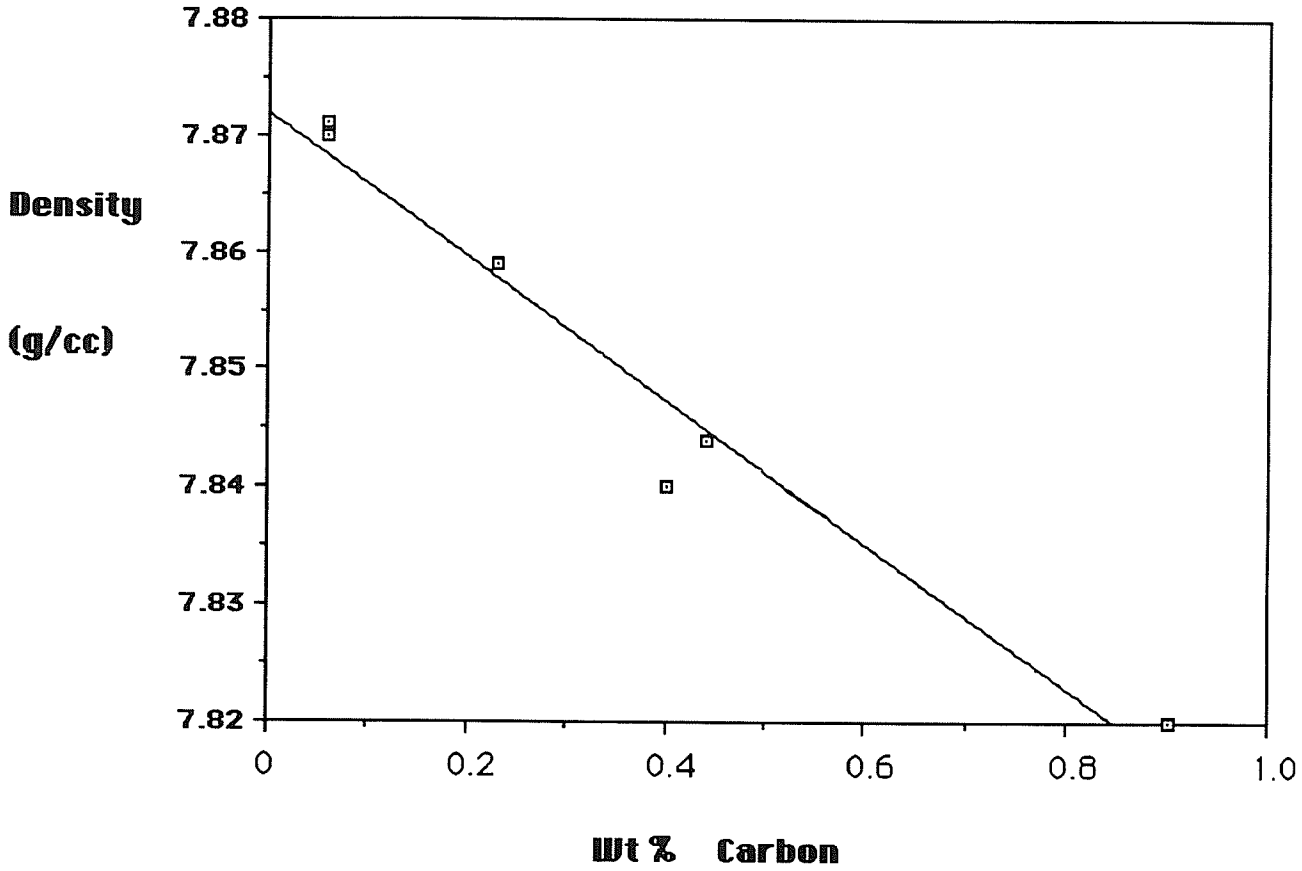

Figure 70 Density of Carbon Steels.[29,30]

Graphite fragmentation and recrystallization was not evident in either the hot swaged material, used in the compression and tension tests, or the hot and subsequently cold swaged material, see Figures 24, 26, 53, 55, 58, 59, 61, and 64 through 68. It is believed that the recrystallization temperature of graphite is quite high, possibly as high as 1600°C to 1700°C. The exact method in which graphite crystallizes from the melt is questionable and many theories exist. One such theory may help to explain why such a high temperature is required to initiate recrystallization. This theory is known as the "phase boundary" or "bubble" theory. It states that graphite will evolve only if it is protected by the presence of a phase boundary during crystallization. If phase boundaries are absent carbides or diamond will form in lieu of graphite. The phase boundaries

suggested in this theory arise from the presence of CO gas bubbles existing in the melt due to the following reaction:

$SiO_2 + 2C > Si + 2CO$

It follows that graphite is formed and begins to crystallize while the iron is still in the liquid state and it therefore will remain stable (ie not recrystallize) at the relatively low temperatures, 750 to 1000°C, used in the experimental portion of this thesis. Further proof that the graphite crystallizes when the iron is still in a liquid state comes from the existence of floated, primary graphite spheroids that have often collided and remained in direct contact with each other upon solidification.[31] See Figure 71. A final statement supporting this comes from the ASM Metals Handbook, "The amount and form of the graphite in ductile iron are determined during solidification and cannot be altered by subsequent heat treatment."[32]

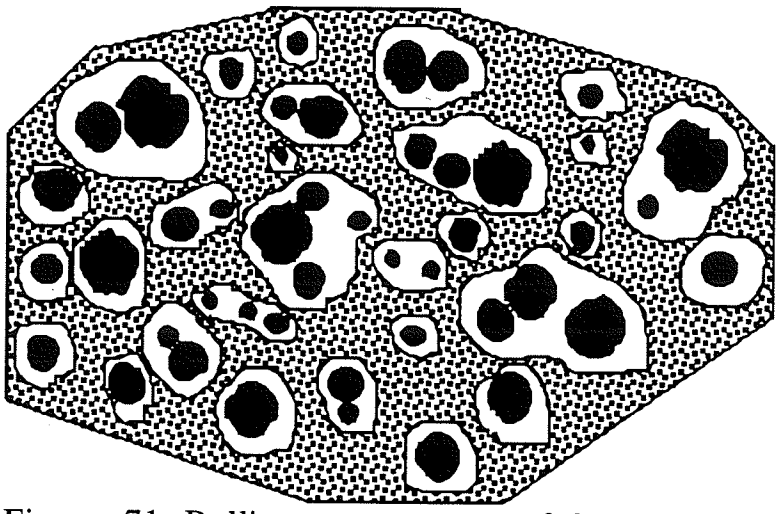

Figure 71 Bull's eye structure of hypereutectic ductile cast iron. This schematic representation shows floated graphite spheroids, many of which are in physical contact with one another.

When a material is made superplastic it is done so that it can become more versatile, with more potential applications. It is important that the material, with its refined microstructure, does not deviate to a great extent from its room temperature properties, when used or tested under these conditions. This is another area where the swaged ductile cast iron fails. Even though no room temperature testing was performed on the swaged material it is well known that ductile cast iron inherits the majority of its properties from the fact that the graphite is in the nodular form. Foundries consider nodularity to be a very rigid parameter. Extensive deviation from the desired shape will result in non-acceptance during the early stages of the quality control phase. Since the swaged graphite did not recrystallize it can not be expected to retain its room temperature properties.

Other grain refining processes could be explored that could produce the desired results. One such possibility would be to use a grade of ductile cast iron with even lower amounts of graphite. It is known that the ferrite to austenite phase transformation process is a successful method of grain refinement in iron alloys.[33] If phase transformation was attempted on ductile cast iron, the lower graphite content might take on the role of minor inclusions, rather then a second phase, that would possibly have little effect on superplastic properties. Alternatively these graphite nodules, even though present in limited quantity, could continue to be detrimental by causing the initiation and propagation of cracks due to a low resistivity to tensile separation.

One other method that might be worth consideration would be to limit the amount of graphite and introduce sufficient levels of carbides that would act as a second harder phase perhaps able to stabilize austenite grain growth. Carbide levels could be increased with the addition of manganese, chromium, vanadium, boron, tellurium or molybdenum. By limiting the amount of graphite and increasing the amount of carbide in the matrix, detrimental conditions in the room temperature properties are likely to result, which could limit the application of ductile cast iron as an engineering material.

7.0 CONCLUSIONS

It is quite obvious that the mechanical and thermal processes used, in this thesis, to promote superplasticity in ductile cast iron were unsuccessful to the extent that the material was not made superplastic however certain insight was gained. Properties, strain rate sensitivity, low flow stress, etc., that are important for the existence of superplasticity were not achieved sufficiently in either the as received material or the swaged material. These properties were, surprisingly, fairly similar in the two materials. A notable exception is the as received material performed remarkably better in compression, since it did not fail in the catastrophic fashion that the swaged material did. It is evident that the second phase, graphite, is quite possibly one of the biggest stumbling blocks preventing the occurrence of superplasticity. The reason for this is due to the nature of its formation and its ability to remain stable and not recrystallize over the expected range of superplastic temperatures.If the problems with graphite recrystallization and hence graphite refinement could be overcome, there are still other complications intrinsic to this particular grade of cast iron that would have to be surmounted. One of the foremost of these would be to attempt to increase the presence of graphite in the microstructure. If the amount of graphite was doubled or even tripled by volume percentage and well distributed, the possibility of superplasticity would probably increase. Grain growth would be limited due to the relatively low solubility between graphite and austenite, i.e. by increasing the amount of graphite, diffusion of iron from one

austenite grain to another will be inhibited by the second phase, graphite.

Hot rolling should be considered if graphite recrystallization is realized. This deformation process will give greater freedom and could possibly provide the most effective results if the process is studied extensively. If both the graphite and the austenite could be refined sufficiently by the thermomechanical processing performed in this work, other important superplastic characteristics could result. Grain boundaries would possibly become high angled, the tendency for grains to separate might be suppressed and grain boundary sliding and grain rotation may also take place. The word, if, should be stressed because, as mentioned earlier, it does not appear to be possible to initiate graphite recrystallization and thus proper refinement.

If graphite recrystallization is not possible, a different direction might be necessary if ductile cast iron is to be made superplastic. The phase transformation process might prove to be a useful method of grain refinement. Graphite would have to be present in low enough concentrations since there would be no need for a second phase.

8.0 REFERENCES

1. J. R. Cahoon, University of Manitoba, private communications.

2. Stephen I. Karsay, Ductile Iron 1 Production, Quebec Iron and Titanium Corporation (1976).

3. ASM Metals Handbook Volume 15, 9th Ed, Castings.

4. ASM Metals Handbook Volume 1, 9th Ed, Properties and Selection: Irons and Steels.

5. ASM Metals Handbook Volume 15, 9th Ed, Castings.

6. K. A. Padmanabhan and G. J. Davies, Superplasticity, Springer-Verlag, Heidelberg, (1980).

7. J. Pilling and N. Ridley, Superplasticity in Crystalline Solids, The Institute of Metals, London, (1989).

8. W. A. Backofen, I. R. Turner and D. H. Avery, Trans. ASM 57 (1964).

9. O. D. Sherby, B. Walser, C. M. Young and E. M. Cady, Scr. Metall., Vol 9, pp. 569-574, (1975).

10. J. Wadsworth, O. D. Sherby, J. Mat. Sci., Vol 13, pp. 2645-2649 (1978).

11. B. Walser and O. D. Sherby, Met. Trans., Vol 10A, pp. 1461-1471, (1979).

12. O. D. Sherby, T. Oyama, D. W. Kum, B. Walser and J. Wadsworth, J. of Metals, pp. 50-56, (June 1985).

13. G. S. Daehn, D. W. Kum and O. D. Sherby, Met. Trans., Vol 17A, pp. 2295-2298, (1986).

14. O. A. Ruano, L. E. Eiselstein and O. D. Sherby, Met. Trans., Vol 13A, pp.1785-1792, (1982).

15. W. J. Kim, J. Wolfenstine, G. Frommeyer, O. A. Ruano and O. D. Sherby, Scr. Metall., Vol 23, pp. 1515-1520, (1989).

16. Y. Tanaka and K. Ikawa, J. Japan. Inst. Metals, Vol 38, pp. 865-871 (Sept 1974).

17. Y. Tanaka and K. Ikawa, Trans. JIM, Vol 17, pp. 73-82, (1976).

18. Y. Tanaka and K. Ikawa, 44th International Foundry Congress, pp. 51-60, (1977).

19. Y. Otoguro, K. Hashimoto, O. Seya, A. Chida, K. Sato, M. Meguro, M. Ueno, Nippon Steel Tech. Report No. 15, pp. 40-54, (June 1980).

20. X. J. Zhang and G. H. J. Bennett, Ironmaking and Steelmaking, Vol. 15, No. 6, pp. 323-328, (1988).

21. K. Chijiiwa and M. Hayashi, J. Japan. Foundrymen's Soc., Vol. 51, pp. 395-400, (July 1979).

22. K. Chijiiwa and M. Hayashi, J. Japan. Foundrymen's Soc., Vol. 51, pp. 457-462, (Aug. 1979).

23. K. Chijiiwa and M. Hayashi, J. Japan. Foundrymen's Soc., Vol. 51, pp. 575-580, (Oct. 1979).

24. Y. Tanaka and K. Ikawa, Trans. JIM, Vol 17, pp. 73-82, (1976).

25. O. D. Sherby and J. Wadsworth, Prog. in Mat. Sci., 33/3-A, pp. 178, (1990).

26. O. D. Sherby and J. Wadsworth, Prog. in Mat. Sci., 33/3-A, pp. 178, (1990).

27. O. D. Sherby and J. Wadsworth, Prog. in Mat. Sci., 33/3-A, pp. 177, (1990).

28. J. R. Cahoon, University of Manitoba, private communications.

29. Metals Handbook, 9th ed., Vol. 1, Am. Soc. for Metals, pp145, (1978).

30. The Making, Shaping and Treating of Steel, United States Steel, pp. 929, (1957).

31. Stephen I. Karsay, Ductile Iron 1 Production, Quebec Iron and Titanium Corporation, pp. 19-20, (1976).

32. ASM Metals Handbook Volume 15, 9th Ed, Castings.

33. John A. Wert, J. of Metals, pp. 36, (September 1982).